RHEOLOGY OF RODLIKE NANOPARTICLE SUSPENSIONS IN LYOTROPIC LIQUID CRYSTALLINE POLYMERS

by

Ana Raquel Cameron Soto

A dissertation submitted in partial fulfillment of the requirements for the degree of

DOCTOR OF PHILOSOPHY

in

Chemical Engineering

UNIVERSITY OF PUERTO RICO

MAYAGUEZ CAMPUS

2013

_____	_____
Aldo Acevedo, PhD President, Graduate Committee	Date
_____	_____
Ubaldo M. Córdova-Figueroa, PhD Member, Graduate Committee	Date
_____	_____
María Martínez Iñesta, PhD Member, Graduate Committee	Date
_____	_____
Agnes Padovani, PhD Member, Graduate Committee	Date
_____	_____
Paul Sundaram, PhD Representative of Graduate Studies	Date
_____	
Aldo Acevedo, PhD Chairperson of the Department	_____ Date

ABSTRACT

Liquid crystalline polymers are ideal to develop oriented and anisotropic materials. The incorporation of a nanoparticle may improve or add properties to a matrix. Small concentrations of particles smaller than the liquid crystal structural features do not affect the structure of the phase, or consequently, its properties. Similarly, small loadings of cylindrical particles may modify the rheological and electrical properties of a liquid crystal. Yet, unfavorable effects will be expected as the loading increases. It was expected that rod-like nanoparticles may be incorporated into a liquid crystalline polymer and oriented along the nematic director. Moreover, both components may be oriented using external fields. Therefore, solutions of cylindrical nanoparticles and liquid crystalline polymers may be useful to obtain oriented multifunctional materials.

In this research, the rod-like nanoparticle loading effect on the rheological and viscoelastic properties of both an isotropic and a liquid crystalline polymer solutions were determined. The inclusion of multiwalled carbon nanotubes and halloysite nanoclays up to 0.45 wt% does not affect the viscosity, neither the viscoelastic properties, of a liquid crystalline hydroxypropylcellulose solution. A maximum viscosity and viscoelastic moduli were obtained at 10 wt% of the halloysite. No indication of percolation neither changes on the polymer dynamics was obtained suggesting that the nanoparticle were oriented along the nematic director. A decrease of the steady-state viscosity and viscoelastic properties of isotropic polymer solutions was observed at small particle loadings. ζ - potential measurements demonstrated the

formation of core (nanoparticle) – shell (polymer) structures. POM measurements suggest that the polymer shell around the halloysite nanoclays have a preferential orientation on a macroscopic scale.

The effect of the application of an electric field on the rheological and viscoelastic properties was also determined for both a non- and electrorheological polymer solution loaded with multiwalled carbon nanotubes. It has been demonstrated that an electric field is not a feasible method to control the orientation of carbon nanotubes suspensions since it promotes the agglomeration of the nanoparticles, affecting the properties of a non-electrorheological hydroxypropylcellulose polymer solution. Yet, the application of a flow field can be used to obtain materials with oriented rod-like nanoparticles.

RESUMEN

Los polímeros líquidos cristalinos son ideales para ser utilizados en el desarrollo de materiales orientados y anisotrópicos. Incorporar nanopartículas a una matriz polimérica puede añadir o mejorar las propiedades de dicha matriz. Pequeñas concentraciones de partículas isotrópicas, de un tamaño menor que la longitud estructural de la fase líquida cristalina, no afectan la estructura de dicha fase y, por consiguiente, sus propiedades. Similarmente, si partículas cilíndricas son incorporadas en dicha matriz, cambios favorables pueden ser inducidos al utilizar una concentración pequeña partículas. Sin embargo, un deterioro de dichas propiedades se espera al aumentar la concentración de partículas. Se espera que partículas cilíndricas puedan ser incorporadas en un polímero líquido cristalino y orientarlas a lo largo del director nemático. Además, tanto los nanotubos como los polímeros líquidos cristalinos pueden ser orientados mediante la aplicación de un campos externo. Por lo tanto, soluciones de nanotubos y polímeros líquidos cristalinos pueden ser útiles para desarrollar materiales orientados y multifuncionales.

En esta investigación, el efecto de añadir partículas cilíndricas en las propiedades reológicas y viscoelásticas de soluciones poliméricas en estado isotrópico y líquido cristalino fue determinado. La inclusión de partículas hasta una concentración de 0.45 porciento por peso de nanotubos de carbono de paredes múltiples o haloisita no afecta significativamente la viscosidad en estado estacionario, ni las propiedades viscoelásticas de una solución líquida cristalina de hidroxipropilcelulosa. Un valor máximo tanto en la viscosidad como en los módulos

elásticos se obtuvo al añadir una concentración de haloisita de 10 porciento por peso. Los resultados no demuestran la percolación de las partículas ni cambios en la estructura de la fase líquida cristalina, lo que sugiere que las partículas están orientadas a lo largo del director nemático. Por otra parte, una disminución en la viscosidad y en las propiedades viscoelásticas se observó al añadir pequeñas concentraciones de partículas a una solución isotrópica. Medidas del potencial ζ sugieren que este efecto es debido a la formación de estructuras de núcleo y coraza, en las cuales el núcleo está compuesto por las nanopartículas y la coraza por moléculas de polímero. Imágenes ópticas sugieren que la capa de polímero alrededor de la haloisita posee una orientación en una dirección preferencial en una escala macroscópica.

Por otro lado, el efecto al añadir un campo eléctrico en las propiedades reológicas y viscoelásticas fue determinado tanto para una matriz electroreológica como otra que no lo es, ambas con nanotubos de carbono de paredes múltiples. Se demostró que un campo eléctrico no es un método adecuado para controlar la orientación de nanotubos de carbono, ya que el mismo fomenta la aglomeración de las nanopartículas afectando las propiedades de una matriz que no responde a campos eléctricos. A pesar de esto, la aplicación de un flujo puede ser utilizado para obtener materiales con partículas cilíndricas orientadas en una dirección preferencial.

To my grandma (Gina), an admirable and exemplary woman…

ACKNOWLEDGMENTS

Firstly, I would like to thank Mariana Moraca and Dra. María M. Martínez-Iñesta, the persons through whom I had the opportunity to meet my future advisor and undertake this challenge six years ago. Dr. Aldo Acevedo, thanks for always believing in me. I really appreciate your patience, guidance, advice, and the opportunities to develop and improve some of my skills.

Thanks to my lab-mates for your suggestions and collaboration. Thanks to Vivian Florián, Anthony González, Gaby (Félix) Miranda, and Mariel Santiago for the support, friendship, and talks related to research, life, and everyday issues. Thanks to Rafael Henríquez for the trust and the enriching opportunity of mentoring you.

Thanks to the PR LSAMP - Bridge to the Doctorate Program, the Puerto Rico NASA Space Consortium, Alfred P. Sloan Foundation, and the Chemical Engineering Department for the financial support, professional exposure, and educational opportunities offered throughout these years.

To all my friends, Gaby (Ángel) Santos, Anthony, Fernando Mérida, and Gretselle Carreras thanks for the support during the moments of stress and the shared joys. Thanks to all the persons that collaborated with me, and directly or indirectly contributed to the success of this research work.

Thanks to all the members of my committee for your suggestions and to my family for the support.

TABLE OF CONTENTS

LIST OF FIGURES

NOMENCLATURE

c - concentration

c_{IN} – concentration at which the transition of an isotropic and a liquid crystal occurs

c_N – concentration at a fully nematic phase

d – diameter

D – strain rate tensor

D_r – rotational diffusivity

D_{r0} – dilute rotary diffusivity

$\overline{D}_r$ – average rotational diffusivity

$\widehat{D}_r$ – orientation dependent rotary diffusivity

E' – dimensionless electric field strength

E – electric field

g – Onsager internal field factor

G – dimensionless shear rate

G'' – loss modulus

G' – storage modulus

k_B – Boltzmann's constant

L – length

M_n – number average molecular weight

M_w – weight average molecular weight

M_z – z-average molecular weight

n – director

N_1 – first normal stress difference

q – aspect ratio

$\mathfrak{R}$ – rotational operator

R_{NP} – radius of the nanoparticles

S – order parameter

t – time

T – temperature

u – unit vector

U – strength of nematic potential

U_e – potential of an external field

U_{scf} – mean field nematic potential

Superscript:

E – elastic contribution

Greek symbols:

α – orientation of the director

β – constant of the rotational diffusivity equation (2.3)

$\boldsymbol{\delta}$ – unit vector (2.6)

δ – polymer shell thickness

ϕ – volume fraction

angle between the molecule and the director (2.10)

ϕ_e – effective volume fraction

ϕ_m – maximum packing fraction

ϕ_{NP} – volume fraction of the nanoparticles

γ – correction factor for rods ends effects (2.2)

$\dot{\gamma}$ – shear rate

η – viscosity

η_0 – zero shear rate viscosity

η_P – relative viscosity of a particle suspension

η_M – relative viscosity of the polymer matrix

η_r – relative viscosity

η_s – solvent viscosity

$[\eta]$ – the intrinsic viscosity

$\boldsymbol{\kappa}$ – velocity gradient tensor

μ – permanent dipole moment

ν – number concentration

θ – angle between the molecules and the director (2.1)

angle between the molecules and the electric field or z-axis (2.9)

σ – stress

τ – dimensionless time

Ψ – orientation distribution function

ζ_{str} – viscous drag coefficient

Chapter 1

INTRODUCTION

Polymers are the most commonly used matrices in the automobile, structural, optical, and electronics industry, since they enable the development of diverse materials. The incorporation of adequate nanoparticles may enhance or incorporate additional properties, such as thermal [1-4], mechanical [1, 2, 4-7], chemical [8], electrical [4, 7, 9], rheological [10-12], and barrier properties [13, 14], providing the opportunity to develop multifunctional materials at lower capital costs. Nevertheless, the addition of some nanoparticles, such as clays, may result in the confinement of the polymer chains [15, 16]. This aspect is important since it has been demonstrated that the dynamics of filled polymers differs significantly from that of the neat polymers [10, 15].

An interesting subgroup is the liquid crystalline polymers (LCPs). LCPs are anisotropic fluids, that is, they have some orientational order at rest (molecules tend to align in the same direction). Moreover, they may have partial positional order, the molecules' centers of mass tend to lie on lattice points. Consequently, LCP materials have high strength, high molecular orientation, anisotropic physical properties, and high resistance to chemical and moisture uptake. Additionally, they have low viscosity in the nematic melt state (i.e., the state in which molecules only have orientational order), which allows for easier processing and thus cheaper fabrication. Another potential advantage of these complex fluids is the ability of their stiff molecules to be oriented by an electric, magnetic, or flow field. These properties may be useful to

obtain oriented materials with excellent mechanical, electrical, and thermal properties. In addition, these properties may be attractive in police, military, automobile, sport, aircraft, and aerospace industries. For example, Kevlar is a LCP applied in airframe systems, aircraft interiors, and electronic systems [17]. As an additional advantage, the liquid crystal (LC) texture, rheological, mechanical, and optical properties, and the isotropic to nematic (I-N) phase transition may be altered by particle inclusion and by the shape or degree of anisotropy of the particles.

It has been shown that isotropic particles can alter the rheological properties of a LCP. For example, they can eliminate the negative normal stress differences at small loadings [18-20], result in the destruction and recovery of the alignment of the LC mesogens [21], and enhance the viscosity of the suspensions [19, 20]. Nevertheless, only a few reports elucidate the effect of particle inclusion on a LCP matrix.

Some of the fundamental aspects of this problem are similar to those of low molecular weight LCs. It has been shown that, at small loadings, isotropic particles do not change the I-N phase transition of a low molecular weight LC [22], nor the liquid crystallinity of the LC [23]. Moreover, low concentrations of anisotropic nanoparticles did not affect the electric [24-26] and rheological properties [27], nor the LC ordered phase [26-28].

In spite of the similarities between the fundamental aspects of LCPs and low molecular weight LCs, the concentration threshold at which an effect will be observed on the properties of the matrix should be different for both systems. Consequently, we are interested in elucidating the effect of nanotube inclusion on the phase behavior and rheological properties such as the steady-state viscosity and viscoelastic moduli of a LCP matrix. The effect of the nanoparticle addition on the electrorheological

properties of both a non-electrorheological and electrorheological LCP matrix will be determined in order to verify the feasibility of use an electric field to control the orientation of both the polymer molecules and nanoparticles. Furthermore, the relationship between the rheological properties and the structure of the system will be determined in order to transfer that knowledge to the development of a continuous process for an oriented and reinforced material.

1.1 Summary of the Following Chapters

The next chapter intends to provide a comprehensive overview of the effects of isotropic and anisotropic particles on LC phases and their physical properties, mainly rheological properties, both from a theoretical and an experimental perspective. It is divided in three parts: (1) a brief review of the most important properties of neat and filled LC matrices, (2) a discussion of the orientation techniques to align both polymer and cylindrical particles, and (3) the most relevant theoretical aspects to model the rheology and electrorheology of LCP. Next, in Chapter 4 the methodology and studied systems used on the research project are discussed. Then, the experimental results, rheology and electrorheology, are discussed in the subsequent chapters (chapter 5 and 6, respectively). Finally, the general conclusions are presented in the last chapter.

Chapter 2

BACKGROUND

2.1 Introduction

In this section the properties and rheological features of liquid crystalline polymer matrices will be described. The experimental and theoretical effects of particle loading and shape on those properties will be discussed. Finally, the most relevant aspects of the molecular theory of Doi-Edwards will be provided with the intention of describing the orientation of rod-like molecules when an external field is applied to the system.

2.2 Liquid Crystalline Solutions

Oblate, rods, or elliptic molecules (generally semirigid molecules) are generally responsible for liquid crystalline phase formation. The nematic (N) phase has only orientational order at rest, as illustrated in Figure 2.1. It also indicates that the liquid crystalline phases might be induced due to temperature or concentration changes. Lyotropic polymers are those for which the liquid crystal phase arises by increasing the polymer concentration in a given solvent. Thermotropic polymers are those in which the liquid crystal phase arises with an increase in temperature from the solid phase. Optical microscopy and x-ray scattering are useful techniques to determine the phase type and LC structure [29-31]. Moreover, optical microscopy, differential scanning calorimetry, and rheology can be used to determine the liquid

crystal phase transition concentration or temperature [29, 31, 32]. The main focus of this work is on lyotropic polymers, which typically show a nematic phase.

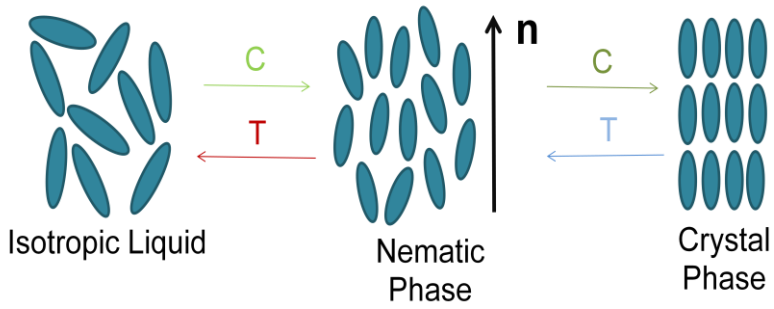

Figure 2.1. Phase transition exhibited by liquid crystals due to concentration or temperature changes. The direction of the average orientation of the nematic phase is given by the director (n).

The parameters necessary to completely describe the nematic phase are the director and order parameter. The director (**n**) is a unit vector that describes the direction of the average orientation of the molecules, whereas the order parameter (S) describes the degree of orientational order. The order parameter is defined as:

$$S = {}^{3}/_{2}\langle \cos^2\theta \rangle - {}^{1}/_{2} \qquad (2.1)$$

where θ is the angle between the molecules and the nematic axis (or director), and the brackets represent an average over all the molecules. The order parameter is used to describe the deviation of the molecular orientations from the director. For example, for an isotropic phase S = 0, because there is no order. On the other hand, for an ideal nematic phase in which the molecules are perfectly parallel to each other (and to the director), S = 1.

The anisotropy of the LC phases results in an optically birefringent sample [29, 32]. Usually, optical micrographs are composed of a range of beautiful colors due to the distorted or inhomogeneous director field of a LC matrix. These distortions are called textures.

The rheological properties, flow properties such as the viscosity, are important from a processing point of view because they can be correlated with the orientation of the LC phase. Complex rheological properties of LCPs are characteristic of the anisotropic internal structure of these systems, and show unique and special features such as a negative steady-state first normal stress difference (N_1) [33-36] and an oscillating transient shear stress [37-39]. N_1 is defined as the difference between the components of the normal stress tensor, σ_{11} and σ_{22}. A positive value of N_1 indicates that the plates tend to push apart and a negative value represents the opposite. Some lyotropic LCPs show a negative N_1 over a specific shear rate range, and this range depends on the polymer concentration and molecular weight [32]. In this region, there is an oscillation of the director about a steady state value due to the competition between tumbling and steady alignment of the director domains [40]. The transient shear stress of LCPs has an oscillatory response, and usually between 50 and 100 strain units must be applied to obtain a steady-state value [37-39]. These aspects are a consequence of the flipping of the director of a domain and a gap-averaged director orientation dependence on the radial position.

Moreover, rheology may be a complimentary tool to obtain the LC phase transitions by determining the polymer concentration effect on the steady-state viscosity [34, 41]. Figure 2.2 illustrates the effect of polymer concentration on the steady-state viscosity of aqueous hydroxypropylcellulose (HPC) solutions [42]. An

initial increase in the viscosity is observed, which at small polymer concentration is proportional to the cubic of the polymer concentration. The viscosity drop is attributed to the onset of the nematic phase (c_{IN}), due to the oriented molecules show a lower resistance to movement because they may slide past each other more easily. It is usually characteristic of a biphasic phase, phase in which both an isotropic and a liquid crystal phase coexist. However, the viscosity begins to increase with increasing concentration when a fully nematic phase is obtained (c_N) due to excluded volume interactions. The existence of these phases is usually corroborated by polarized optical microscopy (POM) or other structural probes.

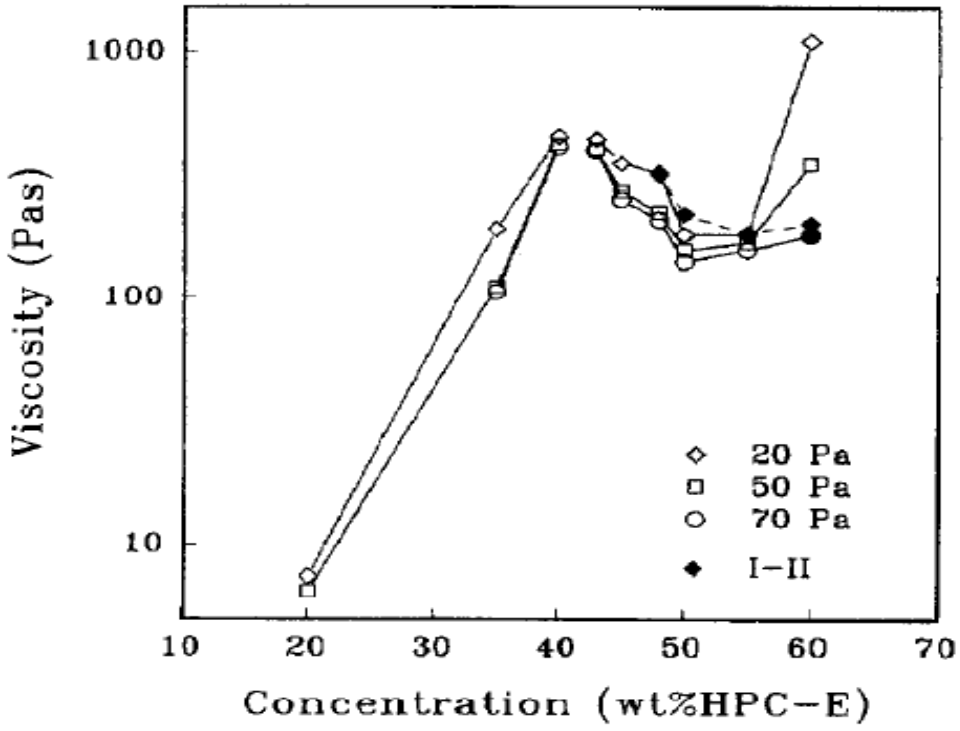

Figure 2.2. Polymer concentration effect on the steady-state viscosity of aqueous hydroxypropylcellulose (HPC) solutions at different constant stress. Reproduced from Walker, Wagner (1994) [42].

Another rheological feature of the LCs is that they may be aligned by a flow field [32]. Generally, there is a difference between the director of the bulk phase and the boundary surfaces when a shear flow is applied to a LC layer between two parallel plates. This would be due to the influence of the bounding surfaces on the LC director. As the velocity increases, the greater fraction of the bulk phase is oriented along the flow direction and the boundary layer at the surface of the wall is thinner. Therefore, the rheological properties are measured so that the bulk gap is sufficiently greater than the boundary gap, so that the boundary director layer may be neglected. A similar mechanism occurs for materials that have dielectric or magnetic anisotropy, but the external force will be an electric or magnetic field, respectively, instead of a flow field [43, 44]. On the other hand, a combination of fields, as for example shear and electric fields, can also be used to orient LCs. In this case, there is a competition of forces, in which the orientation of the LCs molecules (with a dielectric or magnetic anisotropy) depends of the relative magnitude of the applied fields.

2.3 Filled Liquid Crystals

The phase behavior and rheology may be distorted by particle inclusion and by the shape or degree of anisotropy of the particles. In this section, the effect of isotropic and anisotropic particles on rheological and optical properties is discussed.

Some experimental studies focus on the determination of the effect of particle inclusion on the rheological, optical, and mechanical properties of LC matrices. In the case of isotropic particles suspended in LCPs, authors have reported: 1) an increase in viscosity with particle loading governed by shear rate instead of shear stress for isotropic matrices [18-20] and a damped oscillatory response on flow reversal experiments, which indicates that the rheological response is governed by the LC

textures [18, 20]; 2) the obstruction of the LCP orientation along the flow direction due to a complex and unsteady flow field in between the particles, which caused positives values for N_1 on the studied shear rate range [18-20] and a decrease in the overall orientational order under flow with particle loading, especially when nanoparticles were used [20]; 3) lower characteristic time scales of the transient experiments (faster transients) with particle loading caused by a weak coupling between the particles and the LCP, which reduce the texture length scale [18, 20]; 4) an organization of the particles under high shear rate, in rope-like structures, independently of the anisotropy of the polymer matrix [19]; 5) a destruction and recovery of the planar alignment of the LCP matrix with the addition of nanoparticles due to the organization of the particles and the excluded volume interactions that result in hexagonally packed rods [21]; 6) a lower glass transition temperature for LCP nanocomposites with 15wt% of nanoparticles related to a lower packing density of the polymer molecules [45]; and 7) a displacement of the nematic to isotropic (N-I) and glass transition temperature of LCP composite to higher value due to the particles surface induced ordering of the LCP molecules [46]. In addition, it was demonstrated that the addition of particles of the same order of magnitude as the structural features of the polymer in solution did not suppress the director tumbling of the polymer solutions [18], but when smaller particles were used greater damping was observed [20]. Another study by small-angle x-ray scattering (SAXS) demonstrated that a concentration of 0.007 volume % of nanoparticles do not affect the liquid crystallinity of a LCP matrix, a concentration lower than the concentration used in the studies previously discussed [23]. Moreover, the effect of particle inclusion on the properties

of low molecular weight LCs should be analogous to the high molecular weight LC or LCP.

It has been stated that particles with an average diameter between 0.7 and 1.5 nm, significantly smaller than the ones used in the studies previously discussed, did not change the N-I transition of a low molecular weight LC [22]. Low particle loading and particles with a diameter smaller than the LC structural features do not have any effect on the LC phase, and consequently, on its properties. However, there is a critical loading at which a lower degree of orientational order results with the particle loading. At high particle loading ordered structures may be obtained, such as lamellar domains, at which the dynamics of the flexible polymer chains may change due to confinement.

From a theoretical point of view, a homogeneous nematic phase, present from the N-I volume fraction up to approximately 0.53, was predicted for hard spheres with a diameter (d) equal to the diameter of hard rods with an aspect ratio (q) equal to three [47]. Moreover, an homogeneous stable mixture was predicted for a system composed by soft spherocylinders with an aspect ratio of five and hard spheres with a diameter equal to the length of the spherocylinders for volume fractions below 0.38 (the maximum concentration studied) [48]. However, for hard sphere ($d = d_{rods}$) and rod ($q = 3$) mixtures with particle volume fraction higher than 0.53 macroscopic phase separation was expected [47]. Simulations predict micro-phase separation or lamellar structures due to the addition of particles, for hard particles and parallel hard spherocylinders with an aspect ratio equal to or larger than 5 [49]. The experimental studies, discussed above, worked with particles concentrations lower than the critical concentration for which a macro- or micro-phase separation was predicted.

Anisotropic particles such as nanotubes (NTs) may induce interesting changes in LC properties since those nanoparticles have a diameter smaller to the structural features of LC molecules and aspect ratio one or two orders of magnitude higher than those of the LC molecules. Some investigations determined an unfavorable effect on the mechanical properties of a LCP with fiber loading due to a change in the orientation and poor wetting [50]. Furthermore, phase separation was reported for the inclusion of nanotubes to LCs at concentration greater than 0.15 wt% [28].

On the other hand, it has been demonstrated that loadings up to 1 or 1.5 wt% improve the thermal stability [51-53] and mechanical properties [53] of thermotropic LCP nanocomposites. The integration of those nanoparticles in LCP nanocomposites was demonstrated by x-ray diffraction measurements [51], and the promotion of the liquid crystalline phase on the surface of the NPs by POM [54]. Other works reported a shift of the I-N transition temperature to higher values with low nanotube loadings (less than or equal to 1wt%) [22, 51, 52, 55, 56] and an increase in the dielectric anisotropy with low carbon nanotube (CNT) loading [57], which suggests an alignment of the nanoparticles along the director. Other studies of NT dispersion in a low molecular weight LC matrix showed: that small concentrations (on the order of 10^{-3} wt%) do not affect the LC order nor the dielectric anisotropy [24], a displacement of the LC-I transition to lower temperatures [58-60], the dispersion and stabilization of low nanoparticle concentration by the LC [56, 61-64], an electrical percolation threshold at concentrations less or equal than 0.1 wt% [25, 26, 55], the integration of the nanoparticles on the LC ordered phase [26-28, 60, 65-68], the improvement of the thermal stability with loadings up to 0.5 wt% [52], and a slight increase in the viscosity and viscoelastic moduli of the matrix for loadings up to 0.5 wt% [27, 53, 69].

The existence of stronger anisotropic interactions between carbon nanotubes and aromatic LCs have also been demonstrated [26] and strong anchoring effects on the nanotube surface for concentrations of 0.1 [25] and 0.007 wt% [57]. Therefore, the discrepancies between positive and negative effects, previously discussed, suggest a strong interplay among the interactions between the nanoparticles and the LCs. Stronger interactions may produce a nematic phase with a stronger nematic potential, and consequently, improve the characteristic properties of a LC phase.

From a theoretical point of view, the effect of anisotropic particles on the LC properties may be described by studies that consider a mixture of two polydisperse hard rods of different lengths with the same diameter or, similarly, with the same length and different diameters. In these studies, three phase equilibrium was obtained for systems with a large discrepancy between the lengths or diameters of the rods, asymmetric length distribution, and small fraction of long rods [30, 70-75]. However, the phase coexistence disappears when the polydispersity of both length distributions increases [71]. Alternatively, a highly polydisperse system causes strong fractionation [30, 71-73, 76-78] (shorter rods prefer to remain in the isotropic phase, and longer rods in the nematic phase) and a broader biphasic region [70, 71, 78]. For a log-normal length distribution, three phase equilibrium was predicted above a threshold polydispersity, but it disappears at very large polydispersities [72, 77]. Also, phase equilibrium can be found for weakly polydisperse systems with a small molar fraction of longer rods, but direct observation of this peculiar phase is difficult [72, 77]. Usually, both LCPs and nanotubes mixtures are highly polydispersed, thus making observation of the phenomenon even more difficult. The predictions for polydispersed systems composed of two rod-like molecules, such as the triple phase equilibrium and

fractionation on the biphasic phase, have been seen experimentally for ternary solutions of schizophyllan (M_w = 800 and 65.8 or 132 kDa, $M_z/M_w < 1.3$) and *fd* virus (D_{thick}/D_{thin}) ≤ 3) with different length and diameter ratio, respectively [75, 79, 80]. However, the triple phase equilibrium was not observed on ternary poly(n-hexyl isocyanate) solutions with an average molecular weight of 244 and 20.9 kDa (M_z/M_w ≤ 1.1), 244 and 68 kDa ($M_z/M_w \leq 1.1$), and 29.7 and 99.2 kDa ($M_z/M_w \leq 1.9$) [81, 82].

The major advantage of incorporating cylindrical particles to a liquid crystal is to obtain ordered materials because the particles can be oriented along the liquid crystal director due the inherent self-orientation properties of the LC matrices. Furthermore, rod-like nanoparticles, due to their geometric similarity with the polymer molecules, should not significantly affect the phase behavior below a threshold concentration, and above it, the system will behave as a pseudo dispersed system. Besides using liquid crystals, other techniques may be used to align both the nanorods and LCs (such as electric, flow, and magnetic fields).

2.4 Orientation Techniques

An inherent desire of the material industry is to obtain better, multifunctional, and efficient materials. It has been theoretically predicted and experimentally demonstrated that if the particles dispersed on a polymer matrix are aligned in a preferential direction, its mechanical and other physical properties may be improved [1, 5, 83]. Some alignment techniques are used to align LCPs and proposed to align cylindrical nanoparticles such as the use of magnetic, flow, and electric fields.

A technique commonly used is the application of shear forces [63, 84-89]. It has been demonstrated that these forces are useful to reinforce the mechanical properties of the final sample in the shear direction. However, electric and dielectric

properties decrease in both the shear and perpendicular direction when a dilute and well dispersed system is used [90].

In the case of the alignment of both nanotubes and/or LCs using a magnetic field, the alignment is due to their anisotropic magnetic susceptibility. There is some evidence of the use of this technique to align liquid crystal polymers [43], nanorods in a LC matrix [63, 91, 92], and carbon nanotubes dispersed in a polymer matrix [93, 94] along the magnetic field direction. A similar technique is the application of an electric field, which produces an alignment of nanotubes and polymers with a permanent dipole and dielectric anisotropy [43, 44, 95-98].

It has also been demonstrated that application of electric field induces electric dipoles in carbon nanotubes, causing the formation of network structures between the electrodes [99-105]. The elongation of nanotube clusters dispersed in a LC matrix by electric fields was demonstrated, independently of the anisotropy of the matrix, suggesting the orientation of the nanotubes in the electric field direction [106, 107]. Migration of them to the anode [99, 100, 108, 109] or the cathode [110], caused by electrostatic forces, was observed. Migration to a specific electrode may be due to the presence of some impurities on the nanotubes left from the synthesis procedure that imparts some net charge to them. In a related study, a detrimental effect on the LC phase results from the application of an AC electric field to a nanotube and LC mixture due to the deformation of the LC director field by a translational motion of the nanorods between the electrodes [24, 101]. Furthermore, Shah and coworkers demonstrated a reversible N-I transition with the application of an electric field on nanotubes/LC solutions due to a local heating caused by the short-circuiting of long nanotubes [111]. Park and Ma, with their respective collaborators, observed alignment

of nanotubes dispersed in a polymer matrix along the field direction and coarsening of the aligned clusters due to the lateral migration of the aligned nanoparticles, which create conductive percolation paths [102, 103]. Other research groups use an applied electric field to align the nanorods, while the solvent was being evaporated or during the curing process to obtain oriented films [95, 112].

Combining the application of an electric field and shear flow is a useful technique to orient nanoparticles or molecules along a specific direction depending on the relative field strengths. This technique can maximize mechanical and electrical properties. Suspensions and LCPs that undergo a rapid alteration of its rheological properties when subjected to an electric field are electrorheological (ER) fluids. In the case of suspensions, the electric field induces the formation of chains of particles along the field direction. Consequently, the resistance to flow perpendicular to the chains increases proportionally to the square of the electric field strength [32].

Also, it has been demonstrated that LCPs, such as poly(n-hexyl isocyanate) (PHIC), are oriented along the electric field direction or have shown a positive response (their rheological properties increase) with the application of an electric field [44, 98, 113]. However, a negative effect on the rheological properties of nanotubes in solutions was reported (their rheological properties decrease), which decrease with an increase in the field strength. When nanowires are used, a positive effect was obtained [114]. The negative effect was attributed to a phase separation in the form of layered structures, followed by an alignment along the electric field direction in the form of ropes by an electrophoresis or dielectrophoresis mechanism.

Nematic LC phase are proposed to induce an alignment along the LC director of cylindrical nanoparticles as a great method to develop oriented materials [27, 28,

63, 64, 66, 68, 91, 115-121]. However, most of these studies have used surfactants to disperse and form the LC media. They demonstrate the integration of the nanoparticles in the LC matrix without destroying the LC phase [27, 28, 64-67, 119]. Moreover, cylindrical materials such as carbon nanotubes have the ability to form liquid crystalline phases, which provides the possibility of developing materials with a greater nematic potential and better orientation [87, 122-126]. Therefore, it has been demonstrated that some materials which exhibit a LC phase may be used efficiently to orient the nanorods along the director [63, 64, 97, 115, 117, 119-121, 127] and the manipulation of the orientation will depend on the possibility of changing it using external fields.

However, most of these methods are not suitable for the preparation of nanocomposites, since they cannot be transferred to continuous processing or are limited to laboratory scale processes. For example, orientation with LC surfactants is not feasible for polymer composites applications since there is no efficient method to solidify the polymer melt or solution without adding stress to it, which may cause a loss of the LC phase and the nanorod orientation. In spite of all the efforts to achieve a better orientation, no successful technique which allows a controlled and reproducible production of oriented nanostructures has been developed.

2.5 Dynamic Molecular Theory of Doi and Edwards

The dynamics and feature rheological properties of rod-like polymers can be understood and explained, from a molecular point of view, by the dynamic molecular theory developed by Doi and Edwards. Doi's theory provides a mathematical description of the orientation of the molecules when an external field is applied to the

system. Additionally, some authors found alternative solutions when a shear force alone or in combination with electric fields is applied to the liquid solution.

As it is shown in Figure 2.3, a solution of Brownian rod-like polymers may be classified in the following concentration regimes: dilute, semidilute, and concentrated [128]. These regimes can be expected in a specific range of number concentration (ν). The number concentration can be related to the volume fraction (ϕ) as $\phi = \pi d^2 L\nu/4$, where L is the length of the rod.

Figure 2.3: Concentration regimes for rod-like molecules at specific number concentrations (ν); d and L refer to rods the diameter and length of the rods, respectively.

In a dilute solution ($\nu < 1/L^3$), the rods are able to rotate freely without the interference of others rods. The position of a rod in this region is constantly changed by thermal agitation or Brownian motion. The mean square displacement of a unit vector **u**, which is parallel to the axis of symmetry of a rod molecule, is directly related with the rotational diffusion constant. The dilute-solution rotary diffusivity (D_{r0}) shows the rate at which a particle reorients by Brownian motion. Doi and Edwards define it as [128]:

$$D_{r0} = \frac{3k_B T(\ln\left(L/d\right) - \gamma)}{\pi\eta_s L^3} \tag{2.2}$$

Where k_B is the Boltzmann's constant, T is the absolute temperature, η_s is the solvent viscosity, and γ is a correction factor of the rod end effects. The value of γ commonly used is 0.8, which was calculated based on the point force approximation [129].

In the semi-dilute regime ($1/L^3 << \nu << 1/dL^2$), the rotation of the rod molecules is restricted by the neighboring molecules. Doi and Edwards developed a cage model to predict the rotational diffusivity (D_r) in this region [130, 131]. This cage was modeled as a cylinder in which other molecules do not penetrate. Its dimensions are limited by their neighbor molecules, and represent the characteristic space within the molecules could move freely by Brownian motion. In this case D_r is defined as:

$$D_r = \beta D_{r0}(\nu L^3)^{-2} \propto \phi^{-2} L^{-7} \ln\left(L/d\right) \tag{2.3}$$

β is a constant that it is estimated as 1350 for perfectly rigid rods based on geometrical considerations [132, 133]. It has been reported that for concentrated solutions of unimodal poly(*n*-hexyl isocyanate) (PHIC) this constant is on the order of ten ($O(10^1)$) [134].

In a concentrated regime, the rod molecules tend to orient in the same direction by excluded volume interactions, inducing an anisotropic or a LC phase. Also, rod like molecules could be oriented with a flow field, causing the orientation distribution of the rods to become anisotropic. In this region, the radius of the cage and the rotational diffusivity becomes dependent of **u**, so it is necessary to define an orientation dependent rotary diffusivity ($\widehat{D}_r$).

Doi developed a molecular theory for the flow effect on the orientation of monodisperse thin-rigid rod polymers [135]. The Smoluchowski equation predicts the probability that the axis of symmetry of a rod-like molecule is oriented parallel to a unit vector **u**. This equation is defined as [136]:

$$\frac{\partial \Psi}{\partial t} = \bar{D}_r \mathfrak{R} \cdot \left[\mathfrak{R}\Psi + \frac{\Psi}{k_B T} \mathfrak{R}(U_{scf} + U_e)\Psi \right] - \mathfrak{R} \cdot [\mathbf{u} \times (\boldsymbol{\kappa} \cdot \mathbf{u}\Psi)] \tag{2.4}$$

where Ψ is the probability that an arbitrarily chosen polymer is oriented in the **u** direction, t is time, $\mathfrak{R}$ is the rotational operator (defined as $\times \frac{\partial}{\partial \mathbf{u}}$), U_{scf} is the mean field nematic potential, U_e is the potential of an external field, and $\boldsymbol{\kappa}$ is the velocity gradient tensor.

For simplicity, Doi and Edwards suggest the use of an orientation independent average diffusivity ($\bar{D}_r$) defined as [128]:

$$\bar{D}_r \equiv D_r \left\{ \frac{4}{\pi} \iint \Psi(\mathbf{u})\Psi(\mathbf{u}')|\mathbf{u} \times \mathbf{u}'| du^2 du'^2 \right\}^{-2} \tag{2.5}$$

An orientation dependent rotary diffusivity gives nonlinearity to the Smoluchowski equation, and consequently, a difficult mathematical analysis. However, this simplification applies if the external perturbation is small.

Once Ψ is computed, the order parameter (**S**) and stress ($\boldsymbol{\sigma}$) tensor [128] could be obtained from the following equations:

$$\mathbf{S} \equiv \langle \mathbf{uu} - \frac{1}{3}\boldsymbol{\delta} \rangle \tag{2.6}$$

$$\boldsymbol{\sigma} = 3\nu k_B T \mathbf{S} + \nu \int \Psi \left(\frac{\partial}{\partial \mathbf{u}} U_{scf} \right) \mathbf{u} d^2 u + \nu \zeta_{str} \mathbf{D} : \langle \mathbf{uuuu} \rangle \tag{2.7}$$

where **δ** is a unit vector, $\langle ... \rangle$ denotes an average over the Ψ, **D** is the strain rate tensor, and ζ_{str} is the viscous drag coefficient, which is defined as [128]:

$$\zeta_{str} = \frac{k_B T}{2 D_{r0}} \tag{2.8}$$

The stress tensor is composed of the elastic terms, due to Brownian motion and the nematic potential of the molecules, and the viscous term, produced by the drag force of the solvent as it flows past the molecules.

2.6 Modified Two-Dimensional Approximation

Marrucci and Maffettone found explicit solutions for the orientational distribution function of nematic rod-like polymers in a shear flow using a two dimensional approach [137]. In this approximation, thin and rigid rod-like molecules were assumed to be oriented to the shear plane, and a parallel geometry is used in the analysis. They could predict negative normal stresses in a range of shear rates, characteristic of tumbling liquid crystalline polymers.

This two dimensional model was modified by Tse and Shine to describe the electrorheological effect of LCPs [138]. In this model, the LCPs molecules are assumed as rod-like molecules, with a permanent dipole along its length axis, and oriented parallel to the shear plane. A parallel geometry, constant shear rate ($\dot{\gamma}$) and uniform DC electric field (E), applied perpendicular to the flow direction, were assumed in the analysis. Figure 2.4 illustrates the modeled system and its coordinates.

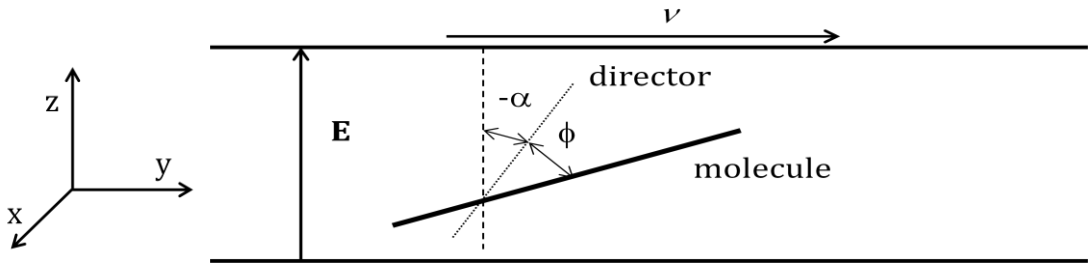

Figure 2.4: Modeled system with coordinates for the application of a constant electric field strength (E) and shear velocity (v).

The orientation of a molecule is given by the following equation:

$$\mathbf{u} = (-sin\theta, cos\theta)^T \tag{2.9}$$

where θ is the angle between a molecule and the electric field or z-axis. The angle θ is composed of:

$$\theta = \alpha + \phi \tag{2.10}$$

Where α represents the orientation of the director and ϕ is the angle between a molecule and the director. The angular velocity of the molecule is defined as,

$$\frac{d\theta}{dt} = -\dot{\gamma}\, cos^2\, \theta \tag{2.11}$$

The two dimensional Smoluchowski equation presented in its dimensionless form is:

$$\frac{\partial \Psi}{\partial \tau} = \frac{\partial}{\partial \phi}\left(\frac{\partial \Psi}{\partial \phi} + \Psi \frac{\partial\left(-U\left\langle \cos 2\phi \right\rangle \cos(2\phi) - E' \cos(\alpha + \phi)\right)}{\partial \phi} \right) + \frac{\partial}{\partial \phi}\left(\frac{\partial \alpha}{\partial \tau}\Psi + G \cos^2\left(\alpha + \phi\right) \right) \tag{2.12}$$

This equation governs the orientation distribution function (Ψ) of the studied system. In the derivation, D_r was assumed constant and the dipolar interactions between the molecules were neglected. A dimensionless time (τ) is defined as $t \times D_r$. The rheology

of the system is governed by three dimensionless groups: (1) the strength of the nematic potential (U), (2) the dimensionless shear rate (G), which is defined as shear rate divided by the rotational diffusivity, and (3) the dimensionless electric field strength (E') that is defined as: $\mu gE/k_BT$, where μ is the permanent dipole moment and g is the Onsager internal field factor. The Onsager internal field factor is defined as a function of the dielectric constant of the medium. It was estimated as 1.5 for concentrated solutions of PHIC, based on experimental data that shows that the electric field dependent dielectric constant is on the order of one hundred ($O(10^2)$) [139]. The value of the permanent dipole moment of polyisocyanates was reported as 1.13 D = 3.77E-30 C-m [140].

The steady-state solution of Ψ was obtained setting the time derivative equal to zero and integrating it analytically. Two boundary conditions are necessary to solve it, the periodicity of Ψ with 2π:

$$\Psi(0) = \Psi(2\pi) \tag{2.13}$$

and the normalization condition:

$$1 = \int_0^{2\pi} \Psi(\phi) d(\phi) \tag{2.14}$$

Finally, the α angle is needed so that the orientation distribution function can be completely defined. To solve both α and S, a fixed point iteration was developed. A 64-point Gaussian quadrature was used to carry out the numerical integrations. A complete description of the algorithm and computer code was detailed by Tse [141].

After a solution for the orientation distribution function is obtained, the stress tensor and, subsequently, the electroviscosity of the system can be calculated. The stress tensor is symmetric without the presence of an electric field. However, σ_{21}

determines the contribution to the shear rate in the presence of an electric field. In this case, 1 represents the flow direction and 2 the velocity gradient direction.

As was discussed previously, the stress tensor is composed of both elastic and viscous contributions. For small shear rates (less than 10 (1/s), the elastic contribution to the stress tensor dominates over the viscous one, so the elastic stress will be used to obtain the electroviscosity. The elastic contribution to the shear stress, for small deformations, is given as:

$$\frac{\sigma_{21}^{E}}{\nu k_B T} = -\sin 2\alpha \langle \cos 2\phi \rangle - \frac{1}{2} \mathrm{U} \langle \cos 2\phi \rangle \left\{ \sin 2\alpha \left(\langle \cos 4\phi \rangle - 1 \right) + \cos 2\alpha \langle \sin 4\phi \rangle \right\}$$
$$- \frac{1}{4} \mathrm{E}' \left(\sin \alpha \langle \cos \phi \rangle + \cos \alpha \langle \sin \phi \rangle + \sin 3\alpha \langle \cos 3\phi \rangle + \cos 3\alpha \langle \sin 3\phi \rangle \right) \qquad (2.15)$$

The superscript E refers to the elastic contribution. The electroviscosity is obtained as:

$$\eta^{E} = \frac{\sigma_{21}^{E}}{G D_r} \qquad (2.16)$$

The applicability of the model to describe the steady-state viscosity dependence on the shear rate and electric field strength of nematic PHIC/*p*-xylene solutions was demonstrated [82, 113, 134, 141]. Figure 2.5 and 2.6 shows the polymer concentration and molecular weight effect on the electrorheological behavior of PHIC/p-xylene solutions at constant temperature and shear rate. A quantitative agreement between the experimental and the model data was obtained, especially at low shear rates.

In conclusion, it has been demonstrated that the orientation of both nanotubes and some liquid crystalline phases may be changed with the application of an electric, magnetic, and/or flow field, and that a liquid crystalline phase may induce an alignment on the nanoparticles along the director direction. For this reason, we

propose that the self-organizing properties of a liquid crystalline polymer matrix and its inherent processing flexibility to orient cylindrical particles to develop novel materials with better and more controlled orientations. Moreover, these properties and the electric polarizability of carbon nanotubes may be combined with an electric and flow field to develop nanocomposites with a controlled orientation.

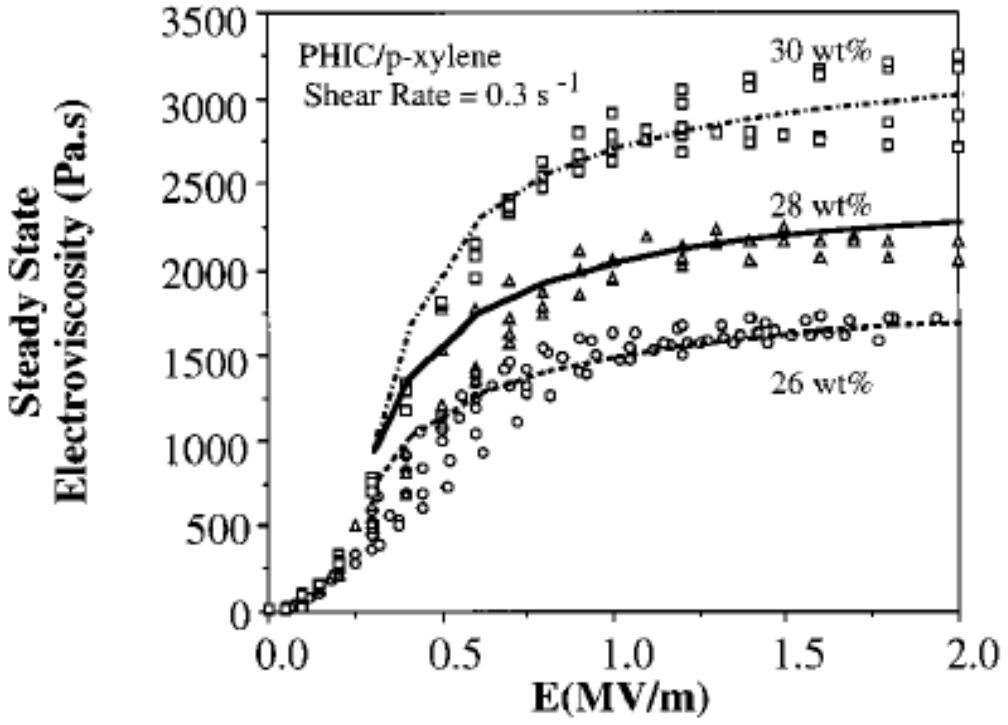

Figure 2.5: Polymer concentration effect on the steady-state electroviscosity of PHIC/*p*-xylene solution at 0.3 (1/s) and room temperature. Symbols and lines represent the experimental and the modeled data, respectively. Reproduced from Tse 2000 [113].

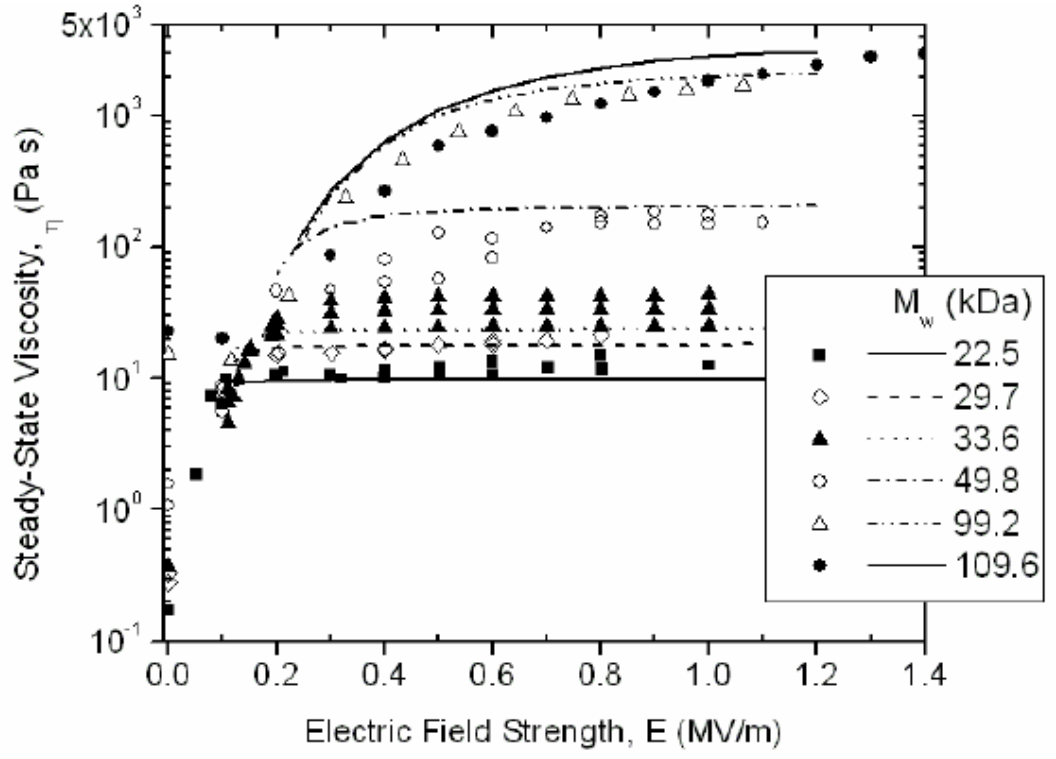

Figure 2.6: Molecular weight dependence on the steady-state electroviscosity of PHIC/*p*-xylene solutions at 1 (1/s) and a concentration 1.25 times the concentration in which the isotropic becomes unstable. Symbols and lines represent the experimental and the modeled data, respectively. Reproduced from Acevedo 2005 [134].

Chapter 3

OBJECTIVES

3.1 Main Objective

Determine the structural and rheological changes with the addition of rod-like nanoparticles to a liquid crystalline polymer solution

3.2 Specific Objectives

Determine the effect of nanoparticle loading on the phase behavior of a LCP solution.

Determine the dependence of nanoparticle loading on the viscoelastic properties of a LCP matrix.

Determine the effect of nanoparticle loading on the steady-state rheology of both an isotropic and a liquid crystalline polymer solution.

Determine the dependence of nanoparticle loading on the electrorheological (ER) effect on a non-electrorheological and an electrorheological matrix.

Chapter 4

EXPERIMENTAL: MATERIALS AND METHODOLOGY

4.1 Introduction

A system composed of hydroxypropylcellulose loaded with multiwalled carbon nanotubes (MWCNTs) and halloysite nanoclays (HNCs) was used first. This system is relevant as a nanocomposite from natural resources (i.e. a cellulose derivative). Additionally, poly(*n*-hexyl isocyanate) was used as a synthetic electrorheological polymer matrix. In this section the materials, characterization techniques, and equipment used in our research are discussed in detail.

4.2 Particles

Rod-like nanoparticles such as multiwalled carbon nanotubes and halloysite nanoclays were used as the dispersed phase. Functionalized MWCNTs were also used to improve the dispersion of the nanoparticles in the LC matrix.

4.2.1 Multiwalled Carbon Nanotubes

Carbon nanotubes are anisotropic and light materials with a high aspect ratio, excellent mechanical, thermal, and electrical properties. These particles can form nematic liquid crystal phase with concentration changes [122-126]. The CNTs can be electrically polarized, have the ability to be charged, and have considerable potential as solid state actuators with mechanical response to applied electric fields. MWCNTs

are the most common CNTs used in the material industry due to their lower production costs compared with single-walled CNTs.

CNTs are typically incorporated in a polymer matrix to improve their structural, electric, and mechanical properties. The principal advantage is that significant changes in these properties can be obtained at a low loading percentage [1, 10]. Nevertheless, the principal challenge of CNTs is obtaining a uniform dispersion since van der Waals attractions between rods cause their aggregation and clustering [142]. A way of improve the dispersion of the nanoparticles is changing their surface functionalization.

Raw MWCNTs (Lot #: 04619DC) with an outer diameter between 20 and 30 nm and a length between 0.5 and 2 μm were obtained from Sigma-Aldrich. Well-dispersed solutions were obtained using *m*-cresol as a solvent. In addition, carboxylated MWCNTs (c-MWCNTs) with a diameter less than 8nm and length between 10 and 30μm were obtained from Cheap Tubes. A 30wt% acetic acid (AA) aqueous solution was chosen as the adequate solvent to obtain a good macro-dispersion of CNTs for concentrations up to 1 wt%. Isocyanate MWCNTs (i-MWCNTs) were also obtained using the commercial c-MWCNTs, following the procedure detailed by Zhao to improve the dispersion in *p*-xylene solutions [143].

The synthesis procedure consisted in mixing 1g of c-MWCNTs in 100mL of anhydrous acetone using a magnetic stirrer, and then adding 2.5g of toluene 2,4-diisocyanate to the solution. The functionalization was undertaken at 50°C and in a nitrogen atmosphere for 24 hours. The nanotubes were filtered and re-dispersed in dry acetone to remove residuals. Then, the CNTs were dried at 50°C. The nanoparticles

were characterized using thermogravimetric analysis and Fourier transform infrared spectroscopy before and after the functionalization.

4.2.1.1 Thermogravimetric Analysis and Fourier Transform Infrared Spectroscopy

The presence of the functional groups of interest was confirmed by Fourier transform infrared spectroscopy (FTIR), and the organic content attached to the nanoparticles was estimated by thermogravimetric analysis (TGA). Those experiments were done simultaneously in a TGA coupled with a FTIR. TGA-FTIR experiments were performed in a TA Instruments TGA 2950 coupled with a Thermo Scientific Nicolet FT-IR 6700 under an air atmosphere at a 10 ºC/min temperature ramp from 20 to 900 ºC.

Figure 4.1 shows the TGA curves corresponding to the functionalized MWCNTs with carboxylic or isocyanate groups. Both nanoparticles have a water content of 3.4 ± 0.1 wt%. The organic content of the c-MWCNTs was about 3.8 wt%, consistently with the COOH content (3.86 wt%) reported by the manufacturers. In the case of i-MWCNTs, there was a first organic weight loss of 6.8wt% at ~ 271°C and other one of 8.5 wt% before the decomposition of the nanotubes begins. Zhao and coworkers demonstrated that toluene 2,4-diisocyanate react stochiometrically (1:1) with the carboxylic groups. In our reaction the total organic content was 0.0008 and 0.0009 mol/g for the c-MWCNTs and i-MWCNTs, respectively.

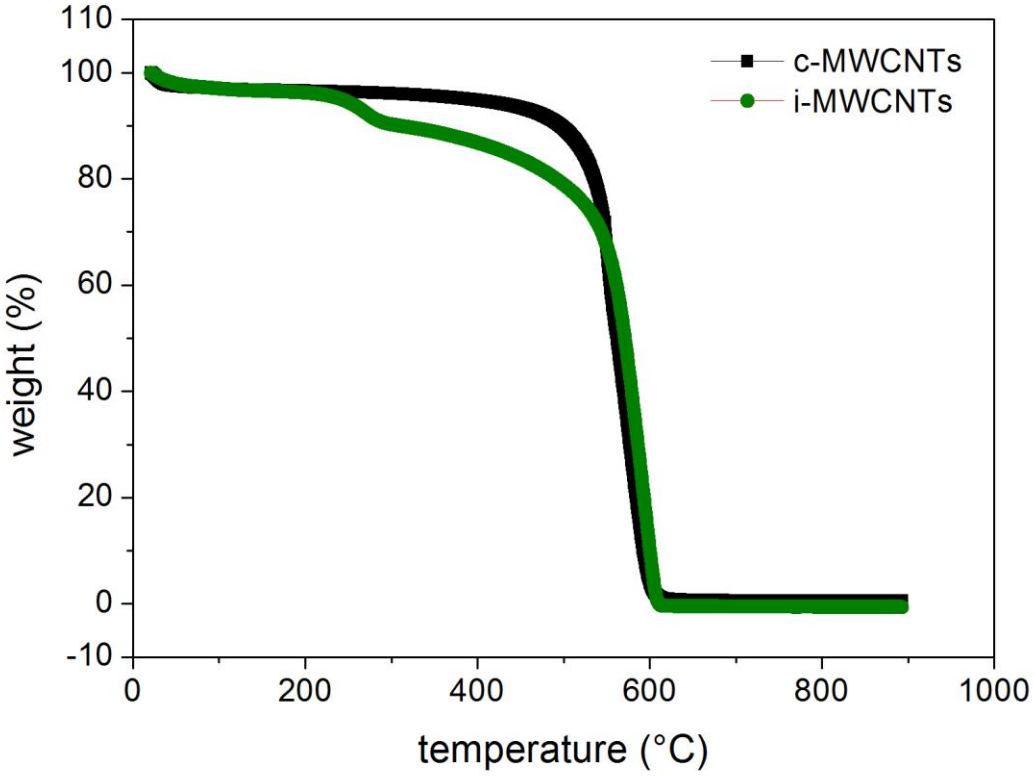

Figure 4.1: TGA curves for the functionalized MWCNTs, c-MWCNTs (black line) and i-MWCNTs (green line).

FTIR is a useful tool to identify the functional groups responsible for each weight loss. As Figure 4.2 shows, the FTIR spectra have characteristic peaks of carboxylic and CO_2 stretching at 1700, 2300, 3700 cm^{-1}, for temperatures between 150 and 450°C. Peaks characteristic of the nanotube structure decomposition at 750 and 3750 cm^{-1} appear at higher temperatures. On the other hand, the peaks corresponding to an ortho-disubstituted ring, NH, N=O, C=O and/or C=N, N=C=O, and N-H stretching appear at 750, 1400, 1600, 1700, 2300, and 3500, respectively for temperatures between 150 and 500°C, as Figure 4.3 shows. This demonstrates that the isocyanate functionalization was successfully done.

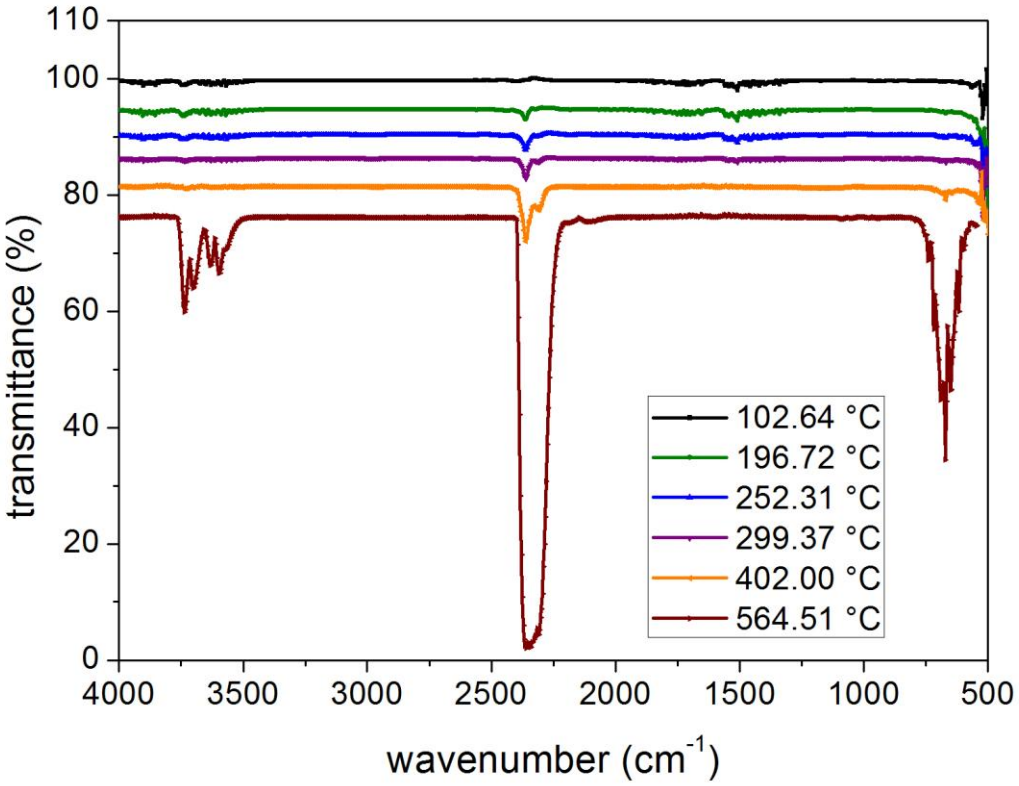

Figure 4.2: FTIR curves for the c-MWCNTs at different temperatures.

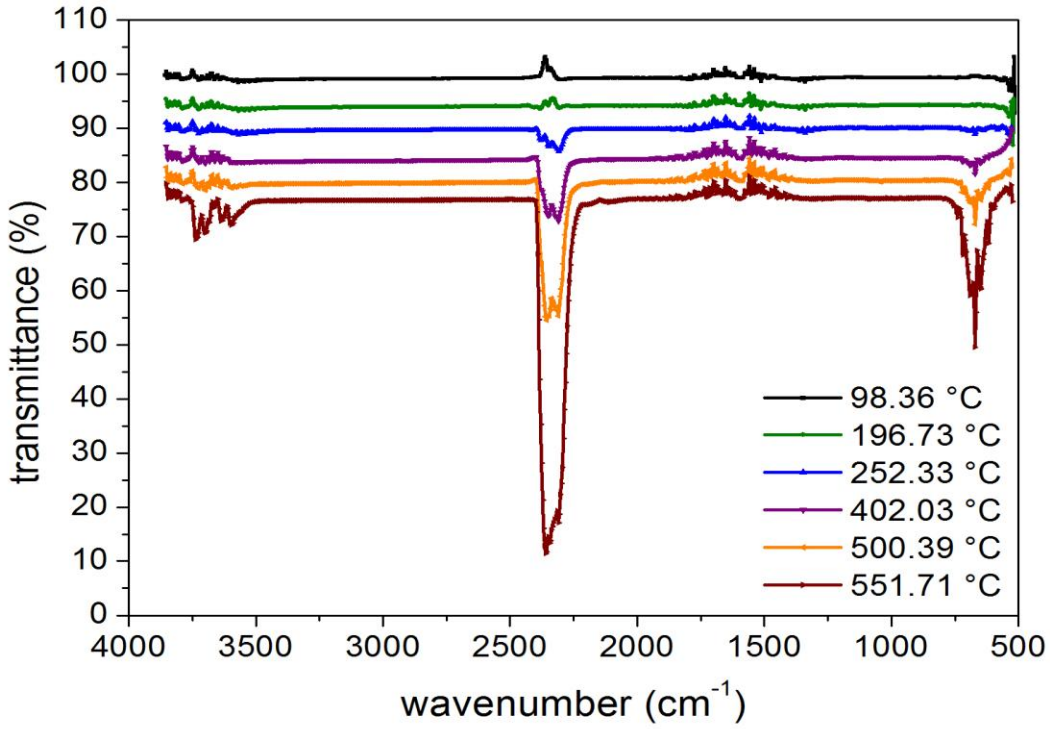

Figure 4.3: FTIR spectra for the i-MWCNTs at different temperatures.

4.2.2 Halloysite Nanoclays

Halloysite nanoclay is a layer silicate clay mineral with a nanotubular structure. Its inner and outer layer is mainly composed of Al-OH and Si-O groups, respectively. It is well known that at pH between 2-12, the HNCs were negatively charged due to the outer surface groups with a little contribution from the inner ones [144-146]. The main application of those nanoparticles is the development of high quality ceramics [147]. However, their biocompatibility [145, 146], their ability to improve the mechanical properties of the main matrix [146, 148], and their applicability in biomedical applications such as controlled drug release [149] and biomimetic nanoreactor [150] have been demonstrated.

FTIR measurements suggest interaction between the amino and hydroxyl groups of the chitosan molecules and the Si-O bonds of the HNCs via electrostatic attractive interactions and hydrogen bonding in dilute aqueous acetic solutions [146]. Consequently, the polymer molecules wrap the nanotube as demonstrated by zeta potential results. This report also demonstrated that HNCs could be effectively dispersed in acetic acid aqueous solutions. So, it could be considered as an alternative nanoparticle, which could be well-dispersed in hydroxypropylcellulose/acetic acid aqueous solutions.

HNCs with a diameter and length of 30-70nm and 1-3μm were obtained through Sigma-Aldrich (Batch #: 09514DJ). A 30 wt% acetic acid aqueous solution was chosen as the solvent.

4.3 Polymers

Hydroxypropylcellulose and poly (n-hexyl isocyanate) were chosen as the model polymer matrices. The first one is a relevant material in biological applications and the other polymer in electrorheological ones. In this section the general characteristics of each polymer are described, and some relevant aspects such as liquid crystalline behavior and the molecular weight distribution corresponding to the sample used in future analyses.

4.3.1 Hydroxypropylcellulose

HPC is a biopolymer used as an ophthalmic protectant, lubricant, and binder in the pharmaceutical industry, and a thickener in the food area. This polymer is a cheaper non-electrorheological matrix. Furthermore, it is commercially available from Sigma Aldrich (Batch #: 17009PD). It is soluble in water and other organic solvents.

In addition, it is capable of forming an anisotropic liquid crystal with changes in concentration or temperature. The molecular weight distribution and liquid crystalline behavior of HPC in *m*-cresol and in acetic acid aqueous solutions will be discussed in the next sections. *M*-cresol was chosen as the solvent for the electrorheological characterization.

4.3.1.1 Liquid Crystalline Behavior

Liquid crystalline behavior was observed using an Olympus BX 51 polarized optical microscope coupled with a Canon EOS Rebel Tli Camera. Solutions were prepared in 5 wt% increments to identify the range of the phase transitions. Then, smaller increments were used to determine the phase transition with a precision of ±1 wt%. A drop of the solution was sandwiched between a microscope slide and a glass cover, and then observed in the microscope. Different solvents were used depending on the nanoparticles or experimental conditions.

Navard and Fried with their respective coworkers demonstrated that HPC solutions in pure acetic acid exhibit a I-N transition and a fully LC phase at a polymer concentration around 30 and 35 wt%, respectively [41, 151]. When aqueous AA solutions were used as solvents, the concentration at which a fully LC phase is obtained moves up to a maximum concentration of 47 wt%, which represents the transition that corresponds to pure water solutions [151]. The phase behavior of HPC solutions in a solution of 30wt% AA was determined (Figure 4.4).

Isotropic solutions (solutions below 30 wt%) do not transmit light due the random orientation of the molecules. However, at a concentration of 30 wt%, nematic regions dispersed in an isotropic matrix were observed, so this concentration was taken as the isotropic-to-nematic transition concentration. The concentration at which

a fully liquid crystalline solution was obtained is 43 wt%. A concentration of 20 and 50 wt% was chosen for future characterizations of the nanoparticle loading effect on an isotropic or LC phase, respectively.

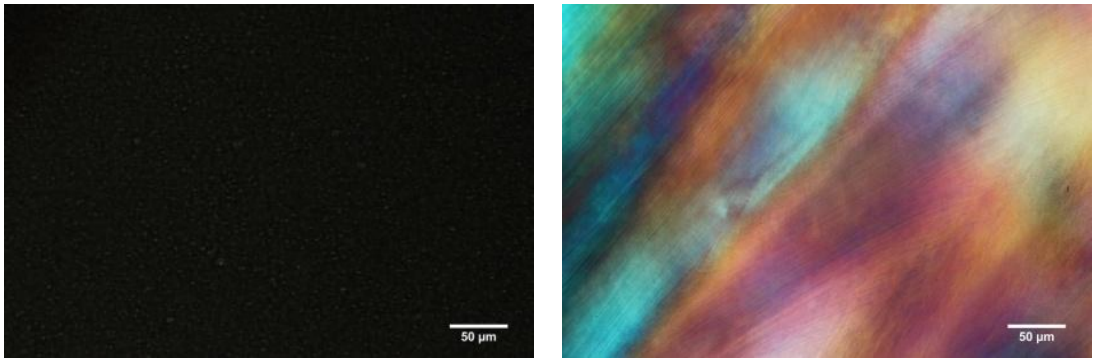

Figure 4.4 Textures of 30 (left) and 43 (right) wt% of HPC/acid aqueous solutions demonstrating a biphasic phase which contains a LC droplets dispersed in an isotropic phase (left) and a fully LC phase (right)

It have been demonstrated that HPC/*m*-cresol solutions exhibit a liquid crystalline phase at polymer concentrations higher than 30wt% [152]. Based on this, a concentration of 45 wt%, a fully liquid crystalline solution, was chosen as the main matrix for future experiments. To corroborate it, the phase behavior of a 45 wt% HPC/*m*-cresol solution was obtained (Figure 4.5).

Figure 4.5 Liquid crystalline texture of a 45 wt% HPC/*m*-cresol solution at room temperature

4.3.1.2 Molecular Weight Distribution

The molecular weight distribution was determined in a gel permeation chromatography (GPC) system equipped with a PLgel 5µm MIXED-C column, a Brookhaven Instruments differential refractometer (BiDNDC), and a Brookhaven Instruments molecular weight analyzer (BI-MwA). Tetrahydrofuran (THF) was used as the carrier solvent at a flow rate of 0.5 mL/min.

A polymer concentration of approximate 10g/L in THF was prepared for the GPC experiments. The number average (M_n), weight average (M_w) and z-average (M_z) molecular weights of the HPC were 78.23, 87.48, and 97.51 kDa, respectively. Figure 4.6 shows the molecular weight distribution of the HPC that was studied.

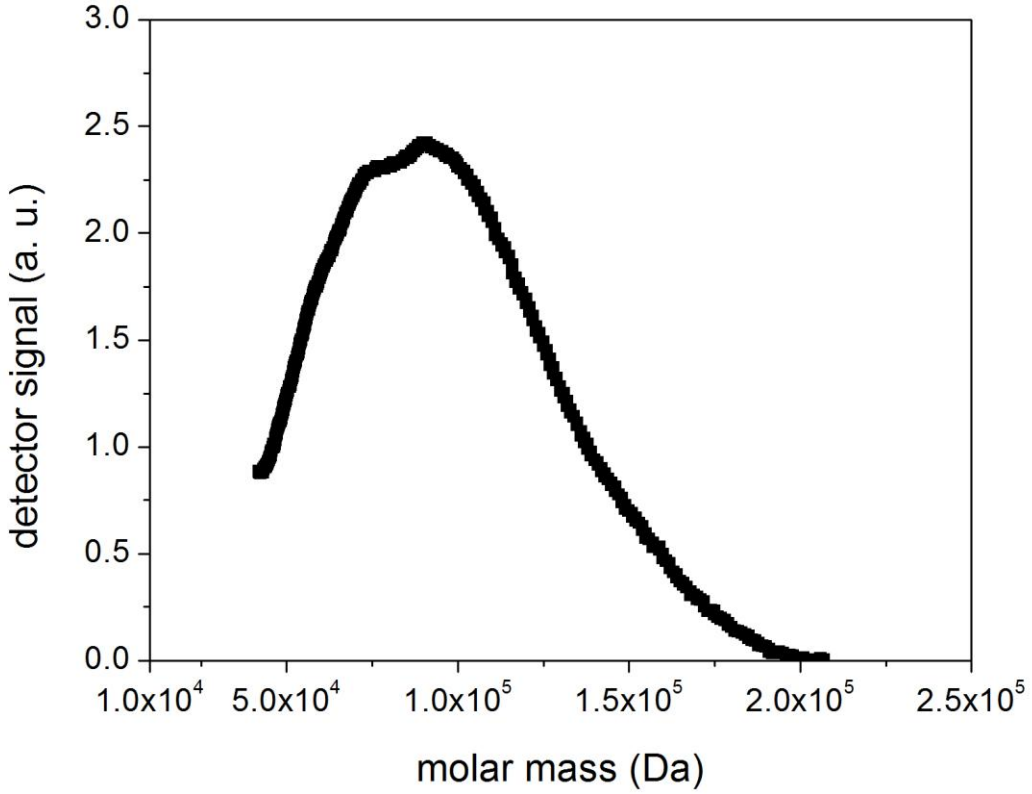

Figure 4.6. Molecular weight distribution of HPC (Batch #: 17009PD).

4.3.2 Poly(n-hexyl isocyanate)

Poly(n-hexyl isocyanate) is an helical synthetic polymer and an electrorheological matrix with a positive ER effect due to its large permanent moment along the helix axis, as has been demonstrated experimentally [113, 134, 140]. This lyotropic polymer is available commercially by Polysciences, Inc (Batch #: 603274). Its nematic state is stable and accessible in organic solvents such as p-xylene [113, 134], toluene [153, 154], and dichloromethane [154]. This chiral polymer does not show optical activity because it is a racemic mixture, that is, it contains equal quantities of left and right handed helices.

4.3.2.1 Liquid Crystalline Behavior

The liquid crystalline behavior was obtained using the same equipment and procedure detailed in the Section 4.3.1.1. The phase transition concentrations were determined, with a precision of 0.5 wt% (Figures 4.7 and 4.8).

Isotropic solutions (concentrations below 22.5 wt%) do not transmit light due the random orientation of the molecules. However, at a concentration of 22.5 wt% nematic regions dispersed in an isotropic matrix were observed, so this concentration was taken as the isotropic-to-nematic transition concentration. A fully nematic solution was obtained at concentration equal to and higher than 31 wt%. A concentration of 10 and 34 wt% was chosen to characterize the nanoparticle effect on an isotropic and LC solution of PHIC, respectively.

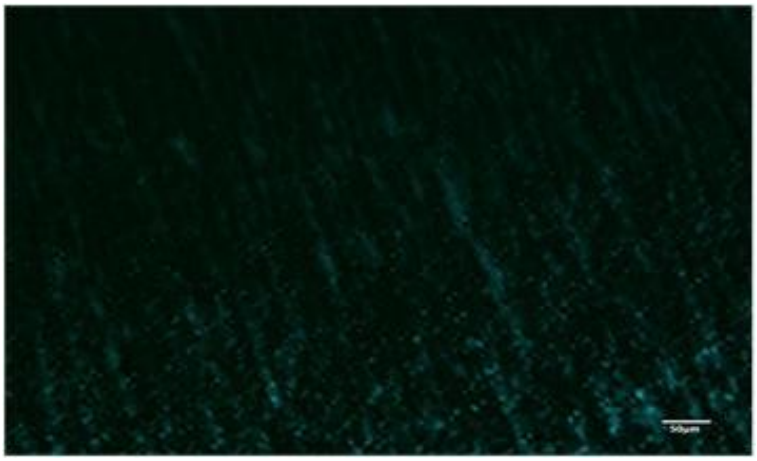

Figure 4.7 Texture of PHIC/p-xylene solution at the isotropic to nematic transition concentration (22.5 wt%) and room temperature.

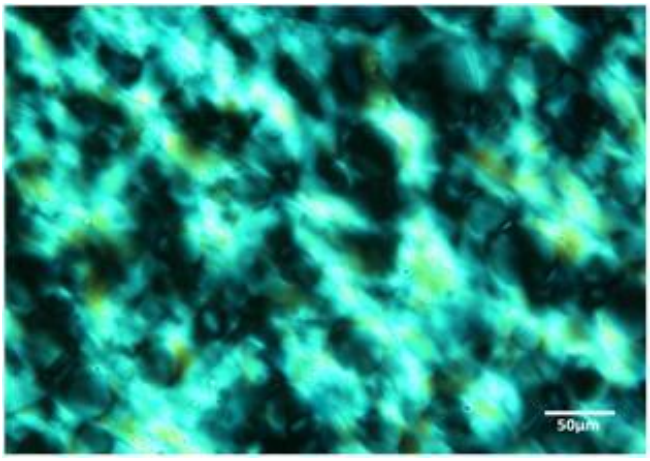

Figure 4.8 Texture of 31.0 wt% PHIC/p-xylene solution, the concentration at which a fully liquid crystalline was first observed, at room temperature.

4.3.2.2 Molecular Weight Distribution

The number average, weight average and z-average molecular weights of the PHIC were 28.74, 79.42, and 184.6 kDa, respectively. Figure 4.9 illustrates the molecular weight distribution of PHIC. The details of equipment and experimental conditions are provided in the Section 4.3.1.2.

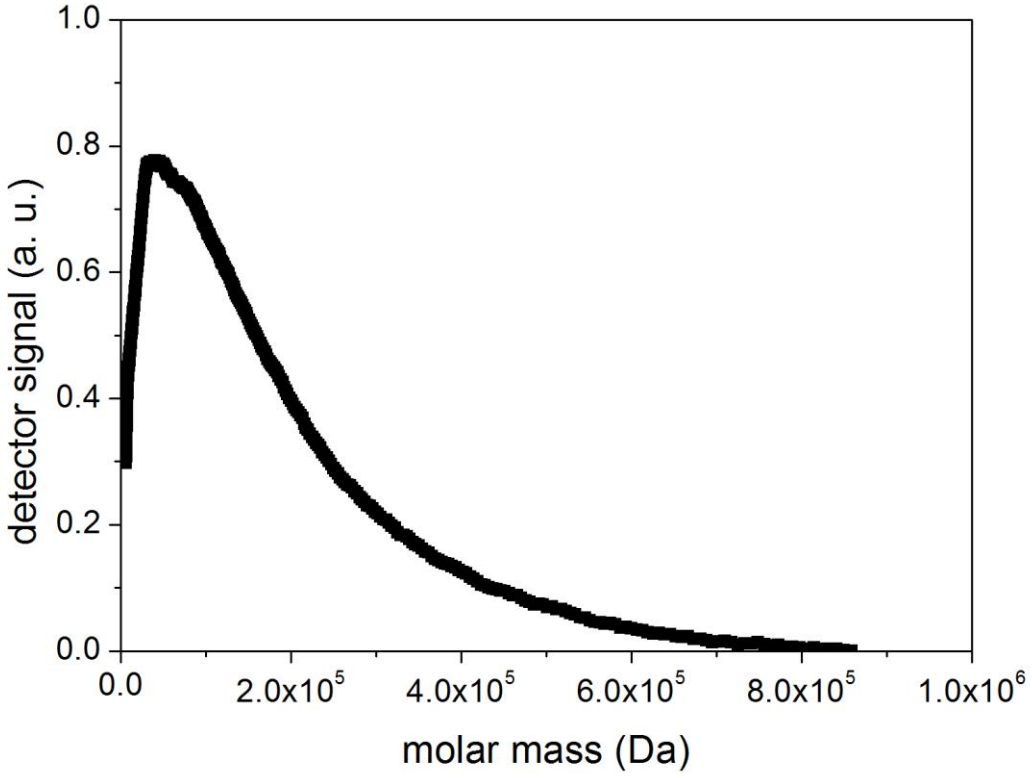

Figure 4.9: Molecular weight distribution of PHIC (Batch #: 603274).

4.4 Solution Preparation

The general procedure to prepare the solutions was firstly dispersing the nanoparticles in the chosen solvent by ultrasonification using a high or low power sonicator. The dispersion method and time were evaluated determining the stability of the nanoparticles in the solvent. Then, the polymer was added and mixed with the dispersed solution, and left standing with occasional mixing up until a uniform mixture is obtained. Finally, the solutions were centrifuged. The dispersion of the solutions was determined by optical microscopy.

Different dispersion methods were tried to optimize the dispersion of the suspensions. The MWCNTs, c-MWCNTs, i-MWCNTs, and HNCs were dispersed

using a microtip probe for ten minutes, a bath sonicator for two hours, the cup horn probe for thirty minutes or one hour, and a bath sonicator for two or three hours, respectively. Cold water was used in both the bath and cup horn to prevent solvent loss during the dispersion process. In addition, a step pulse was used, on for fifty seconds and off for twenty five seconds, when the high power sonicator was used to minimize the heating of the sample.

For PHIC/*p*-xylene solution, the polymer was dried in a vacuum oven at 50°C overnight. The solvent was treated with molecular sieves 4A (Lot #: 05325BV), obtained from Sigma Aldrich, for at least one week before using it. When transferring the solvent to the solution, a syringe fitted with a 0.2µm Nylon filter was used to discard any possible contamination from the sieve particles. Neat polymer solutions were recovered, and purified after the rheological characterization.

The recovery procedure consists of dissolving the PHIC in toluene, and filtering by gravity through a folded funnel filter paper into methanol, where the polymer precipitates. The polymer was filtered and recovered using filter paper with a pore size less than 3µm. Finally, the polymer was dried in vacuum at 50°C overnight.

Some samples prepared using the recovered polymer were prepared in an excess of the solvent. The solutions were left standing with occasional mixing up until a uniform mixture is obtained. Finally, the excess of solvent was removed by evaporation.

4.5 Rheological Characterization

Liquid crystalline polymer has intrinsic rheological properties. In this section the rheological tests and the equipment used to identify these properties will be specified.

4.5.1 Rheometer

Two rheometers were used in the analysis, a Reologica StressTech HR and an Anton Paar MCR 302. The Reologica was used for the electrorheological tests and for the main characterization of c-MWCNTs/aqueous acid solutions.

4.5.1.1 Reologica StressTech HR

A stress-controlled rheometer, Reologica StressTech HR (*ATS RheoSystems*, Bordentown, NJ), will be used to determine the rheological properties of the chosen systems. Parallel plate (upper diameter = 25 mm) geometry was used, at a constant temperature of 25 °C.

The Reologica StressTech HR rheometer coupled with an electrorhelogical cell equipped with a Trek high voltage power supply was used to perform the ER characterization. Parallel plates (d = 25 mm) geometry was used to obtain a uniform electric field, up to a maximum of 3 kV/mm. The power supply has the ability to supply a voltage between 0 up to ± 10 kV. For PHIC/*p*-xylene solutions, the electrorheological characterization was done at constant temperature. Furthermore, a solvent trap with cotton pads was used to retard the solvent evaporation. The humidity of the pads was monitored between the runs.

The operational conditions of the ER cell such as maximum electric field strength and gap between the parallel plates was determined for a constant temperature (25°C) using a viscosity standard (Standard S30000; Lot No. 05101) with a viscosity of 70.4 Pa-s at 25°C. It is a Newtonian fluid, whose viscosity does not depend on the electric field strength, shear rate, or of the gaps used. A gap of 0.5, 0.8 and 1mm and electric field strengths up to 4MV/m were chosen. The data points showed on Figure 4.10 are the average viscosity of a shear rate ramp from 1 to 100 (s^{-1}) at room

temperature. The maximum operational electric field strength was 3 MV/m, since at higher values significant electric arcing was observed. No significant effect on the viscosity was observed at the chosen gaps. However, a gap of 0.8mm was chosen for the further analysis.

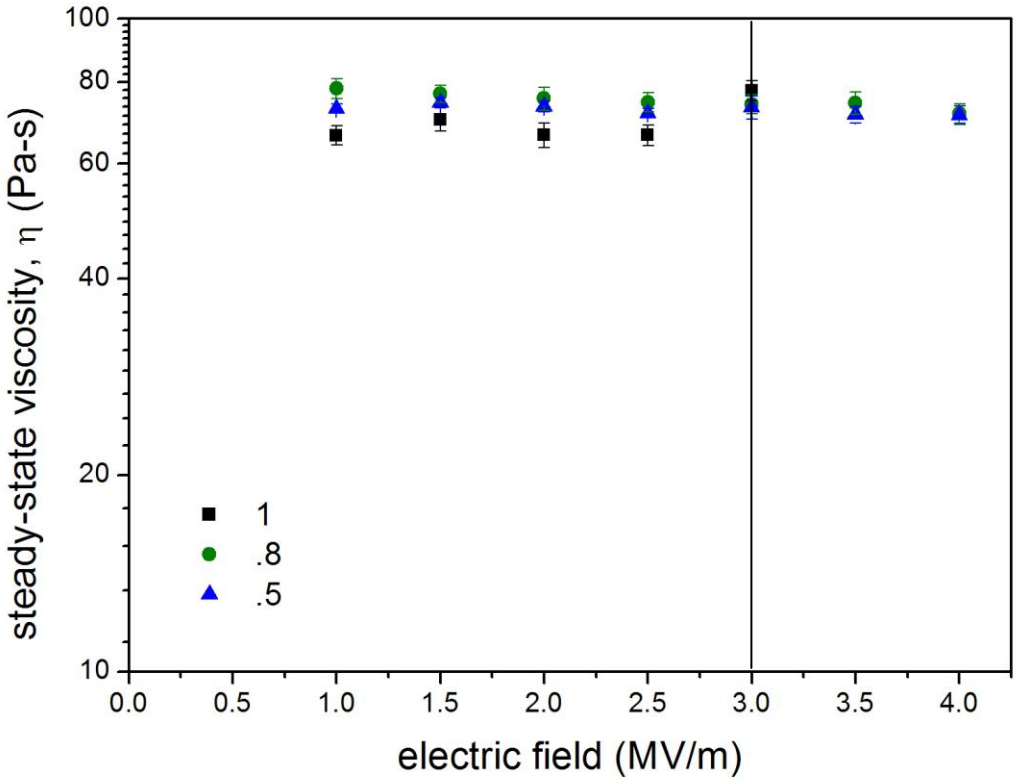

Figure 4.10: Electric field and gap effect on the steady-state viscosity of a viscosity standard (S30000; 70.4 Pa-s at 25°C) at room temperature (the line represent the maximum operational electric field strength, at higher values a significant arcing was observed)

4.5.1.2 Anton Paar

An Anton Paar MCR 302, strain controlled rheometer, was used to determine the rheological properties of the solutions. A parallel geometry was also used (d = 25mm).

For PHIC/*p*-xylene solutions, the rheological characterization was done at constant temperature. Furthermore, a solvent trap with cotton pads was used to retard the solvent evaporation. The humidity of the pads was monitored between the runs.

4.5.2 Rheological Tests

Both transient and dynamic experiments were performed at a constant temperature to determine the particle loading effect on the characteristic rheological properties of the polymer matrix due to possible microstructural interference.

A transient experiment was performed to see the evolution of viscosity while a constant shear rate was applied until a steady-state was reached. For flow-aligned lyotropic LCPs, a local maximum stress, or viscosity was observed at a critical strain unit and then decayed, in some cases showing a local minimum, before finally reaching a steady value. This is related to textural changes due to a disruption of a polydomain structure with the flow [155, 156]. On the other hand, measurements of the steady-state viscosity at a shear rate range (0.1 – 100 s^{-1}) at different particle loading was done to determine their effect on the viscosity, if any. The zero-shear viscosity (η_0) was extrapolated fitting a linear regression to the Newtonian or shear thinning regime obtained at low shear rates, depending on the polymer concentration used. This viscosity was used to obtain the phase transitions by rheological methods, by plotting η_0 vs. polymer concentration for each nanoparticle at the chosen concentrations.

Furthermore, transient experiments were a useful tool to characterize the ER effect of both the neat and loaded polymer matrix. In these experiments, the viscosity of the samples is measured as a function of time at constant shear rate and electric field strength until a steady-state viscosity is reached. The applied voltage was turned on manually at time zero. The steady-state viscosity was calculated by an average of the values taken for the last sixty seconds.

Dynamic experiments were also done to study microstructure change in the composites. These tests are useful to determine if there is some effect of the particle loading on the structural rearrangements within the LCPs. First, the viscoelastic moduli were measured as a function of strain (from 1E-2 to 10%) at constant frequency equal to 0.1, 1, and 10Hz to determine the linear viscoelastic regime. In this region, the viscoelastic moduli are independent of the strain applied, which facilitates its study and modeling. Then, the moduli were measured as a function of the frequency (from 0.1 up to 100Hz) at constant strain and temperature, working always in the linear viscoelastic region. The strain used is small such that it does not disturb the structure of the system, and the stress is controlled by the rates of relaxation present in the matrix. The same procedure was used in the ER characterization always working at constant electric field strength. The applied voltage was turned on manually at time zero, when an electric field was used.

4.6 Polarized Optical Microscopy: Electric Field Effect

The effect of an electric field on the phase behavior of quiescent samples was assessed by polarized optical microscopy using an Olympus BX51 microscope. A custom built glass slide set-up, shown in Figure 4.11, was used. In this configuration, a sample was placed between two square thin copper plates connected to a TreK 610E

high voltage power supply. The applied electric field is perpendicular to the observation axis and its strength corresponds to the voltage divided by the plate separation. Texture plates were recorded as a function of the effect of field strength (up to 0.50 MV/m) and exposure time (up to 5 min) was evaluated. At higher electric fields attraction between the microscope objective and the copper electrodes prevented observations. The drawn current through the sample was directly measured on the power supply as a function of time.

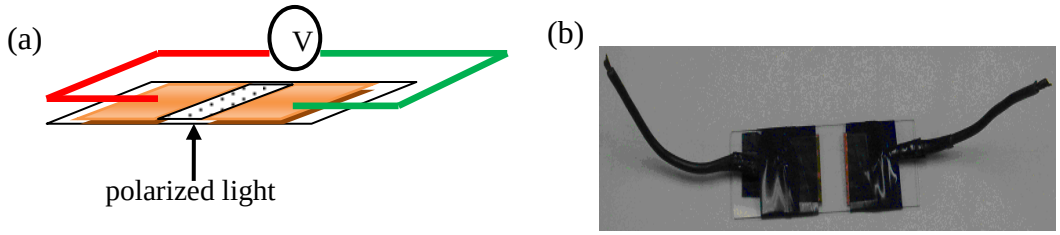

4.11 Custom-built POM slides – (a) schematic diagram and (b) actual set-up

4.7 ζ- Potential Characterization

Dilute solutions of hydroxypropycellulose (HPC), c-MWCNTs, HNCs were prepared using 30 wt% acetic acid aqueous solutions as a solvent. Also, c-MWCNTs-HPC and HNCs-HPC solutions were prepared at polymer:nanoparticle weight ratio equal to 1:1, 5:1 and 25:1, using a constant nanoparticle concentration of 0.1mg/mL. The ζ-potential characterization was done using a Brookhaven 90Plus instrument.

Chapter 5

EXPERIMENTAL RESULTS: RHEOLOGY

5.1 Introduction

In this section the rod-like nanoparticle loading effect on the phase behavior, viscoelastic properties, and steady-state viscosity of LCP solutions will be discussed. Furthermore, the loading effect on the steady-state viscosity and viscoelastic properties of isotropic solutions will also be determined.

5.2 Phase Behavior

The polymer concentration effect on the steady-state viscosity of HPC/AA aqueous and PHIC/*p*-xylene solutions at constant temperature will be discussed in this section. Also, the loading effect on the phase behavior of liquid crystalline solutions will be determined by rheological and optical measurements. Two types of nanoparticles were chosen, MWCNTs (with a surface chemically modified) and HNCs.

5.2.1 Polymer Concentration Effect on the Steady-State Viscosity

The polymer concentration effect on the steady-state viscosity and the nanoparticle loading effect on the phase behavior of HPC/AA aqueous and PHIC/*p*-xylene solutions at constant temperature will be discussed in the next sections.

5.2.1.1 Hydroxypropylcellulose/Acetic Acid Aqueous Solutions

The polymer concentration effect on the steady-state viscosity of neat HPC/AA solutions was obtained at 25 °C (Figure 5.1). A Newtonian plateau followed by a shear thinning region was obtained for both isotropic and biphasic solutions (filled and partially filled symbols, respectively). However, for fully liquid crystal solutions (empty symbols) a three region curve, characteristic of HPC solutions, was obtained. Similar curves were obtained for loaded HPC/AA solutions under the experimental window.

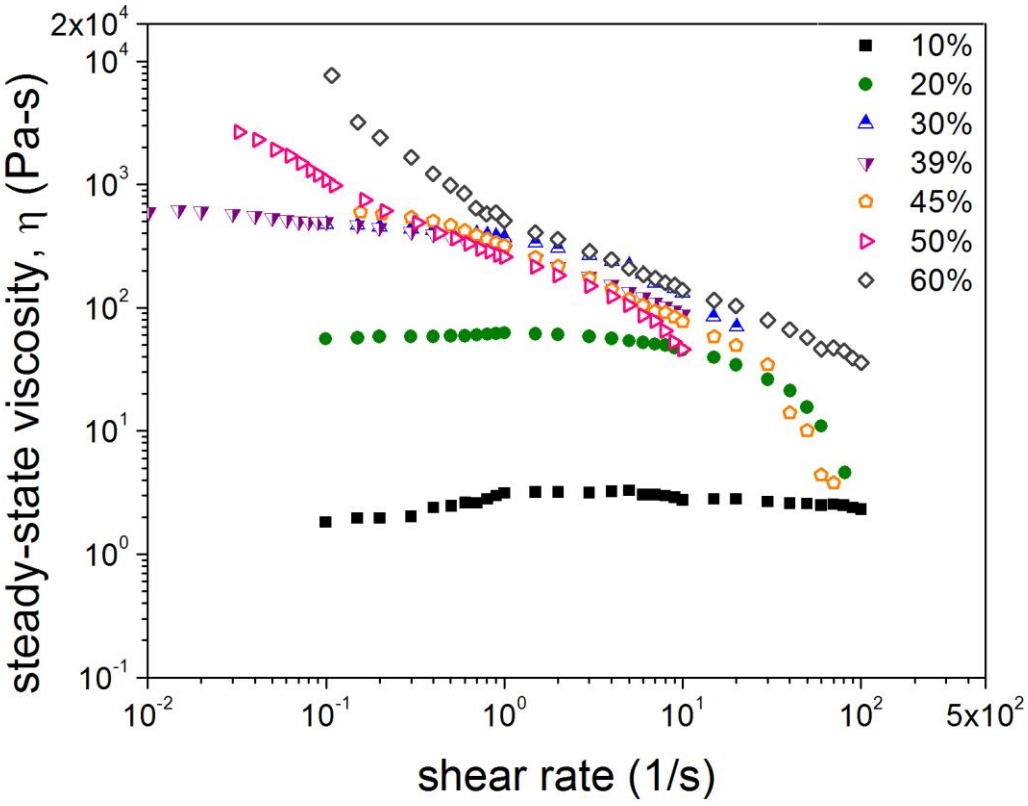

Figure 5.1 Polymer concentration effect on the flow curves of neat HPC/AA aqueous solutions at 25 °C. Full, partially filled, or empty symbols represent isotropic, biphasic, or fully liquid crystalline solutions, respectively.

These viscosity measurements can be used to determine the phase behavior of lyotropic liquid crystalline polymers due to the characteristic behavior of the steady-state viscosity as a function of polymer concentration curve, as discussed previously on the background chapter. Figure 5.2 shows the polymer concentration effect on the zero-shear viscosity of 0 - 0.45 wt% c-MWCNT loaded HPC solutions at 25 °C. The phase transition were identified by vertical lines, which separate the isotropic (I) phase, the biphasic phase (II), and the fully liquid crystalline phase (III). Two important features could be noticed on the plots: (1) phase transitions are unaffected (c_{IN} ~ 35 wt% and c_N ~55 wt%) up to loadings equal to 0.05wt%, while the c_{IN} and c_N was obtained at a slightly higher (~36 wt%) and lower (~52 wt%) concentration, respectively for higher NP concentrations, and (2) there are no significant changes in the viscosity in the isotropic and biphasic zones, whereas there is an increase in the nematic zone (at a polymer concentration of 60 wt%) for 0.05 wt% of c-MWCNTs. The phase transitions where verified by polarized optical microscopy, and discussed in a subsequent section. In general, for this system the phase transitions were not significantly affected with particle loading up to 0.45wt%.

On the other hand, the polymer concentration effect on the zero-shear viscosity of HNC loaded HPC/AA aqueous solutions is show in the Figure 5.3. Similarly to the c-MWCNT system, the c_{IN} transition was not affected with particle loading up to 5wt%. However, the c_N is obtained at a lower concentration (45 wt%), which represent a decrease of 18% compared to the neat polymer solution. For 10 wt% of HNCs, both c_{IN} and c_N transitions were observed at 30 and 42.5 wt%, a decrease of 14 and 23%, respectively. A narrower biphasic gap than for the neat polymer solution was obtained

with particle inclusion. However, a broader biphasic gap was obtained for the higher particle concentration than for lower ones.

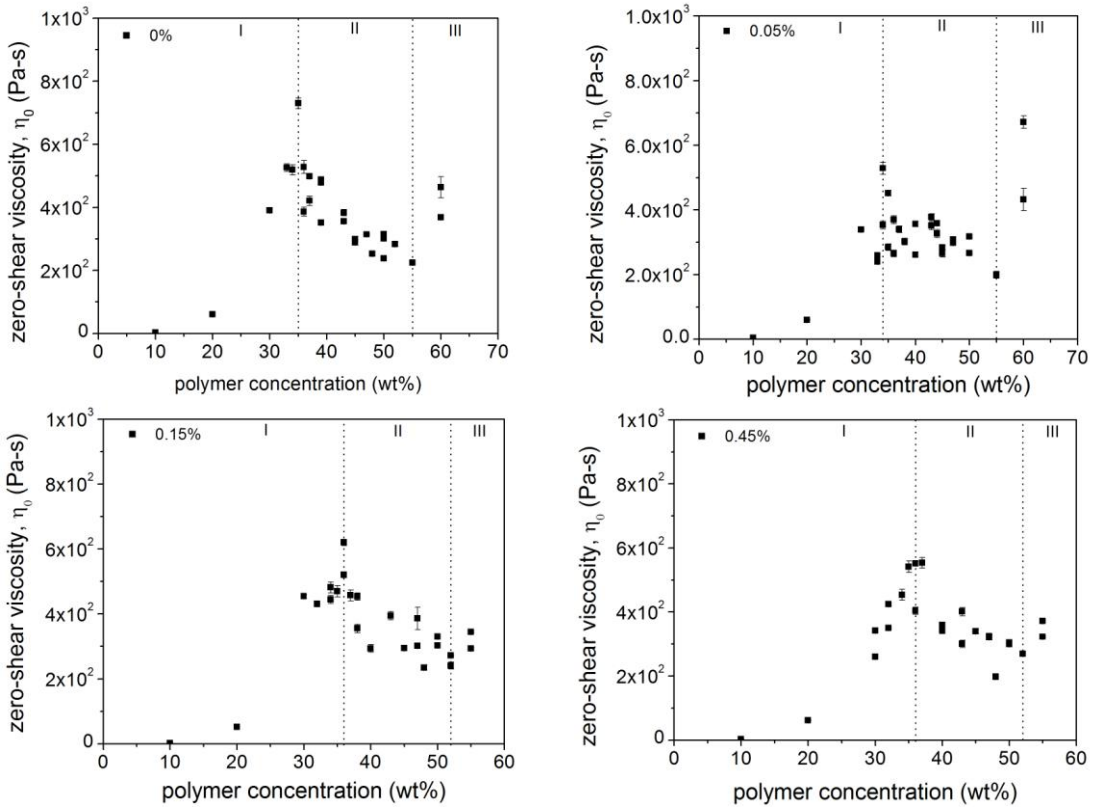

Figure 5.2 Polymer concentration effect on the zero-shear viscosity of 0, 0.05, 0.15, and 0.45 wt% c-MWCNT loaded hydroxypropylcellulose at constant 25 °C. I, II, and III represent the isotropic, biphasic, and the fully liquid crystalline phase zones, respectively. The lines represent the phase transitions for each solution.

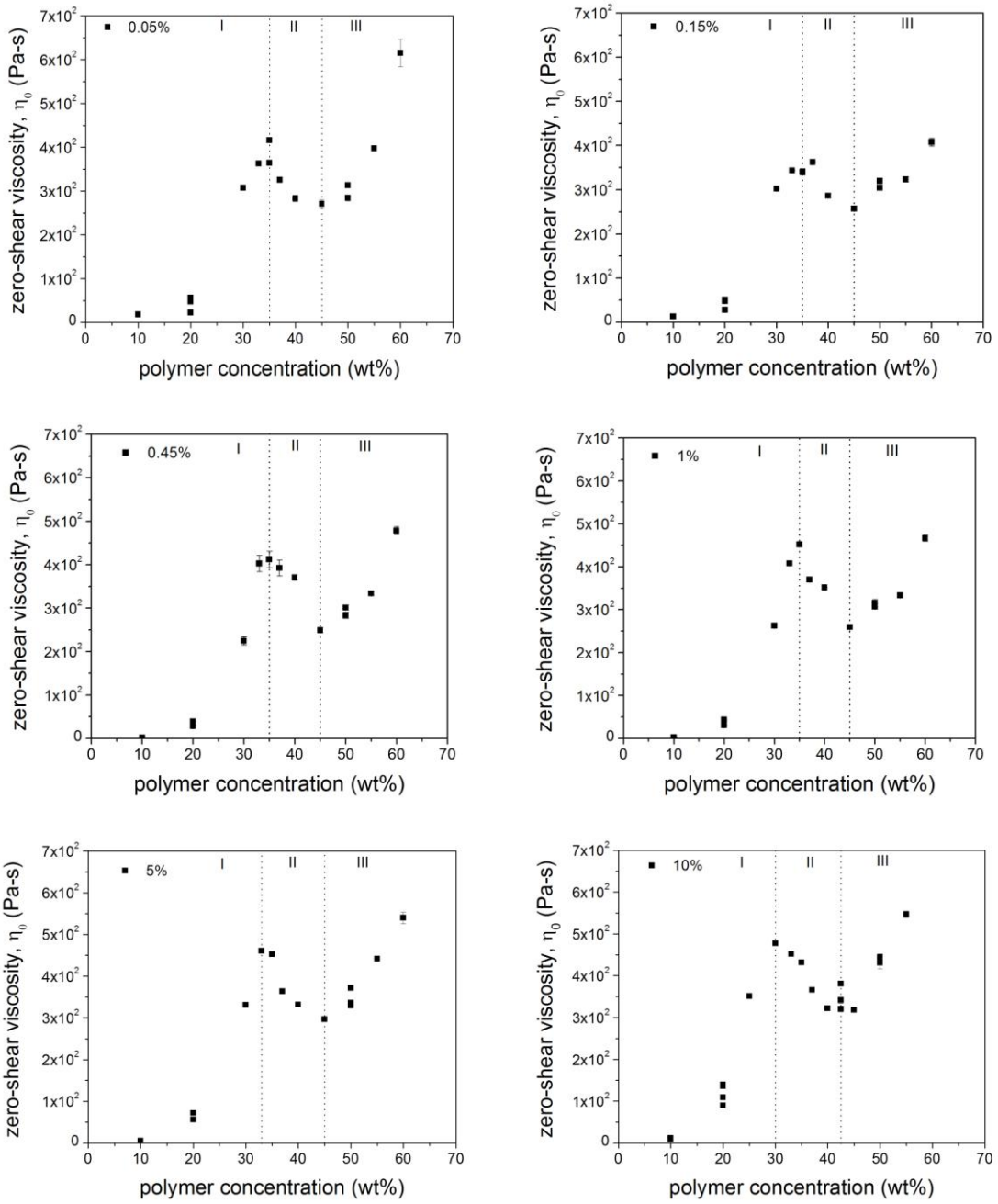

Figure 5.3 Polymer concentration effect on the zero-shear viscosity of the 0, 0.05, 0.15, 0.45, 1, 5, and 10 wt% HNC loaded HPC solutions at 25 °C. I, II, and III represent the isotropic, biphasic, and the fully liquid crystalline phase zones, respectively. Lines represent the phase transitions obtained for each solution.

Figure 5.4 shows a summary of the loading effect on the phase transitions of hydroxypropylcellulose. It demonstrated that the phase transitions were not changed, within the experimental error, with the inclusion of up to 0.45 wt% of c-MWCNTs. Moreover, the phase transitions were improved or obtained at a lower polymer concentration with the addition of 10 wt% of HNCs. A smaller biphasic window was obtained with the inclusion of HNC up to 10 wt%, which may suggest the presence of a highly anisotropic system.

Comparing the results obtained for both systems with previous works: (1) a shift of the c_{IN} to higher concentrations was predicted for semi-flexible molecules, for which the flexibility is distributed along the chain [157] and experimentally observed for *fd* and M13 viruses [158], (2) a shift of the IN transition temperature to higher values for highly anisotropic NPs [159], (3) a narrower biphasic range for a binary mixture of rigid rods and rods with a polymer shell with a lower rigidity [160], persistent semi-flexible molecules [157], and binary mixtures of rigid rods and LC when there is an attractive interactions between them [161], and (4) broadening of the biphasic gap for longer rods [161]. Consequently, the observed features could be related to a combination of stronger anisotropy and attractive interaction between the NPs and the LCP for the HNCs than for the c-MWCNTs.

Previous studies demonstrated the presence of electrostatic interactions and hydrogen bonding between the amino and hydroxyl groups of chitosan and the Si-O groups of the HNCs [146]. Therefore, this supports the idea that the improvement in the liquid crystal transition of the HPC/AA aqueous solution obtained with a high particle loading of HNCs could be due to better interactions between the HNCs and the polymer molecules than for c-MWCNTs. Those interactions and the anisotropy of

the HNCs could be promoting the LC formation on the surface of the nanoparticle, causing an improvement of a c_{IN} at a particle concentration of 10 wt%.

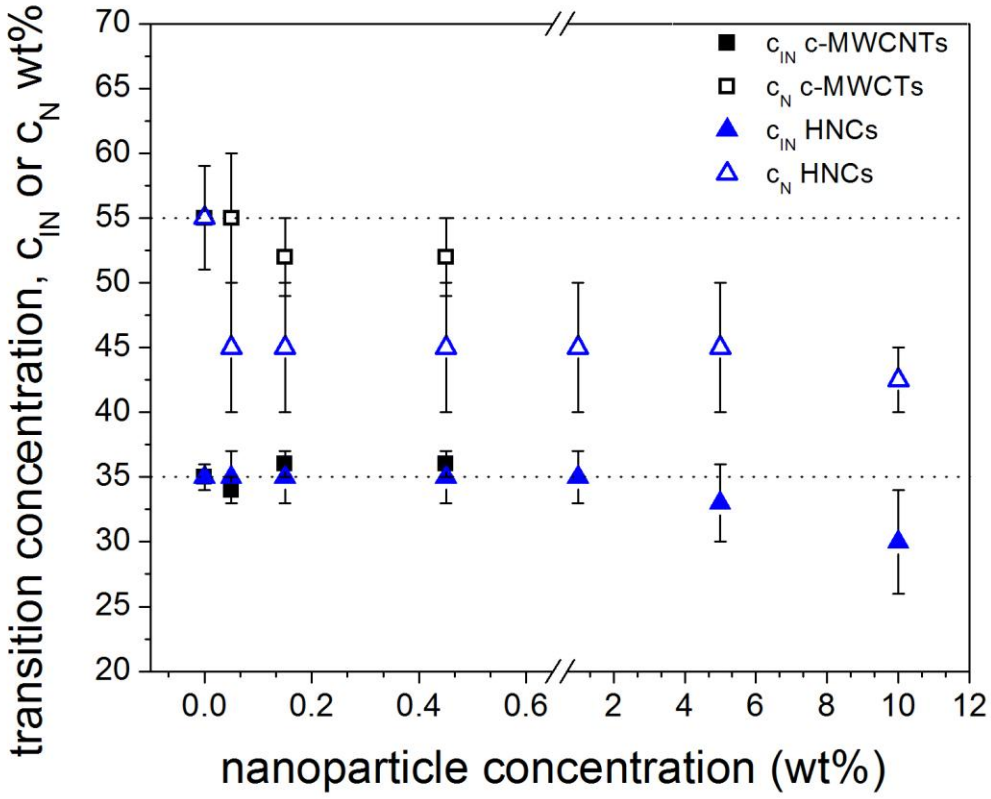

Figure 5.4 c-MWCNT and HNC loading effect on the phase transition concentration (c_{IN} and c_N) of hydroxypropylcellulose using acetic acid aqueous solutions as the solvent. The ragged lines represent the phase transitions of the neat polymer.

At low concentrations, a viscosity scaling closely with a cubic power law was predicted for semi-flexible polymers in the semi-dilute regime by the molecular dynamic theory of Doi-Edwards. The viscosity scaling was calculated for both neat and loaded HPC/AA aqueous solutions and compared with the scaling given by the

theory. The viscosity for the neat, c-MWCNT loaded, and HNC loaded samples scales as the 4.90 ± 0.35, 4.44 ± 0.07, and 3.57 ± 0.11 power, respectively. Those values are higher than theoretical predictions; nevertheless, other authors have reported similar values (5.2) for neat HPC/acetic acid solutions [41]. The discrepancy is attributed to the flexibility of the HPC backbone. However, a lower scaling was obtained for the HNCs loaded solutions, which could suggest that the nanoparticles promote a decrease of the flexibility of the HPC backbone.

5.2.1.2 Poly(*n*-hexyl isocyanate)/*p*-xylene Solutions

The polymer concentration effect on the steady-state viscosity of PHIC solutions was obtained at room temperature (21-25 °C) and at a shear rate range from 0.1 to 100 s^{-1}. Figure 5.5 shows the flow curves for neat PHIC/*p*-xylene solutions. A Newtonian plateau followed by a shear thinning region was obtained for all the polymer solutions. As discussed previously, the polymer concentration effect on steady-state viscosity it is a useful way to determine the phase transitions of lyotropic LCPs.

The phase transitions of PHIC were not significantly changed by nanoparticle loadings up to 1wt% as it is shown in the Figure 5.6. Both transitions seem to be shifted at lower concentrations for a nanoparticle loading of 1 wt%. However, the c_{IN} and c_N phase transition, determined by POM, were 22.5 and 30 wt%, respectively, for the studied nanoparticle concentrations. In general, the phase transitions characteristic of the PHIC were not significantly changed by nanoparticle loadings up to 1 wt%.

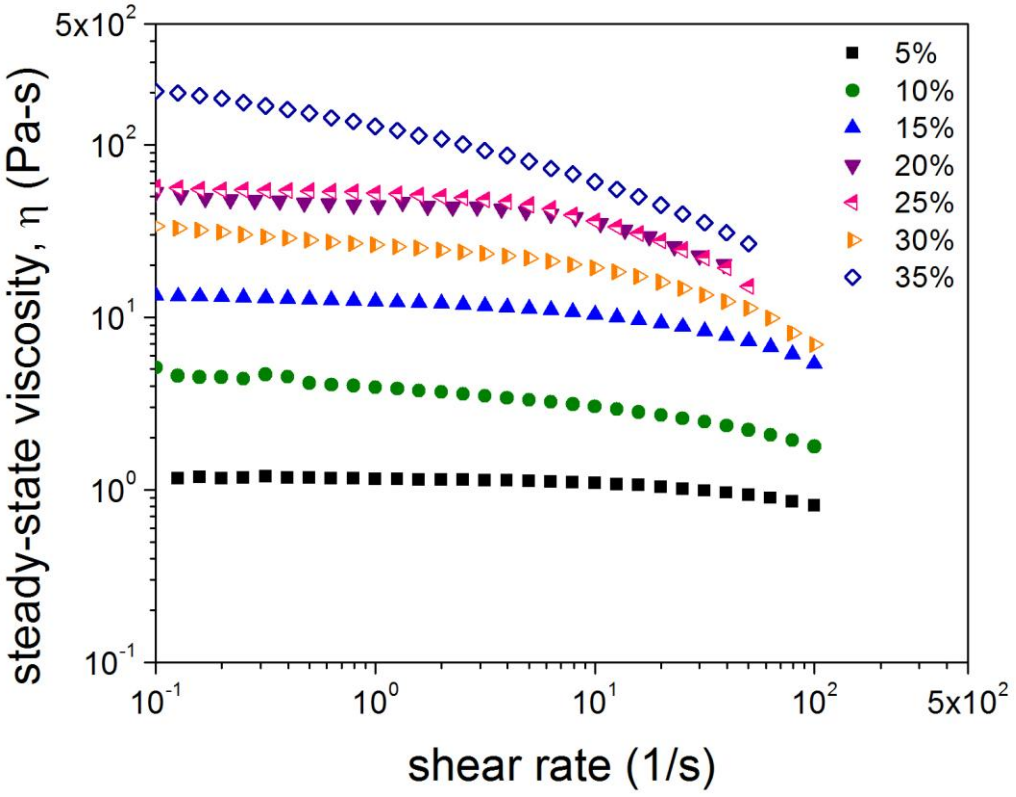

Figure 5.5 Flow curves for neat PHIC/*p*-xylene solutions at room temperature (21-25 °C) for different polymer concentrations. Full, partially filled, or empty symbols represent isotropic, biphasic, or nematic solutions, respectively.

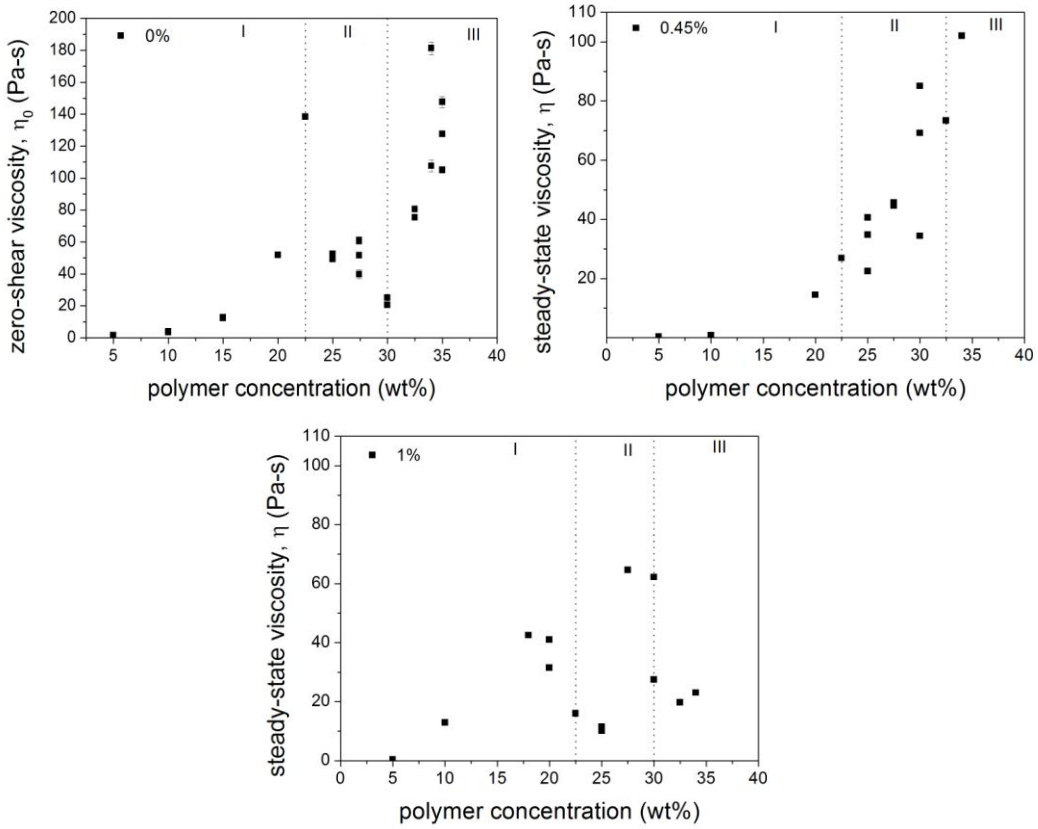

Figure 5.6 Polymer concentration effect on the zero-shear viscosity or the steady-state viscosity at 10 (1/s) of 0, 0.5, and 1 wt% i-MWCNTs loaded PHIC/*p*-xylene solutions at 25 °C. I, II, and III represent the isotropic, biphasic, and the fully liquid crystalline phase zones, respectively. Lines represent the phase transitions determined by polarized optical microscopy for each solution.

The viscosity scaling of the isotropic solutions was obtained and compared with the scaling law given by the molecular dynamic theory of Doi-Edwards. The viscosity scales as the 2.50 ± 0.14, 2.40 ± 0.46, and 3.16 ± 0.24 power for the 0, 0.45, and 1 wt% loaded PHIC solutions, a similar value to the theoretical predictions. It have also been reported higher scaling values (on the order of 3.9 power) for PHIC/*p*-xylene solutions [82, 141].

5.2.2 Optical Micrographs of Isotropic, Biphasic and Liquid Crystalline Polymer Solutions

The loading effect on the phase behavior of HPC/AA aqueous solutions was also determined by POM measurements. No effect was observed on the isotropic to nematic transition with the addition of c-MWCNTs and i-MWCNTs up to 0.45 and 1wt%, respectively, the maximum studied concentration (data not shown). However, some birefringence around the particles was observed independent of the nanoparticle concentration for the HNC/HPC system. The number of particles observed in the solution increase with the HNC concentration (Figure 5.7). The HNC is neither a birefringent nor a fluorescent material. The maximum volume concentration, given by the Onsager theory, at which the HNCs remain isotropic is 0.08 based on their mean diameter and length. Therefore, the nanoparticles by themselves should not show any birefringence at the concentration range investigated. Thus, it has been suggested that the polymer molecules are oriented around the surface of the HNCs. Consequently, the formation of liquid crystalline phase occurs around the nanoclays on a macroscopic scale. Similarly, it has been demonstrated that MWCNTs promote the LC phase formation of a thermotropic liquid crystal polyester at the surface of the nanoparticles by POM measurements [51]. Aromatic interactions between the polymer molecules and the nanoparticles were also demonstrated for that system using Raman spectroscopy.

Figures 5.8, 5.9 and 5.10 show the effect of the inclusion of c-MWCNTs, HNCs, and i-MWCNTs, respectively on the texture of a fully liquid crystal solution (43, 45 and 34 wt% of the corresponding polymer). In all the cases, it was not observed a significant effect on the liquid crystalline phase textures. However, there seems to be a slight phase separation probably due to solubility problems with the

polymer or due to a three phase separation predicted theoretically and observed experimentally for systems such as ternary solutions of schizophyllan.

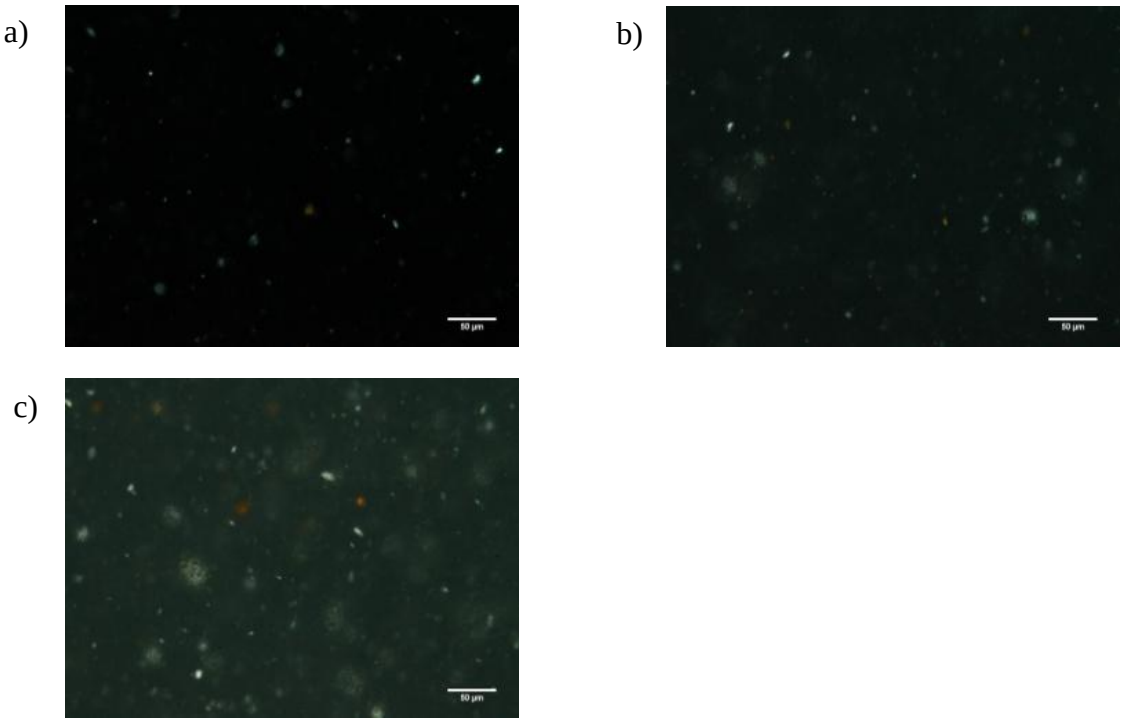

Figure 5.7 HNCs loading effect on an isotropic HPC/aqueous acetic acid solution (20 wt%). HNCs (wt%): 1 (a), 5 (b), and 10 (c)

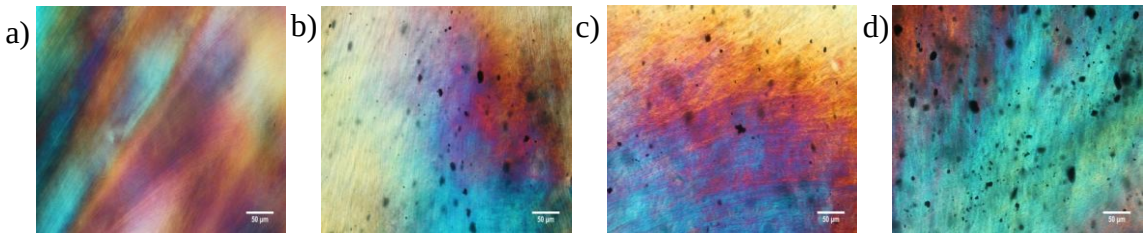

Figure 5.8 c-MWCNTs loading effect on the phase transition of HPC/aqueous acetic acid solutions at concentration (43 wt%) near the transition to a fully liquid crystal phase. c-MWCNT (wt%): 0 (a), 0.05 (b), 0.15 (c), and 0.45 (d)

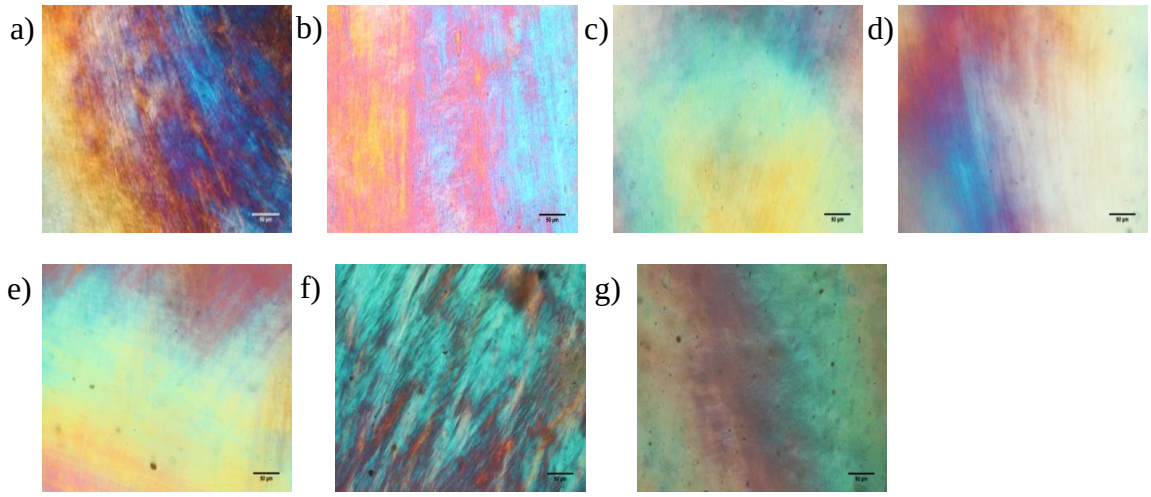

Figure 5.9 HNCs loading effect on the phase transition of 45 wt% HPC/aqueous acetic acid solutions, a concentration near the transition to a fully LC phase. HNC (wt%): 0 (a), 0.05 (b), 0.15 (c), 0.45 (d), 1 (e), 5 (f), and 10 (g)

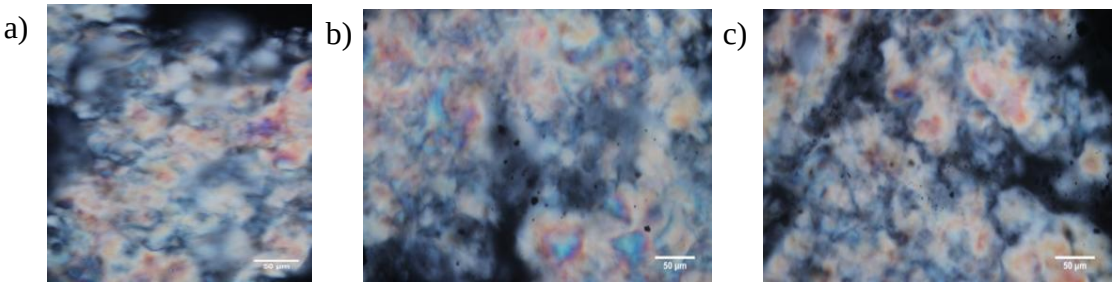

Figure 5.10 i-MWCNTs loading effect on the phase transition of 34 wt% PHIC/*p*-xylene solutions. i-MWCNTs (wt%): 0 (a), 0.5 (b), 1 (c)

In general, c-MWCNTs, HNC, and i-MWCNTs loadings up to 0.45, 5, and 1 wt%, respectively do not affect the phase transitions of a liquid crystalline matrix. The addition of 10 wt% of HNC promotes the formation of a liquid crystalline phase of hydroxypropylcellulose, consequently both c_{IN} and c_N occurs at a lower polymer concentration.

5.3 Dynamic Viscoelastic Properties

The nanoparticle loading effect on the dynamic viscoelastic properties of both isotropic and liquid crystalline loaded HPC/AA aqueous solutions will be discussed in the next section. The viscoelastic properties were determined on the linear viscoelastic region to determine the particle loading effect on the microstructure of the polymer solutions. The frequency range was varied from 0.1 to 100 Hz at a constant strain and temperature.

5.3.1 Linear Viscoelastic Properties of Isotropic Solutions

The c-MWCNTs and HNCs loading effect on the viscoelastic properties of isotropic HPC/AA aqueous solutions (20 wt%) were determined at 25 °C for a frequency range between 0.1 and 100 Hz. No significant effect in the scaling of the viscoelastic modulus of the neat HPC/AA solutions was observed with c-MWCNTs and HNCs loading up to 0.45 and 10 wt%, respectively (Figures 5.11 and 5.12). A minimum and maximum in the loss modulus of 34 and 136% (at 0.1 Hz) was obtained for 0.45 and 10wt% of HNCs, respectively. However the loss modulus was not significantly affected with the addition of c-MWCNTs (changes less than 10%). On the other hand, a decrease of 62% (at 0.1 Hz) in the storage modulus was obtained with 0.15wt% c-MWCNTs. Similarly, a minimum and maximum in the storage modulus of 80 and 71% (at 0.1 Hz) were obtained with the addition of 0.15 and 10wt% HNCs, respectively. Zhang and coworkers also report a decrease in the storage modulus of PE with the addition of single walled CNTs up to 0.2 wt% [162].

On the other hand, an increase of the viscoelastic moduli of an isotropic PHIC solution with the inclusion greater than 0.45 wt% of i-MWCNTs may be observed in Figure 5.13. A maximum loss and storage modulus of 86 and 207%, respectively was

obtained with the addition of 0.7 wt% of i-MWCNTs (at 0.1Hz). However, no significant effect on scaling of the viscoelastic properties of the neat PHIC/*p*-xylene solutions was observed at the studied nanoparticle concentrations.

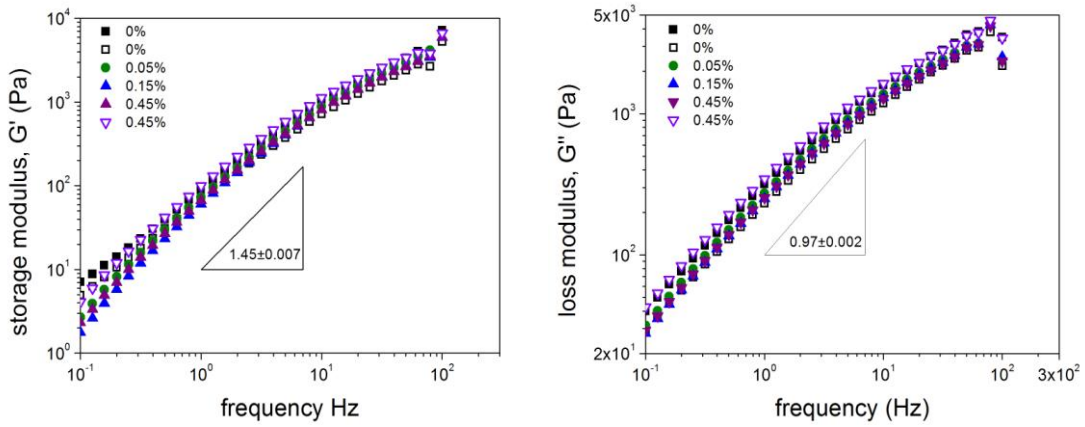

Figure 5.11 c-MWCNTs loading effect on the viscoelastic properties of 20 wt% HPC/AA aqueous solutions at 25 °C and a strain of 6%.

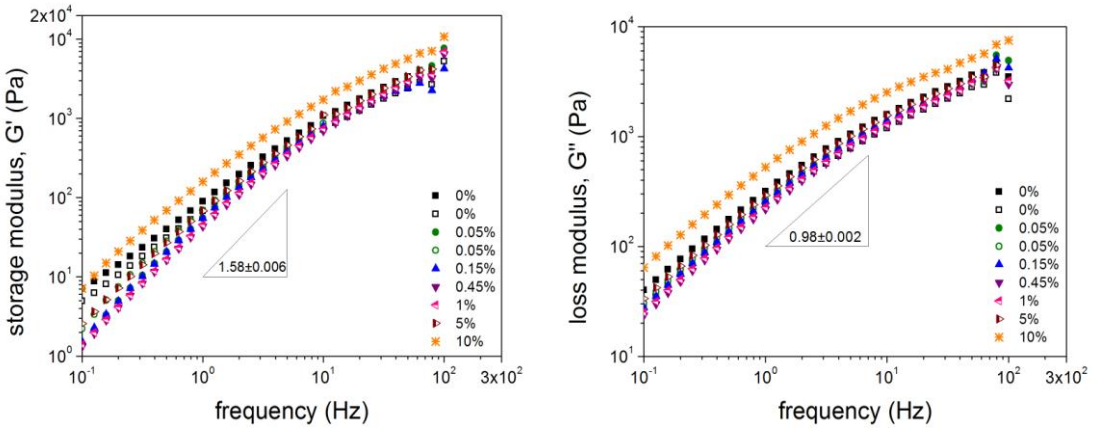

Figure 5.12 HNCs loading effect on the viscoelastic properties of 20 wt% HPC/AA aqueous solutions at 25 °C and a strain of 1.5%.

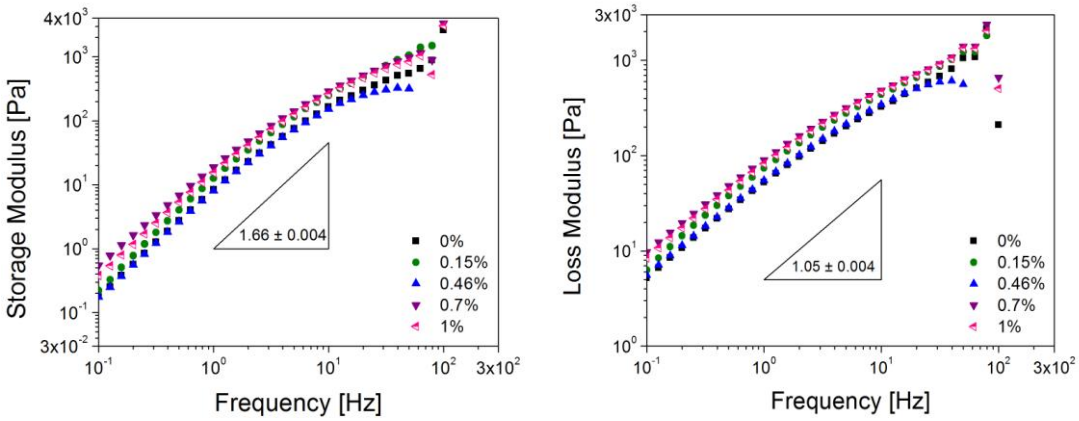

Figure 5.13 i-MWCNTs loading effect on the viscoelastic properties of 10wt% PHIC/*p*-xylene solutions at 25 °C and a strain of 6%.

In general, there is no indication of changes in the polymer dynamics of the solutions. No percolation effect or a plateau on the storage modulus (characteristic of a solid-like behavior) was observed for the studied systems, suggesting that the nanoparticles were well dispersed on the isotropic phase.

5.3.2 Linear Viscoelastic Properties of Liquid Crystalline Solutions

The c-MWCNTs and HNCs loading effect on the viscoelastic moduli of a liquid crystalline HPC solution (50 wt%) are shown in Figures 5.14 and 5.15, respectively. In general, the viscoelastic properties and relaxation times were not significantly affected with particle addition for the studied conditions. There is no indication of changes in the polymer dynamics of the solutions. No percolation effect or a plateau on the storage modulus (characteristic of a solid-like behavior) was observed for the studied systems, suggesting that the nanoparticles were integrated and aligned on the LC phase.

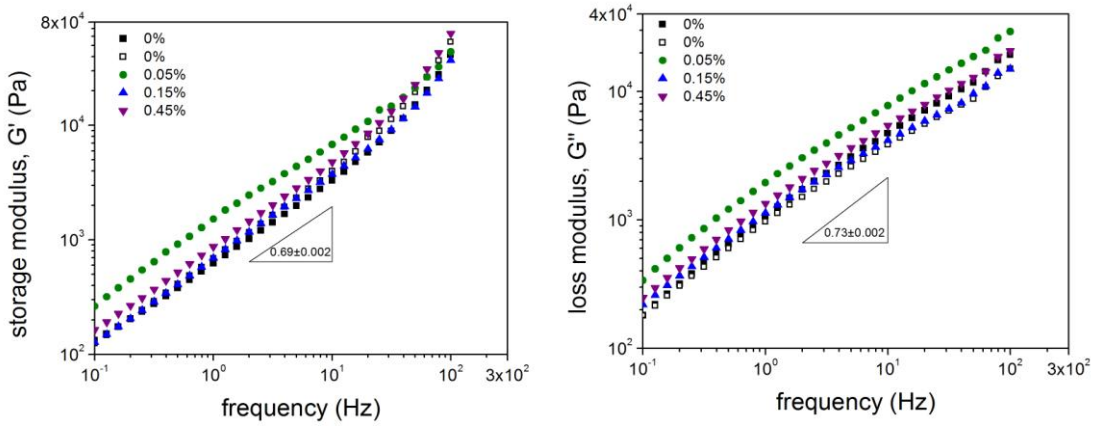

Figure 5.14 c-MWCNTs loading effect on the viscoelastic properties of 50 wt% HPC/AA aqueous solutions at 25 °C and a strain of 0.2%.

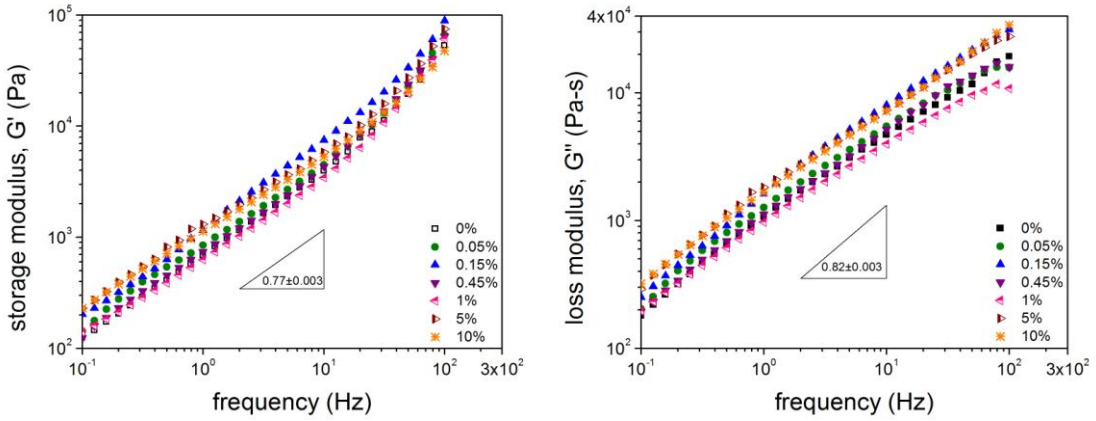

Figure 5.15 HNCs loading effect on the viscoelastic properties of 50 wt% HPC/AA aqueous solutions at a strain less than 0.6 % and 25 °C

5.4 Steady-State Rheology

In this section, the loading effect on the steady-state viscosity will be elucidated at constant temperature for both an isotropic and a liquid crystalline solution. The nanoparticle inclusion effect on the flow dynamics of the polymer molecules will be discussed for both an isotropic and a LC polymer solution.

5.4.1 Loaded Isotropic Polymer Solutions

The rod-like nanoparticle loading effect on the steady-state viscosity of isotropic polymer solutions will be discussed. Moreover, the loading effect on the steady-state viscosity will be predicted and compared with the experimental behavior.

5.4.1.1 Experimental Results

c-MWCNTs, HNCs, and i-MWCNTs loading effect on the steady-state viscosity of isotropic solutions at 25°C was determined (Figures 5.16a, 5.17a, and 5.18a, respectively). All the flow curves exhibit a Newtonian plateau at low shear rates, followed by a shear thinning regime for all the studied systems. The onset of the shear thinning regime is shifted to lower shear rates with loadings higher than 1 wt% of HNCs.

The flow behavior of a polymer suspension may be affected for different parameters that involve both the matrix and the disperse phase. Some authors have been used the relative viscosity at constant shear stress or rate, allowing separate the influence of both the nanoparticles and polymer matrix on the flow behavior of the suspension [163]. It presumes that the nanoparticles enhance the shear rate of the fluid phase so a master curve could be obtained using the relative viscosity at constant stress as the shift factor, B.

$$B = \frac{\eta(\phi)}{\eta(\phi = 0)}\Big|_{\sigma=constant} \tag{5.1}$$

This concept was applied to the studied systems. Some deviations were obtained when the data of c-MWCNT and HNC loaded HPC solutions were collapsed on a master curve. It demonstrates that the flow behavior of the solutions was affected by particle-polymer interactions (Figures 5.19a). However, for these systems the shear thinning

seems to be governed by shear stress. For the loaded PHIC solutions, some greater deviations were obtained may be due to some structure formation or particle-polymer interactions on the flow dynamics (Figure 5.20a).

The shift factor for the systems is shown in Figures 5.19b and 5.20b, which represent the effect on the magnitude of the viscosity compared with the pure polymer solution. Values of B greater than 1 were obtained for HNCs loading greater than 1 wt%, and for 1wt% i-MWCNTs. For HNCs concentrations greater than 0.45 wt%, the shift factor scales linearly with nanoparticle concentration (slope = 0.37±0.03, intercept = 0.65±0.16, R^2= 0.9881). It suggests that for particle loadings higher than 0.45 wt% the particle-polymer interactions do not affect the flow dynamics of the solutions. However, for the i-MWCNTs/PHIC solutions the nanoparticle-polymer interactions seems to affect the flow dynamics of the solutions on the studied experimental concentration range since the shift factor B scales with a polynomial of second order for particle concentrations before and after the minimum value ($y = 6.04x^2-4.22x+1$, up to 0.45 wt%, and $y = 3.23x^2-2.51x+0.8$, from 0.45 to 1 wt%).

Another feature of the steady-state rheology of both MWCNTs and HNCs suspensions is a viscosity decrease with low particle loadings, shown in Figures 5.16b, 5.17b, and 5.18b. This is consistent with the decrease of the viscoelastic properties of isotropic polymer solutions obtained with the inclusion of small nanoparticle concentrations. A similar behavior was observed for all the systems, the viscosity decrease with the addition of small nanoparticle concentrations, reach a minimum value, and then begins to increase. A decrease of 18, 23, and 55% on the zero-shear viscosity was observed with the inclusion of 0.15 wt% c-MWCNTs, 0.45wt% HNCs, and 0.45wt% i-MWCNTs, respectively. Furthermore, a maximum of 22, 206, and 47%

on the zero-shear viscosity was obtained with the inclusion of 0.45 wt% c-MWCNTs, 10wt% HNCs, and 1wt% i-MWCNTs, respectively.

Similar effect was reported with the addition of CNTs to a polyethylene matrix due to the absorption of molecules with the longest relaxation time or highest molecular weight on the CNT surface [162, 164]. In both cases, the effect was suppressed when a PE matrix with a lower polydispersity was used. On the other hand, a viscosity minimum of nematic solutions with loadings of sub-micron carbon black up to 5 wt% was observed only when a larger capillary was used [165], may be due to the some "plasticizing" effect of the nanoparticles. Mackay and coworkers reported a fourfold decrease in the viscosity of polystyrene solutions with 50 wt% of spherical nanoparticles of the same polymer [166]. It is suggested that the nanoparticles produce some changes in the conformation and free volume of the polymer, and which causes cause a non-Einstein behavior. Similarly, Tuteja demonstrated that the non-Einstein behavior was observed only when an entangled and confined polymer matrix was used [167]. Other authors attribute this effect to a well-miscible system [168], selective adsorption of polymer with a higher M_W on the surface of the nanoparticles [169], and the formation of core (nanoparticle) – shell (polymer) structures [170, 171].

In our system, the Si-O or carboxylic groups of the HNCs or c-MWCNTs, respectively, could interact with the hydroxyl groups of HPC. The viscosity decrease is expected to be larger for a system in which there are greater interactions polymer-nanoparticles. Therefore, we could suggest that those interactions cause an unidirectional oriented polymer shell around the nanoparticles and consequently the minimum viscosity, based on the rheological and optical results. Measurements of the

ζ potential of the nanoparticles and the nanoparticles-polymer solutions may confirm this hypothesis.

Figure 5.21 shows that both negatively charged nanoparticles acquire a slightly negative charge, characteristic of the neat HPC/aqueous solutions (-1.48 ± 0.99), at polymer/nanoparticles ratio higher than five. These results demonstrated that the polymer molecules were wrapping the nanoparticles. The ζ potential and POM measurements suggest that the polymer shell around the HNCs was unidirectionally oriented on a macroscopic scale. In the case of the c-MWCNTs, the polymer shell could be randomly organized or oriented on a nanoscopic length scale. Based on these results the formation of a polymer shell around the i-MWCNTs may be presumed too.

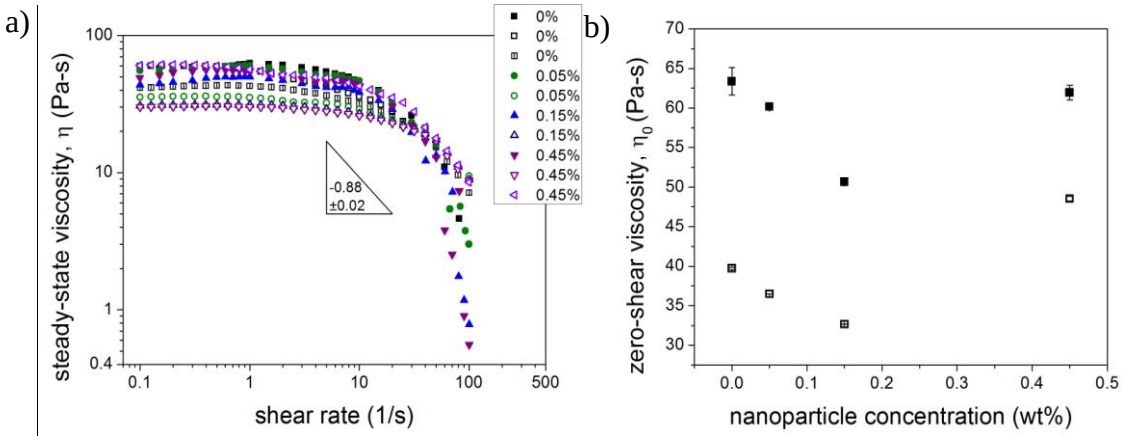

Figure 5.16 a) c-MWCNTs loading effect on the steady-state viscosity of 20wt% HPC/AA aqueous solutions at 25°C. b) nanoparticle loading effect on the zero-shear viscosity. (Closed symbols – data obtained with the ATS Rheologica Rheometer and open symbols – data obtained with the Anton Paar Rheometer)

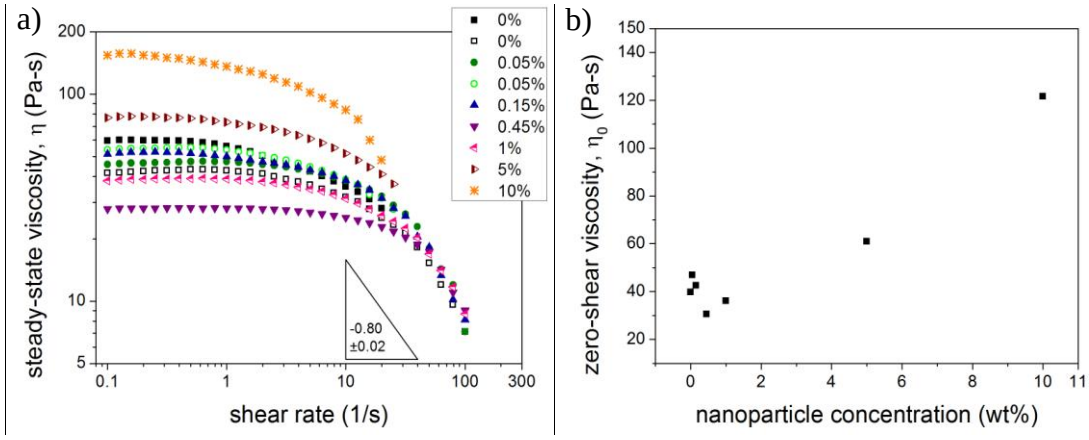

Figure 5.17 a) HNCs loading effect on the steady-state viscosity of 20wt% HPC/AA aqueous solutions at 25°C. b) nanoparticle loading effect on the zero-shear viscosity

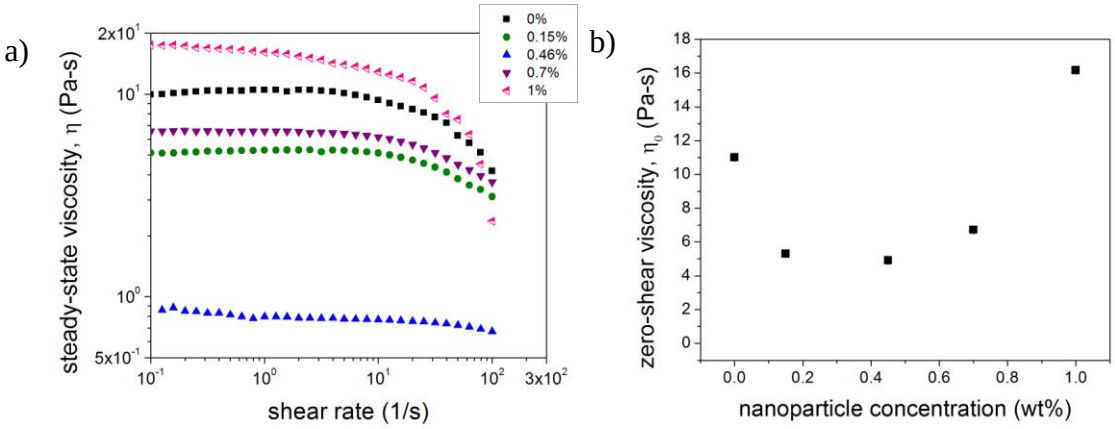

Figure 5.18 a) i-MWCNTs loading effect on the steady-state viscosity of 10wt% PHIC/*p*-xylene solutions at 25°C. b) i-MWCNTs loading effect on the zero-shear viscosity

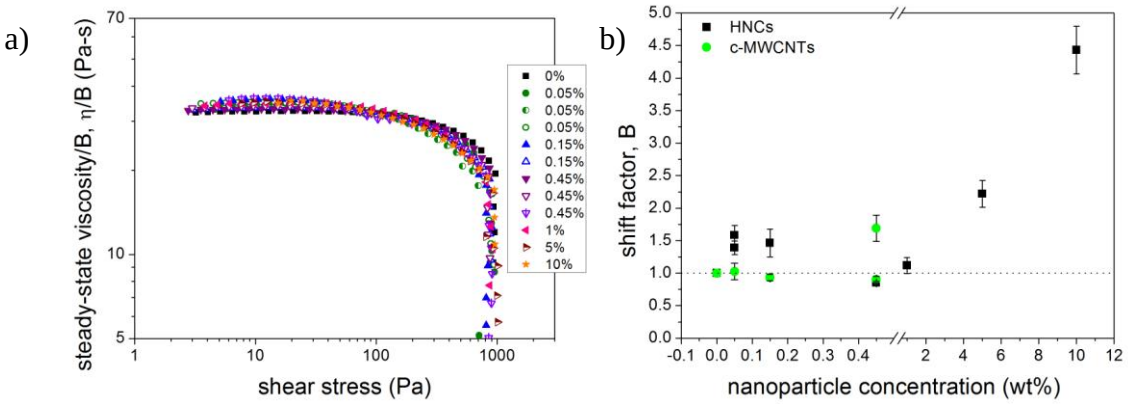

Figure 5.19 a) Master curve of the steady-state viscosity of HNCs (closed symbols) and c-MWCNTs (open symbols) suspensions on 20 wt% HPC/AA aqueous solutions at 25 °C. b) Shift factor as a function of nanoparticle concentration for both the HNCs and the c-MWCNTs

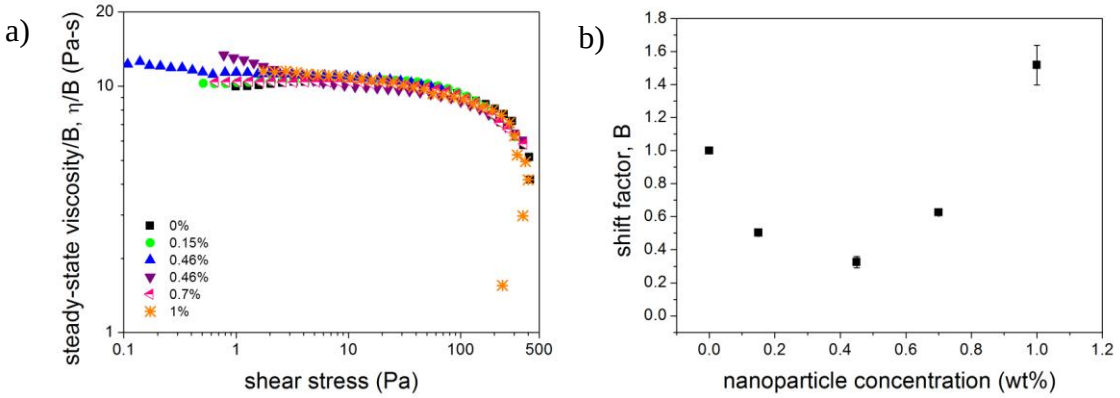

Figure 5.20 a) Master curve of the steady-state viscosity of i-MWCNTs/10 wt% PHIC/*p*-xylene solutions at 25 °C. b) Shift factor as a function of nanoparticle concentration

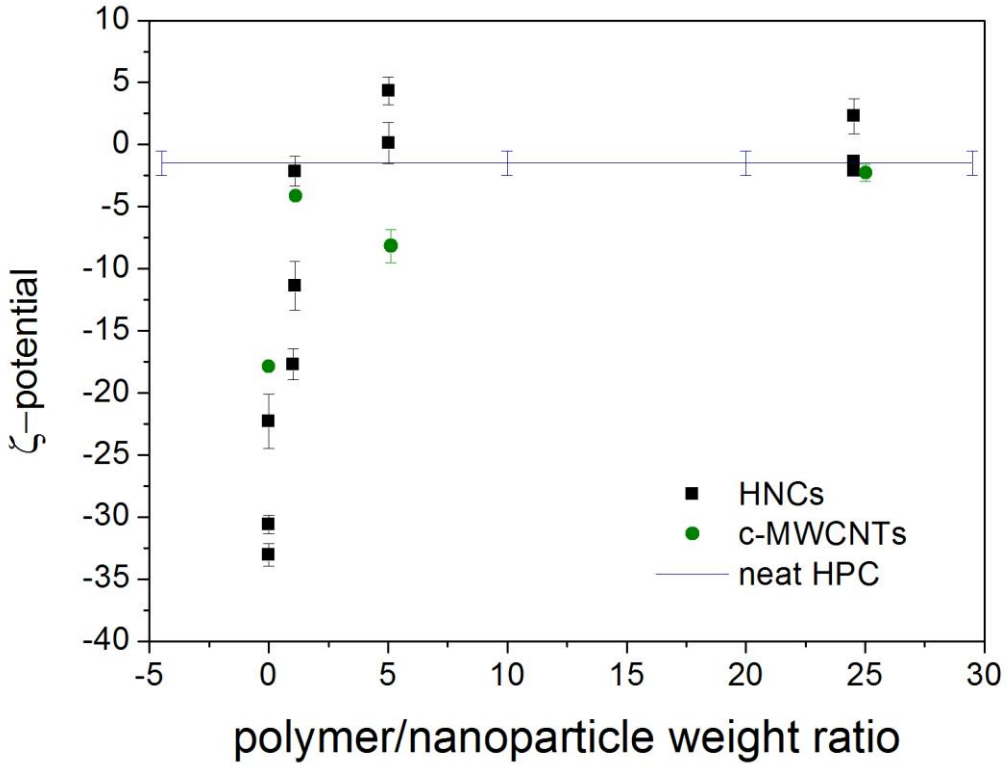

Figure 5.21 ζ-potential measurements of nanoparticle/HPC aqueous solutions at different polymer/nanoparticles weight ratio at 25°C

In conclusion, the adsorption of the polymer on the surface of the nanoparticles was demonstrated. The formation of core-shell structures causes a viscosity decrease at low particle loadings. The inclusion of HNCs promote the formation of a liquid crystalline phase on the nanoparticle surface may be due to the anisotropy of the particles and attractive interactions between the particle and the polymer.

5.4.1.2 Modeling Results

The loading effect on the steady-state viscosity as predicted using a semi-empiric model. The system was assumed to be composed of core-shell (nanoparticle-

polymer) structures dispersed in an isotropic polymer matrix. The principal assumptions were that both the nanoparticles and the polymer molecules are perfect cylinders and the contact area of the polymer molecules (A_P) with the surface of the nanoparticles is a third part of its own area ($A_P = 1/3\pi D_P L_P$, where D_P and L_P is the diameter and length of the polymer molecules, respectively). There are some aspects considered in the model which affect the viscosity of the system: the nanoparticle inclusion, the adsorption of the polymer molecules, and the anisotropy induced by rod-like nanoparticles.

The theoretical concentration scaling (c^3) was used to obtain the viscosity of the matrix (η_M), and hence the adsorption effect on the bulk viscosity. This viscosity was considered on the total contribution until the system reached equilibrium (the mass of polymer on the shell is equal to the mass of polymer added to the suspension). The area of the nanoparticles (A_{NP}) was calculated as the surface area of a cylinder multiplied by the number concentration of nanoparticles on the solution (equation 5.1).

$$A_{NP} = \pi D_{NP} L_{NP} \left(\frac{4\phi_{NP}}{\pi D_{NP}^2 L_{NP}} \right) \tag{5.2}$$

where D_{NP}, L_{NP} and ϕ_{NP} is the diameter, length and volume fraction of the rods, respectively. The polymer molecules adsorbed was obtained, geometrically, as the number of polymer rods needed to cover completely the surface area of the rod-nanoparticle. An adjustable parameter, f_R, was included in the calculus to correct for this assumption (equation 5.2). It was varied from 1 (value corresponding to a homogeneous polymer shell) to 0.0001.

$$\#_{P,\ surface} = f_r \frac{A_{NP}}{A_P} \tag{5.3}$$

The mass of the polymer molecules adsorbed on the surface of the nanoparticles is calculated with the following equation:

$$m_{P,surface} = \#_{P,surface}\left(\frac{M_W}{Na}\right) \tag{5.4}$$

where M_w is the molecular weight of the polymer and Na is the Avogadro's number.

The relative viscosity related to the particle inclusion (η_P) was calculated using the following equations [32]:

$$\eta_P = \left[1 - \frac{\phi_e}{\phi_m}\right]^{-[\eta]\phi_m} (rods) \tag{5.5}$$

$$\eta_P = 1 + 2.5\phi_e + 6.2\phi_e^2\ (sphere) \tag{5.6}$$

where ϕ_m is the maximum packing fraction of the rods (0.91 for hexagonally packed rods [172]) and [η] is the intrinsic viscosity. The effective volume fraction (ϕ_e) was obtained by [32]:

$$\phi_e = \phi_{NP}\left(1 + \frac{\delta}{R_{NP}}\right) \tag{5.7}$$

where δ is the shell thickness and R_{NP} is the radius of the nanoparticles. The intrinsic viscosity was calculated based on the aspect ratio of the cylinders using the following equations [173, 174]:

$$[\eta] = \frac{q^2}{5}\left(\frac{1}{3(ln(2q) - 1.5)} + \frac{1}{ln(2q) - 0.5}\right) + 1.6;\ for\ q > 15\ and\ Pe_r \ll 1 \tag{5.8}$$

$$[\eta] = 0.315\frac{q}{lnq};\ \ for\ q \gg 1\ and\ Pe_r \ll q^3;\ \ \ q = \frac{L}{D} \tag{5.9}$$

Finally, the overall bulk viscosity was obtained multiplying the experimental viscosity obtained for the neat polymer solution ($\eta_{P,\ neat}$), the relative viscosity of the

matrix, the relative viscosity due to particle addition, and the factor f_a to consider the anisotropy induced by the nanoparticles, if any (5.10). This factor was treated as an adjustable parameter that goes from 0.0001 to 1 (value when there are no effects due to anisotropy).

$$\eta_{effec} = \begin{cases} \eta_M(\eta_{NP})\eta_{P,neat} f_a & IF\ \eta_M > 0 \\ (\eta_{NP})\eta_{P,neat} f_a & IF\ \eta_M = 0 \end{cases} \quad (5.10)$$

The effect of loading "soft" nanoparticles and the adsorption of polymer molecules on the surface of the nanoparticles on the relative viscosity (η_r) of the bulk solution was calculated for different values of the adjustable parameters (f_a, f_r, and δ). Figure 5.22 shows the values obtained for the HNC loaded isotropic HPC solution, considering that the nanoparticles behave as rods (5.22a) or spheres (5.22b). This effect was also determined for the c-MWCNTs/HPC and i-MWCNTs/PHIC systems, and a similar effect was obtained. The steepest increase in the relative viscosity was obtained for cylindrical, rather than spherical particles. Increasing the polymer shells around the nanoparticle simultaneously cause opposite effects on the relative viscosity, for spheres the "negative" effect predominate (a decrease in the bulk viscosity). The steepest decrease in the viscosity was obtained for a uniform polymer shell.

Values for f_a, f_r, and δ was determined minimizing the root mean square error (f_a = 1, 0.7, and 0.3; f_r = 0.0003, 0.0001, and 1; δ = 21, 1.6, and 5.3; for HNCs, c-MWCNTs, and i-MWCNTs, respectively). A minimum error was obtained assuming that the HNCs and CNTs behave as spheres and rods, respectively. The polymer molecules were assumed oriented perpendicular to the nanoparticle surface. A qualitative agreement between the experimental and the modeled data was obtained (Figure 5.23). However, a significantly lower value of the minimum viscosity was

predicted for the HNCs system, indicating that may be another phenomenon affecting the viscosity that was not considered in the model.

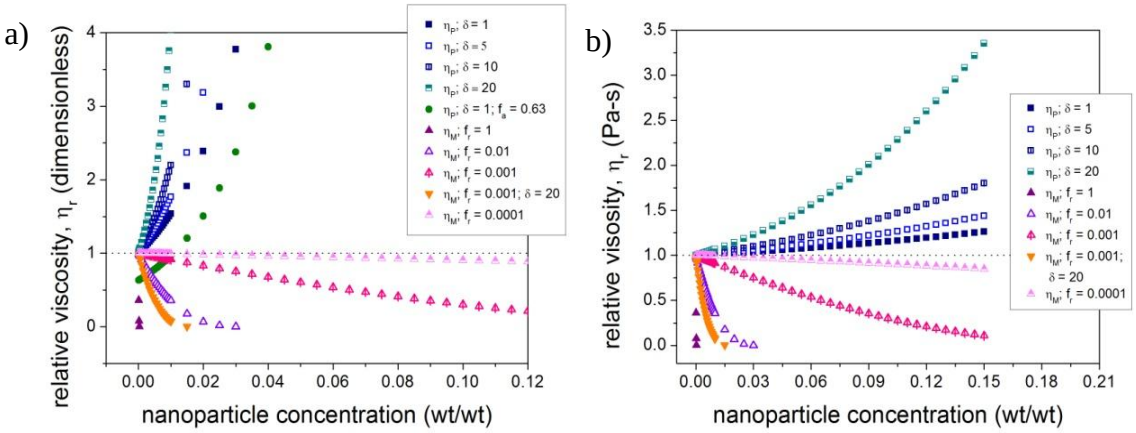

Figure 5.22: Effect of load "soft" nanoparticles (η_p) and the adsorption of polymer on the surface of the nanoparticles (η_M) on the relative viscosity of isotropic HPC solutions loaded with HNC concentration for different parameters f_a, f_r, and δ considering the nanoparticles behave as rods (a) or spheres (b) (the ragged line represent a relative viscosity of one)

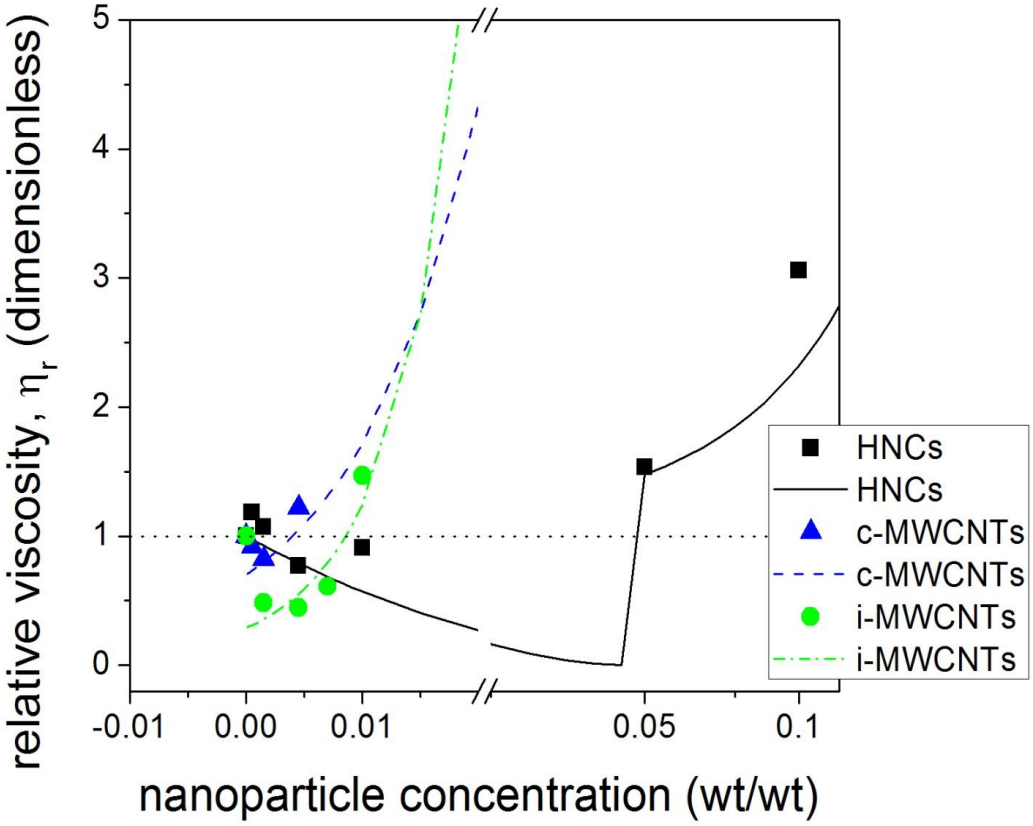

Figure 5.23 Nanoparticle concentration effect on the relative viscosity of isotropic polymer solutions; symbols represent the experimental points and the lines are the modeled data obtained minimizing the root mean square error (f_a = 1, 0.7, and 0.3; f_r = 0.0003, 0.0001, and 1; δ = 21, 1.6, and 5.3; for HNCs, c-MWCNTs, and i-MWCNTs, respectively). Horizontal line represents a relative viscosity of one.

5.4.2 Loaded Liquid Crystalline Polymer Solution

The nanoparticle loading effect on the steady-state viscosity of liquid crystalline solution was determined at 25 °C for HPC and PHIC solutions. As shown in the Figures 5.24 and 5.25, the loaded HPC liquid crystalline solutions behave very similar to the neat polymer solutions and the viscosity scaling with shear rate do not change significantly with particle inclusion ($\dot{\gamma}^{-0.63 \pm 0.003}$). There is an increase in the

viscosity greater than 25 and up to 73%, at 0.2 (1/s), with HNCs inclusion greater than 1wt%. However, the observed effect is lower than the values predicted by Einstein for dilute and non-interactive spherical nanoparticles. In general, we could conclude that the addition of nanoparticles up to 0.45 and 1 wt% for c-MWCNTs and HNCs, respectively did not significantly affect the steady-state viscosity of a neat HPC liquid crystalline solution under the studied conditions. At higher concentrations of the HNCs (up to 10 wt%, the maximum studied concentration) an enhancement on the steady-state viscosity was obtained. This effect it is attributed to a well-dispersed system and better polymer-particle than particle-particle interactions for both suspensions.

The flow curve of loaded PHIC liquid crystalline solutions was not significantly affected by particle loadings up to 1wt% of i-MWCNTs (Figure 5.26; $\dot{\gamma}^{-0.83\pm0.007}$). However, for this system there is a decrease of 35% and 10% (at 0.1 (1/s)) with the inclusion of 0.45 and 1wt% of i-MWCNTs, respectively. This effect may be consistent with the micrographs, previously showed. New samples were prepared this time with an excess of solvent to guarantee a well-disperse polymer solution. Then, the solvent was evaporated until the desired concentration of the components was reached. The flow curves obtained for those samples are show in the Figure 5.27. A consistent and greater decrease in the viscosity was observed, this time the viscosity decrease two order of magnitude (97% at 0.1 (1/s)). This may be due to the particle-nanoparticle interactions promote a perpendicular alignment between them, causing distortions in the nematic phase or the local formation of biaxial liquid crystal phases. Previous reports predict the orientation of the polymer molecules

perpendicular to the nanotubes when there are repulsive interactions between them [161].

The flow behavior of a polymer suspension may be affected for different parameters that involve both the matrix and the disperse phase. Some authors have been used the relative viscosity at constant shear rate, allowing separate the influence of both the nanoparticles and polymer matrix on the flow behavior of the suspension [163]. This concept was successfully applied previously on liquid crystalline HPC solutions loaded with spherical nano and microparticles [18-20]. It presumes that the nanoparticles enhance the shear stress of the fluid phase so a master curve could be obtained using the relative viscosity at constant shear rate as the shift factor, C.

$$C = \frac{\eta(\phi)}{\eta(\phi = 0)}\Big|_{\dot{\gamma} = constant} \tag{5.11}$$

As the shape of the flow curves did not significantly change with particle loading for the studied nanoparticle suspensions, the data was collapsed using this simple vertical shift. A master curve was created that describe both the c-MWCNTs and the HNCs loading effect on the relative viscosity of the LC HPC solutions (Figure 5.28a). Some deviations were obtained at high shear rates due to sample instabilities (sample twist out the gap). This suggests that the flow of the loaded suspensions is dominated by the flow dynamics of the polymer molecules for the studied solutions. The shift factor of the c-MWCNTs did not change significantly with particle loading up to 0.45 wt% (Figure 5.28b). On the other hand, a linear scale with particle loading was obtained for the HNCs (slope = 0.043±0.004, intercept = 1.03±0.016, and R^2 = 0.963), demonstrating that the particle-polymer interactions did not affect the flow dynamics of the solutions. For i-MWCNTs/PHIC solutions, the curve did not change

significantly with the shifting (data not shown) indicating that polymer-nanoparticle interactions affect the flow behavior of the solutions. This may support the hypothesis that both the nanoparticles and the LC molecules tend to align perpendicular to each other.

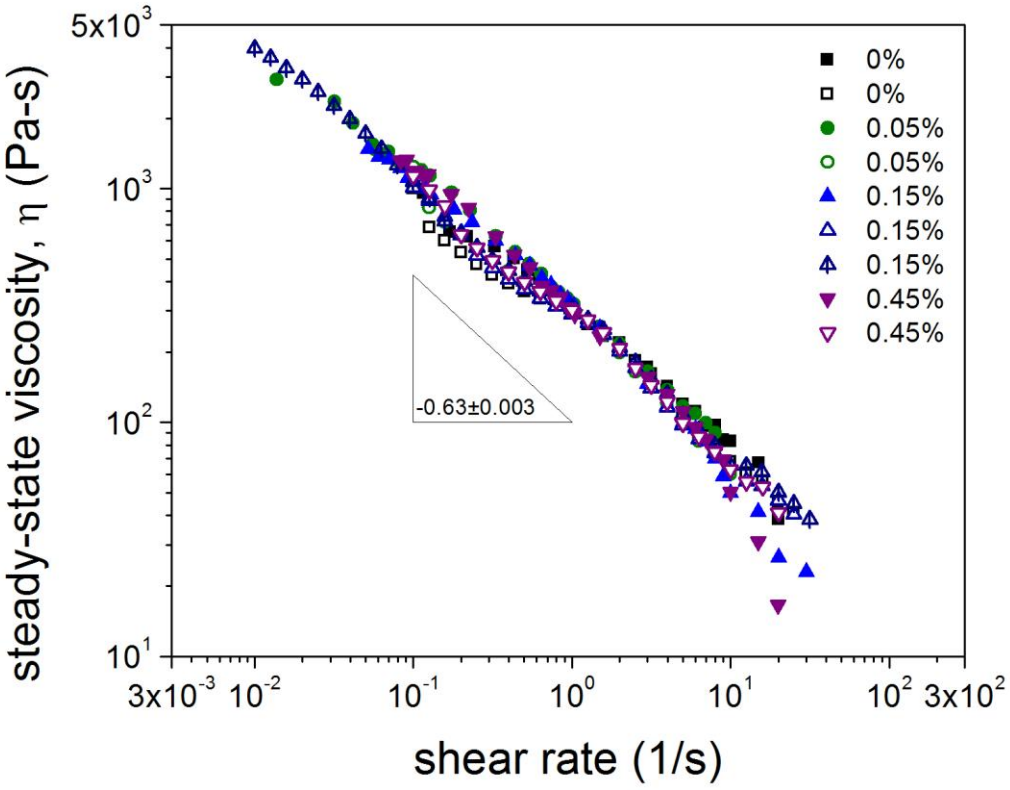

Figure 5.24 c-MWCNTs loading effect on the steady-state viscosity of 50 wt% HPC/ AA aqueous solutions at 25°C (Closed symbols – data obtained with the ATS Rheologica Rheometer and open symbols – data obtained with the Anton Paar Rheometer)

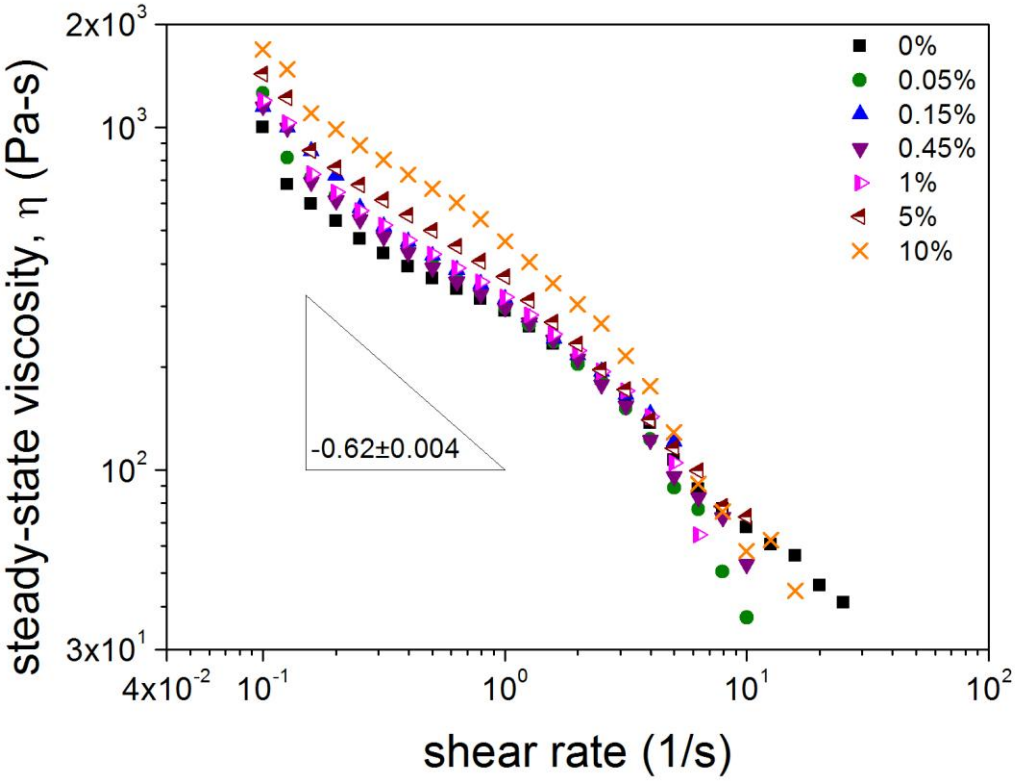

Figure 5.25 HNCs loading effect on the steady-state viscosity of 50wt% HPC/AA aqueous solutions at 25°C

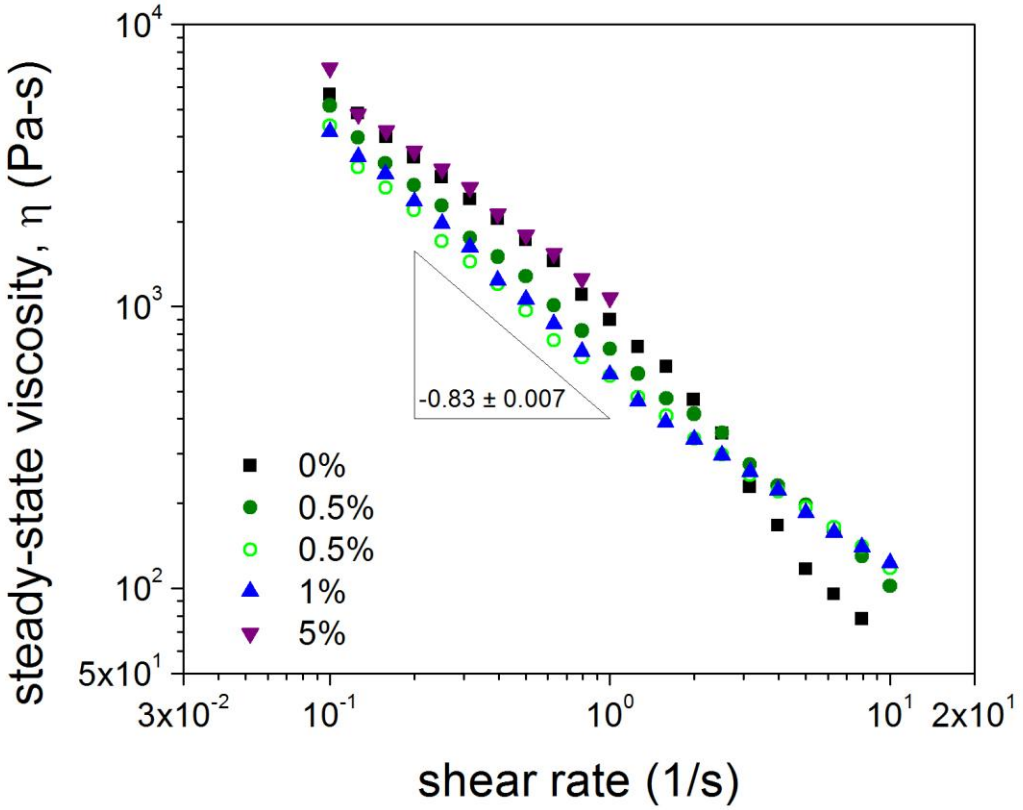

Figure 5.26 i-MWCNTs loading effect on the steady-state viscosity of 34 wt% PHIC/ *p*-xylene solutions at 25 °C

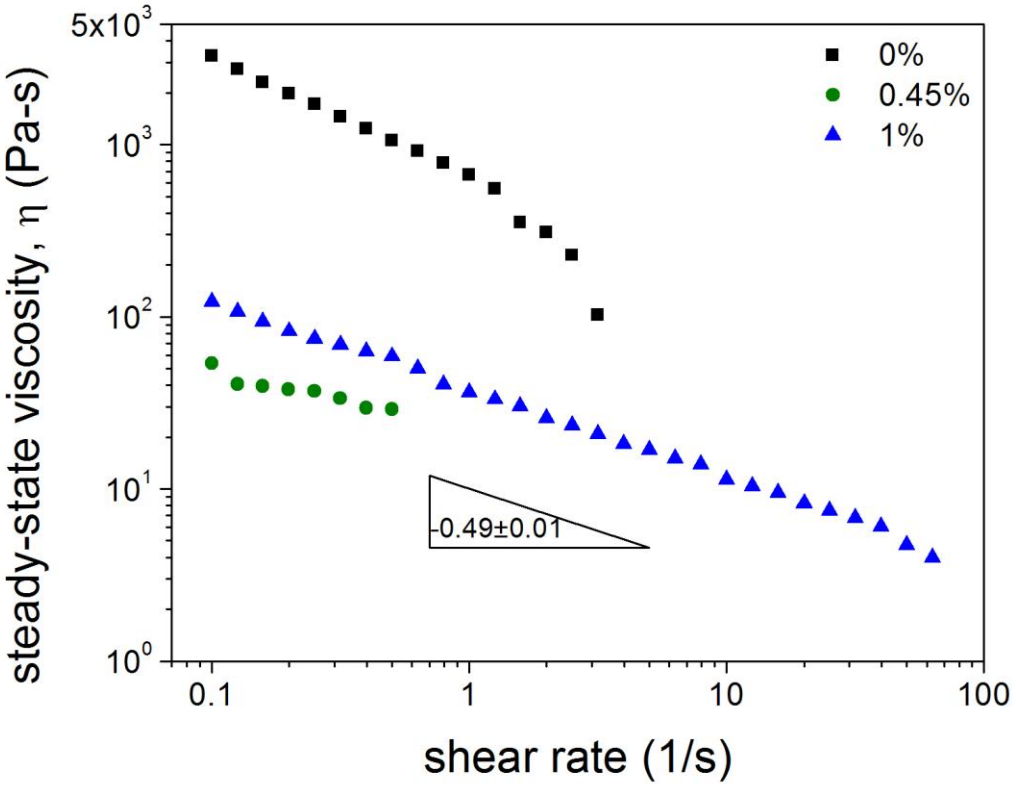

Figure 5.27 i-MWCNTs loading effect on the steady-state viscosity of 34 wt% PHIC/ *p*-xylene solutions at 25 °C (samples prepared with an initial excess of solvent)

a)

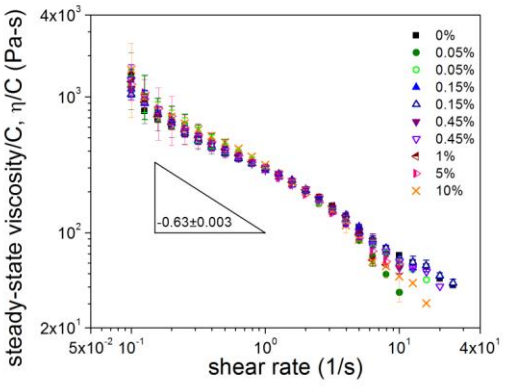

b)

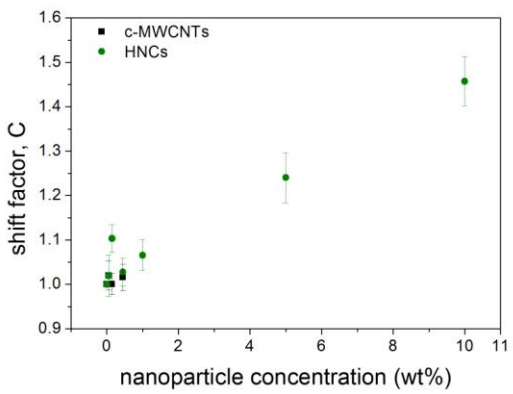

Figure 5.28 Master curve of the flow curves of c-MWCNTs (open symbols) and HNCs (full symbols) loaded LC HPC/AA aqueous solutions.

5.5 Conclusions

The c_{IN} and c_N transitions, characteristic of a LC phase were significantly improved with a high particle loading (HNC/HPC solutions). A viscosity decrease was obtained at low particle loading, independent of the length of the nanoparticles. ζ-potential measurements demonstrated the wrapping of the nanoparticles by the polymer molecules. POM measurements suggest that the polymer shell around the HNCs have a preferential order on a macroscopic scale. In the case of the c-MWCNTs the polymer shell may be randomly oriented or oriented on a nano-scale. The viscosity and viscoelastic properties of the neat LCP matrix were improved by HNCs loadings higher than 1 wt%.

Chapter 6

EXPERIMENTAL RESULTS: ELECTRORHEOLOGY

6.1 Introduction

The loading effect on the steady-state and dynamic electrorheological properties of both a non-electrorheological and an electrorheological matrix will be evaluated and discussed. Also, the electric field effect on quiescent LCP textures corresponding to a non-electrorheological matrix was determined by POM measurements. Finally, the loading effect on the ER properties of PHIC, an ER matrix, was predicted using Tse and Shine modification to the two-dimensional approximation developed by Marrucci and Maffettone.

6.2 Non-Electrorheological Matrix

The steady-state and dynamic ER properties of MWCNT loaded HPC solutions will be discussed in this section. Moreover, the electric field effect on quiescent textures of LC suspensions will be determined.

6.2.1 Steady State Rheology

Transient experiments at constant temperature, 25 ºC, were performed at a constant shear rate, 1 s^{-1}, to obtain the electrorheological behavior of neat and loaded HPC/*m*-cresol solutions, a non electrorheological matrix. The steady-state viscosity was obtained for neat and loaded solutions by averaging plateau measurements over an interval of at least 60-seconds. Error bars correspond to the standard deviation.

The effect of an applied external DC electric field on the steady-state viscosity was elucidated for an HPC solution without and with MWCNTs (Figure 6.1). The neat HPC solution was expectedly observed to be non-responsive to electric fields, since no significant change in the viscosity was measured. On the other hand, the particle loaded solutions showed a decrease in the viscosity, i.e. negative ER effect, with increasing field strength (significantly at field strength higher than 0.5 MV/m). Thus, electric field response is mainly attributed to the nanorod inclusions. An immediate effect was obtained for the 1 wt% MWCNT loaded solution at lower fields. However, the viscosity at a field of 2 MV/m has decreased approximately 92% from that at zero-field, for all the cases.

Two opposite forces, a shear and an electric field force, were acting over the sample. So, to verify if the observed phenomena was as a result of the orientation of the nanoparticles and polymer molecules along the flow direction, the shear rate effect on the electrorheological behavior of 1 wt% loaded HPC/*m*-cresol solutions was determined. As it is shown in the Figure 6.2, a negligible effect in the steady-state viscosity was observed with the application of an external electric field at higher shear rates. This indicates that the negative effect is not due to orientation along the flow direction. In homogeneous ER fluids, high shear forces dominate the orientation of the director, while in the case of heterogeneous ER fluids, shear forces dominate and prevent chain-formation perpendicular to flow.

A negative ER effect on the storage modulus of the carbon nanotube suspensions in silicone oil which disappears as electric field increases was reported by Lozano and coworkers [114]. The effect was attributed to the formation of layered nanostructures, which decrease the modulus, followed by migration of particles to the

electrodes and formation of column-like structures along the electrodes, which in turn increases the storage modulus. Park and coworkers oriented single wall carbon nanotubes (SWNT) through the use of an AC electric field in a photopolymerizable matrix [102]. It was proposed that the SWNT not only aligned with the field, but also migrated laterally to form thick columns between the electrodes.

In both reports, lower field strengths than those from our ER experiments were associated with the formation of the chain-like structures. Nevertheless, our results show a negative change in viscosity over the whole field range. There were no discernible chain-like structures or particle migration to the naked eye. The negative ER effect may be due to formation of small aggregates or bundles and further orientation of those aggregates preferentially along the electric field direction. These phenomena may cause a distortion of the liquid crystal phase, displacing it into the biphasic regime. If this hypothesis is correct, the negative ER effect may be eliminated or decreased when a higher polymer concentration is used.

The polymer concentration effect on the electrorheological behavior of 0.05 wt% MWCNT loaded HPC/*m*-cresol solution was determined, and illustrated in the Figure 6.3. The steady-state viscosity was not significantly affected by the application of an electric field for a solution with a higher polymer concentration or/and nematic potential. It suggests that the high viscosity of the polymer solution hinders the bundling and/or preferential orientation of the nanotubes along the electric field direction.

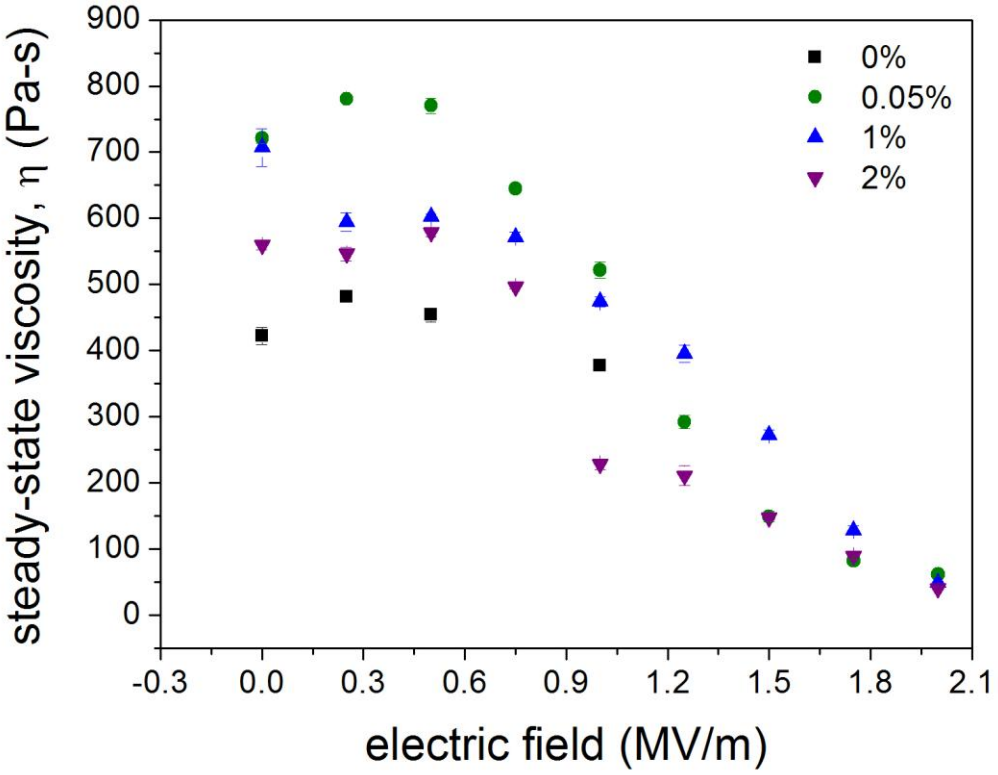

Figure 6.1 Effect of MWCNT loading effect on the steady-state viscosity of a 45 wt% HPC in *m*-cresol solution under an applied external electric field (DC) at constant temperature and shear rate of 25 °C and 1 (1/s), respectively.

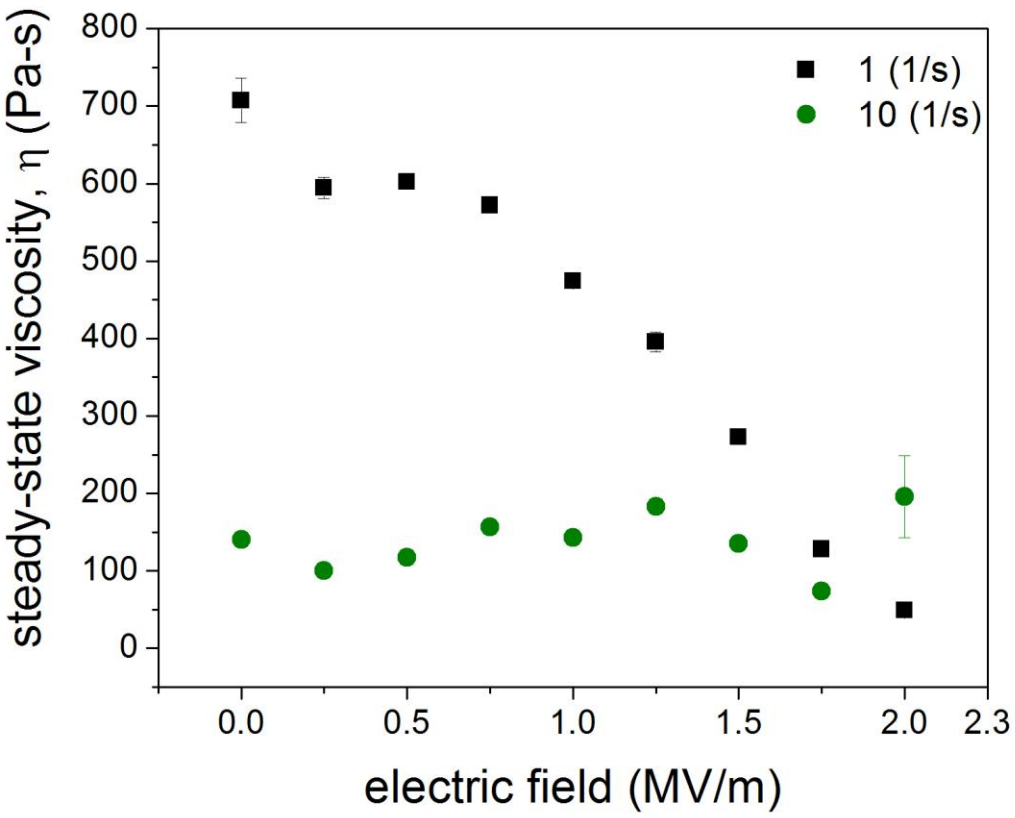

Figure 6.2 Shear rate effect on the electrorheological behavior of 1 wt% MWCNT/45 wt% HPC in *m*-cresol solution at 25 °C.

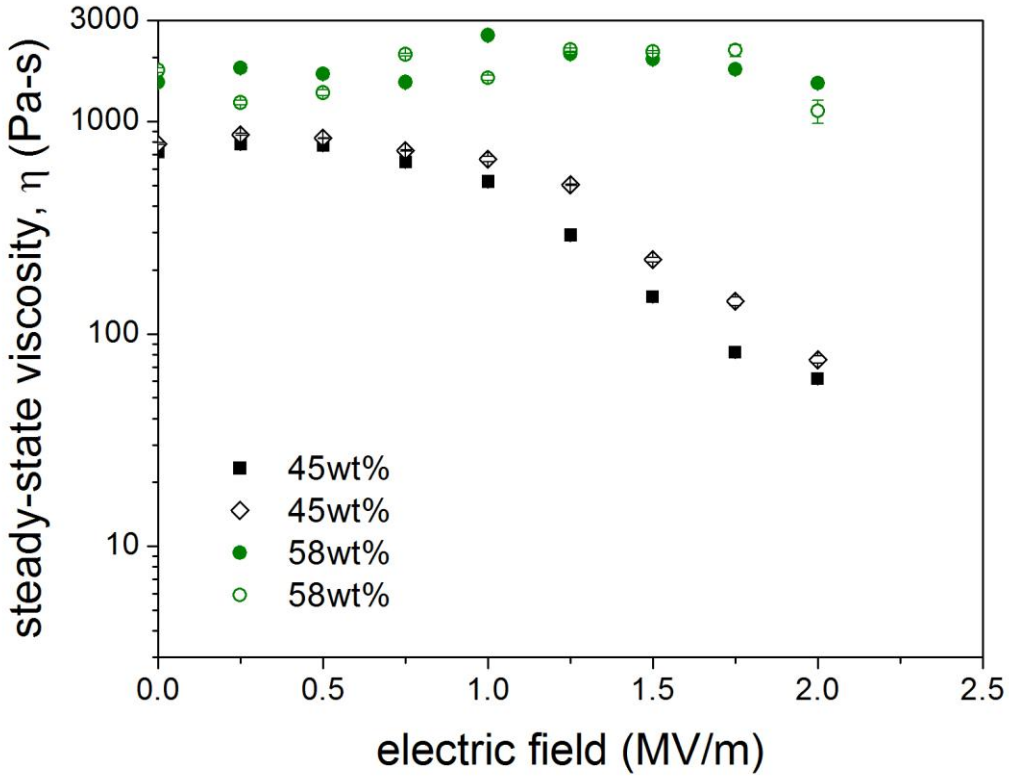

Figure 6.3 Polymer concentration effect on the electrorheological behavior of 0.05 wt% MWCNTs/HPC/*m*-cresol solutions at constant temperature and shear rate of 25 °C and 1 (1/s), respectively.

To verify if the nanotubes were oriented by the electric field, the drawn current was recorded during the transient experiment at constant shear and electric field strength. Figure 6.4 shows the drawn current as a function of time for 0.05 wt% MWCNTs/45 wt% HPC/*m*-cresol at different voltages. The maximum current that could be measured by the equipment is 2000 μA. The drawn current could not be measured, due to the instrument limitation, at a specific range of time for voltages greater than 1kV; samples for which a dramatic increase in the current was observed after it reaches a minimum value. Local maximum and minimum currents were

observed independent of the electric field strength at very short times. For voltages less than 1.2kV (1.5MV/m), an increase in the current with voltage was observed and a steady-state value was measured. For higher voltages, the current seems to steeply increase with time without reaching a measurable steady-state value. This behavior could suggest the orientation of the CNTs along the electric field strength as suggested by Lozano, Park and their respective coworkers [102, 114].

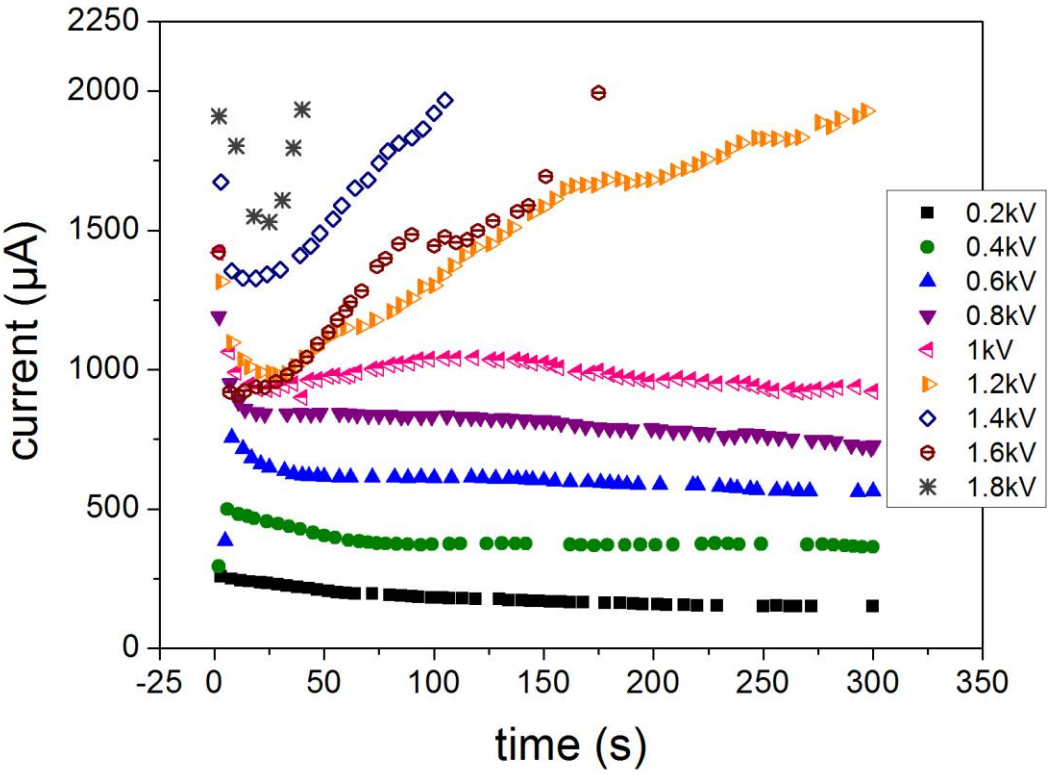

Figure 6.4 Change of drawn current over time for 0.05 wt% MWCNT-loaded HPC/*m*-cresol dispersions during the application of a constant shear rate of 1 (1/s) and a constant voltage at 25 °C and a gap of 0.8mm.

6.2.2 Polarized Optical Microscopy

The effect of the electric field application on quiescent liquid crystalline textures and MWCNT bundles position was determined at room temperature and constant electric field strength to prove the proposed hypothesis. The optical study was conducted at very low particle concentrations (0.05 wt%) to allow direct observation between the polarizer in transmitted mode. Figure 6.5 illustrates the liquid crystalline textures at electric field strength of 0.25 (left) and 0.5 (right) MV/m over a time interval of 5 min. No discernible change in the liquid crystalline texture of 0.05 wt% MWCNT dispersions was observed over a time interval of 5 minutes for electric field strengths below 0.5 MV/m. Neither particle aggregation nor migration of the focused MWCNT bundles was observed. Slight changes on the textures were observed after four minutes when electric field strength of 0.5MV/m was applied. Yet, displacement of bundles was not recorded.

The drawn current is shown in Figure 6.6 for all the analyzed samples. The meager quantitative reproducibility was due to the intentional poor dispersion of the tested samples. Since current is inversely proportional to resistance, an increase in current correlates to a decrease in resistance and vice-versa. No significant changes were observed for a 0.1 MV/m field. For 0.25MV/m, a subtle increase in the current is observed in the first 30 seconds, but it decreases again until it reaches a steady-state. The initial increase of the current is more pronounced at 0.5 MV/m, where it reaches a maximum at 45 seconds and then it decreases. This initial increase in current may be associated with a decrease in resistance which in turn suggests orientation. The decrease may be associated with migration of particles with diminish the effective electron paths across the electrodes. These changes support the proposed mechanism

of Lozano and coworkers [114]. Nevertheless, these changes may be happening at a nano-scale since there were no changes or displacement of the CNTs bundles.

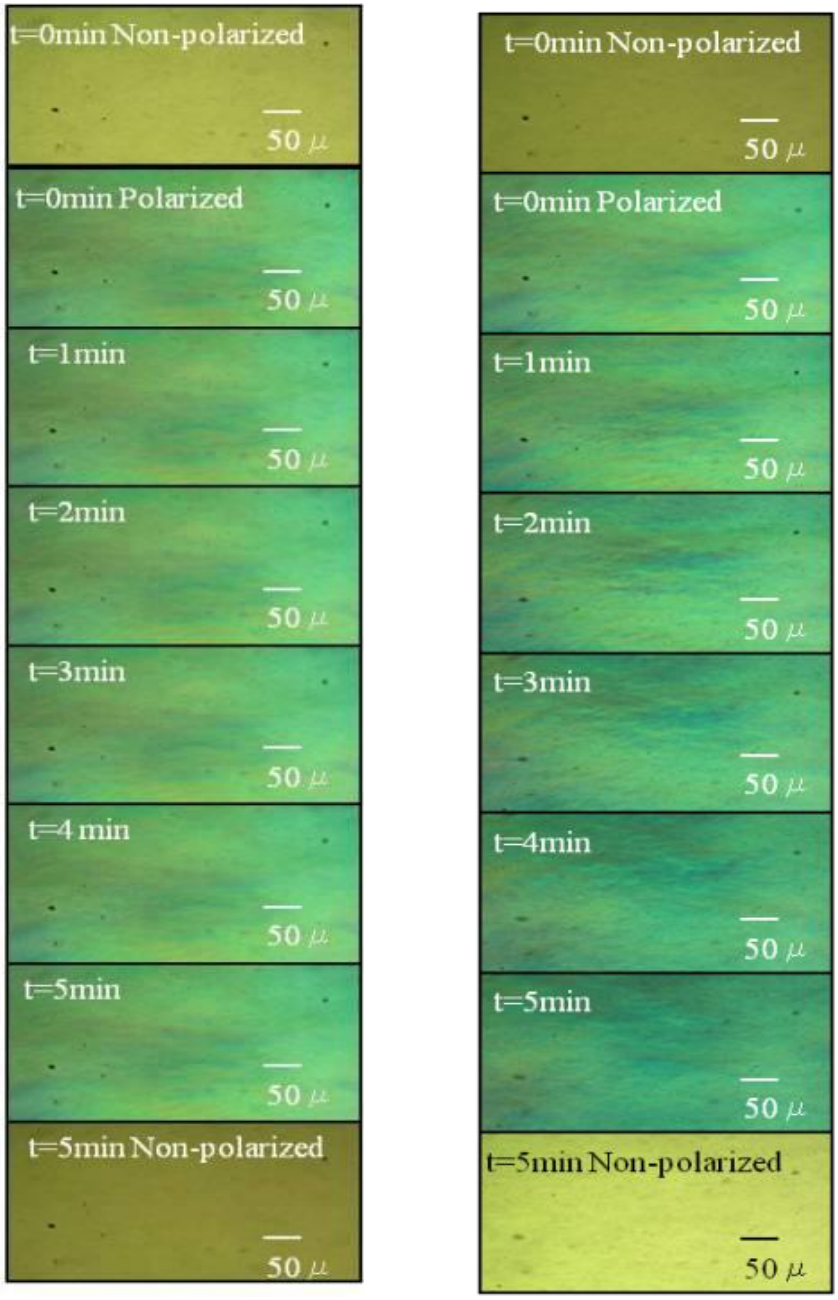

Figure 6.5 Liquid crystal textures of a 0.05wt% MWCNT in a 45wt% HPC in *m*-cresol solution at an applied electric field of 0.25 (left) and 0.5 (right) MV/m as a function of time.

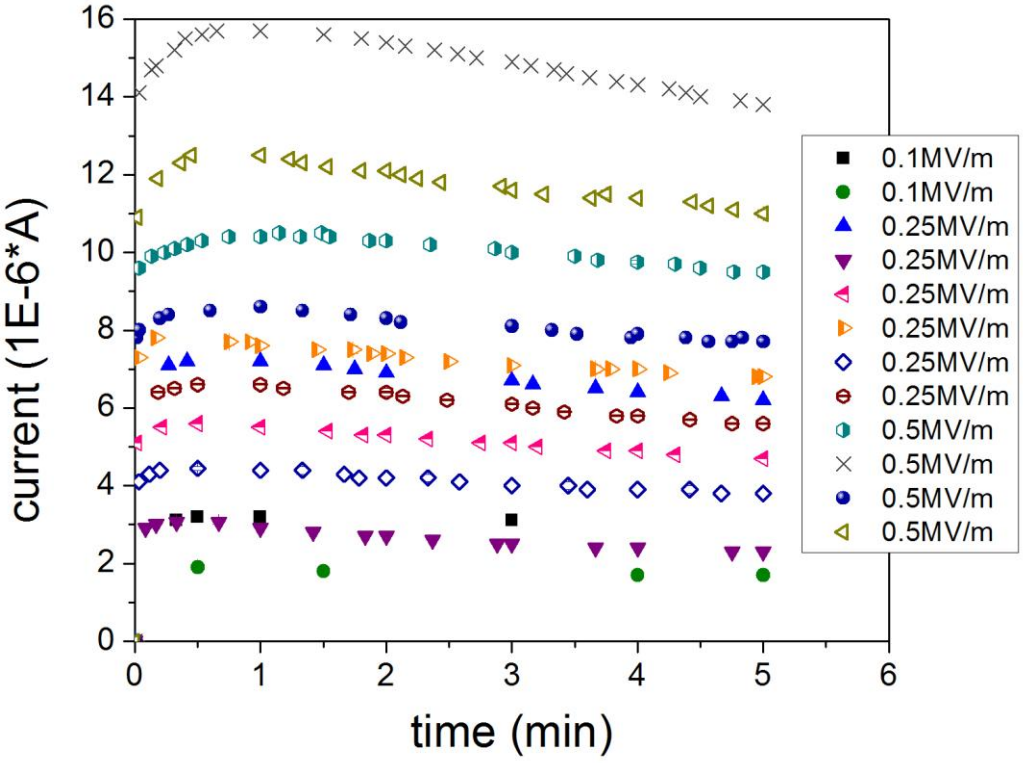

Figure 6.6 Change of drawn current over time for quiescent 0.05 wt% MWCNT-loaded 45 wt% HPC/*m*-cresol dispersions at room temperature and different electric field strengths.

6.2.3 Viscoelastic Properties

The MWCNTs loading effect on the viscoelastic properties of liquid crystalline 45wt%HPC/*m*-cresol solutions were determined at 25 °C and 0.5% of strain for a frequency range between 0.1 and 100 Hz. Figures 6.7 and 6.8 illustrate the electric field effect on the viscoelastic properties of 0.5 wt% and 1 wt% MWCNTs loaded liquid crystalline HPC/*m*-cresol solutions, respectively. No significant effect was observed by the application of electric fields with strength lower than 2 MV/m, independent of the nanoparticle concentration. A solid-like solution was obtained at the highest frequency, independently of the nanoparticle concentration and electric

field strength. However, some features could be distinguished for the 0.5 wt% loaded solution with the application of a higher electric field: (1) both viscoelastic moduli were independent of frequency for frequencies lower than 1 Hz, suggesting the presence of a percolated system; (2) a decrease of both moduli was observed for the frequency range studied with the application of the electric field; (3) an elastic or a solid-like solution (the storage modulus is higher than the loss modulus) was obtained at low frequencies (lower than 1 Hz).

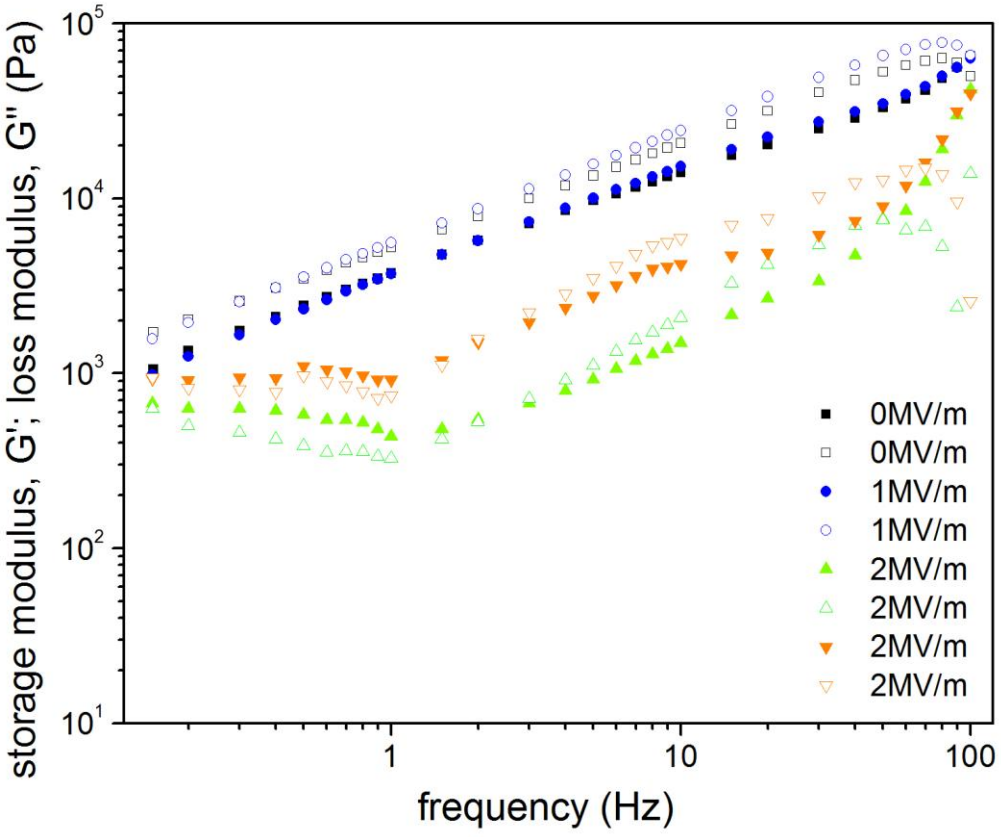

Figure 6.7 Electric field effect on the viscoelastic properties of 0.5 wt% MWCNTs/ 45 wt% HPC/*m*-cresol solutions at a strain of 0.5% and 25 °C

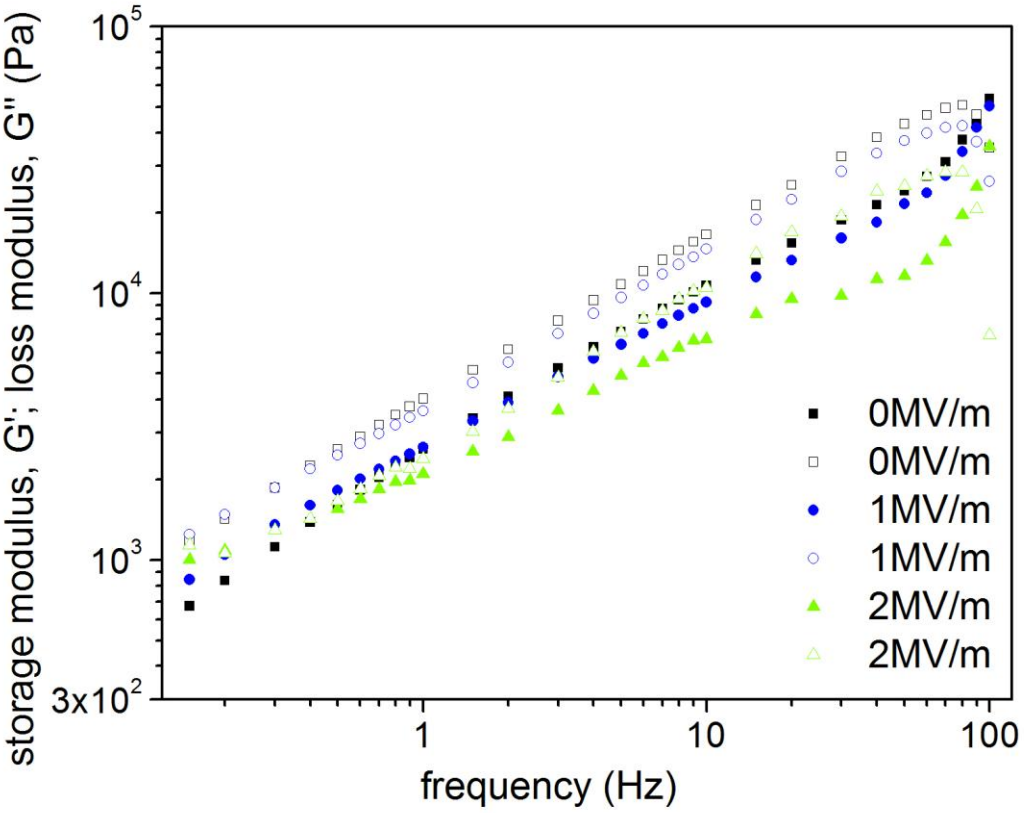

Figure 6.8 Electric field effect on the viscoelastic properties of 1 wt% MWCNTs/ 45 wt% HPC/*m*-cresol solutions at a strain of 0.5% and 25 °C

6.3 Electrorheological Matrix

In this section, the electric field effect on the steady-state electrorheological viscosity will be experimentally determined and theoretically predicted using the Tse and Shine modification to the two-dimensional approach developed by Marrucci and Maffettone.

6.3.1 Theoretical Predictions

The electrorheological behavior of bimodal PHIC solutions has been predicted a priori using the average molecular parameters of the blends and the rotational

diffusivity equation defined by Doi for monodispersed rods. The β constant was found to be 88 for bimodal PHIC solutions [82]. This has been demonstrated to be an effective method to obtain, qualitatively, the basic features of the steady-state electrorheology for blends with a low concentration of a high molecular weight sample. Consequently, it should be a feasible method to predict the effect of nanotube loading on the steady-state electrorheological behavior of PHIC solutions.

The effect of nanotube loading on the steady-state electroviscosity of PHIC solutions was modeled using the Tse modified version of the two dimensional approximation of Marrucci and Maffettone. The system was modeled as a pseudo-polydisperse system. Rod parameters such as density, moment dipole, diameter, and length were obtained using a linear mixing rule. A permanent dipole magnitude with a magnitude equal to 0.01D= 3.33564E-32 C-m was assumed for the carbon nanotubes [175]. PHIC parameters such as its molecular weight, isotropic to nematic concentration transition, and the initial concentration to a completely liquid crystal phase were determined experimentally. The viscosity of *p*-xylene at 25°C was approximate to 0.604mPa-s [176]. The isotropic-nematic phase transition of the pseudo-polydisperse systems of rods were assumed to be the values experimentally founded for neat PHIC solutions, based on experimental results (previously discussed) which demonstrated that it was not significantly affected with carbon nanotube addition (up to 1 wt%).

The rotational diffusivity equation, previously presented, applies for Brownian rod-like molecules. However, rod-like particles with a length greater than 10μm could be considered as non-Brownian rods [32]. The rotational Peclet number (Pe), a dimensionless number, controlled the transition from a Brownian to non-Brownian

behavior of rod-like particles in a flowing suspension $\left(Pe \equiv \frac{\dot{\gamma}}{D_r}\right)$. A particle could be considered as non Brownian under conditions of Pe significantly greater than 1. For model purposes, a Pe higher than 100 was chosen as the critical number in which the system was considered as one of non-Brownian rods.

Folgar and Tucker developed a phenomenological theory in which an effective rotary diffusive process takes in account the fiber-fiber interactions [177]. They define the rotary diffusivity as a linear function of the shear rate. The proportionality constant is called the "Folgar-Tucker constant". Koch calculates an orientational rotary diffusivity using a more rigorous theory [178]. The Folgar-Tucker constant obtained from the Koch's analysis was estimated for shear oriented rods as:

$$\frac{6 \times 10^{-3} \nu L^3}{\left(L/d\right) \ln^2(L/d)} \tag{6.1}$$

This constant was used to obtain D_r for non-Brownian rods.

6.3.1.1 Rod-like Nanoparticle Length and Concentration Effect

The nanoparticle (NP) concentration and length effect on the steady-state electroviscosity of 34 wt% PHIC/*p*-xylene solutions was predicted for constant shear rate and temperature equal to 2 (1/s) and 25°C, respectively (Figure 6.9). PHIC molecules length is on the order of 10^{-1} μm and rod-like nanoparticles, commercially available, have a length on the order of 10^{1} μm. Based on that, the studied lengths were 0.5, 1, 5, and 10μm. A constant diameter of 1.5nm, similar to the diameter of the PHIC molecules, was chosen.

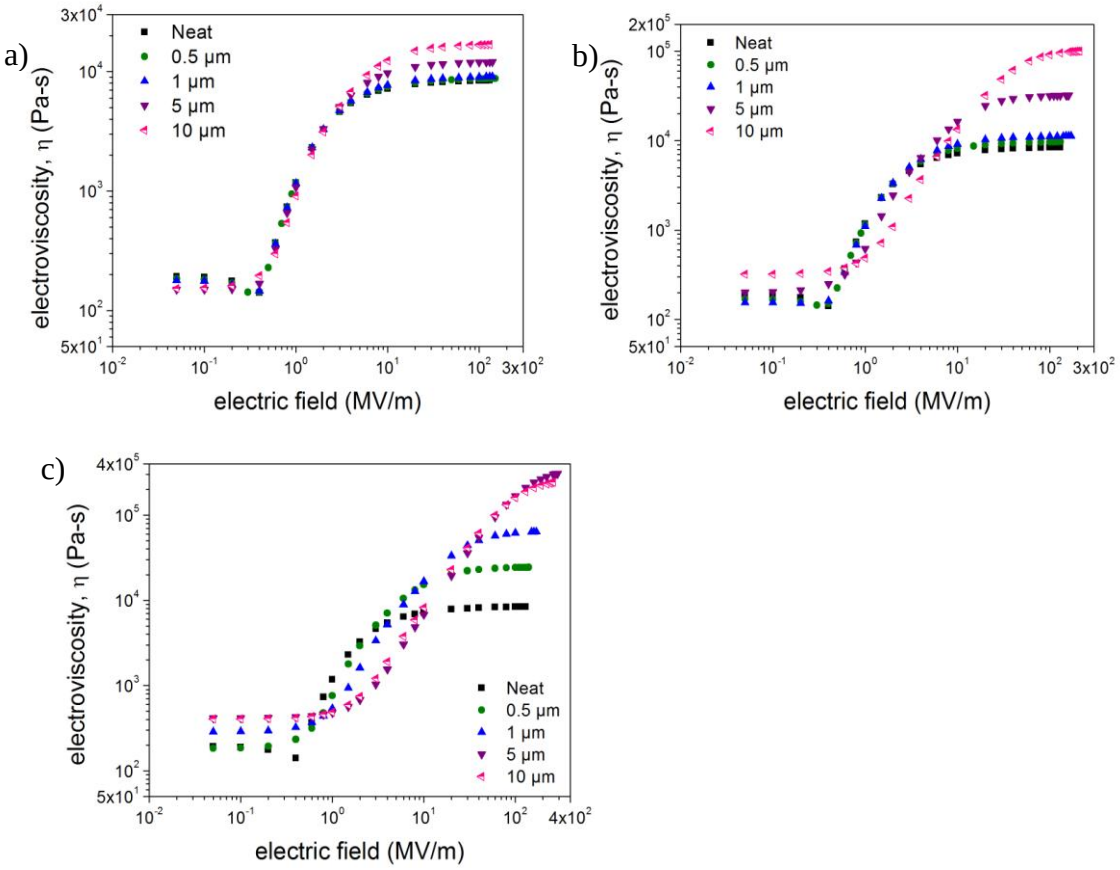

Figure 6.9: Rod-like nanoparticle length effect on the steady-state electrorheological behavior of 34 wt% PHIC/*p*-xylene solutions at 25°C and 2 (1/s) for rod's concentrations of 0.03 (a), 0.12 (b), and 0.96 wt% (c)

Concentrations less than 0.96 wt% of nanoparticles with a length less than 5 μm did not affect the electrorheological behavior of the neat matrix. A concentration equal to 0.96 wt% was found to increase the maximum viscosity and to move the last viscosity plateau at higher electric field strengths, independently of the rod's length. A similar behavior was observed for rod lengths greater than 1μm with nanoparticle inclusion. In addition for 0.96 wt% of NPs with L = 5 and 10 μm, and 0.12 wt% of NPs with L = 10 μm, higher electric fields should be applied to begin the orientation

with the electric field, which seems to be a slower process. Solutions with 0.96 wt% of nanoparticles with length equal and greater than 5μm behave as non-Brownian (NB) rods. In summary, longer rods are more difficult to orient in the electric field direction, but a higher maximum viscosity, up to one order of magnitude more than the value obtained for the neat matrix, could be obtained at higher electric fields.

On the other hand, the nanoparticle concentration effect on the steady-state electroviscosity at zero-field was elucidated for both single and bundles of NPs with the similar properties to the i-MWCNTs experimentally used. Figures 6.10a and 6.10b shows the effect of adding nanoparticles with a diameter and length equal to 8 or 48 nm and 20μm, respectively to a 34 wt% PHIC/*p*-xylene at different shear rates at zero electric field. There is an increase in the electroviscosity with particle addition up to 0.12 wt% (concentration at which the rods begin to behave as non-Brownian rods) when a shear rate of 2 (1/s) was applied, irrespective of the diameter of the nanoparticles. A further increase in nanoparticle concentration did not seem to have a significant effect on the viscosity up to concentrations greater than 4wt%. The plateau viscosity was obtained at smaller concentrations when higher shear rates were applied. Therefore, the nanotube diameter did not change significantly the rheological behavior of rod-like polymers.

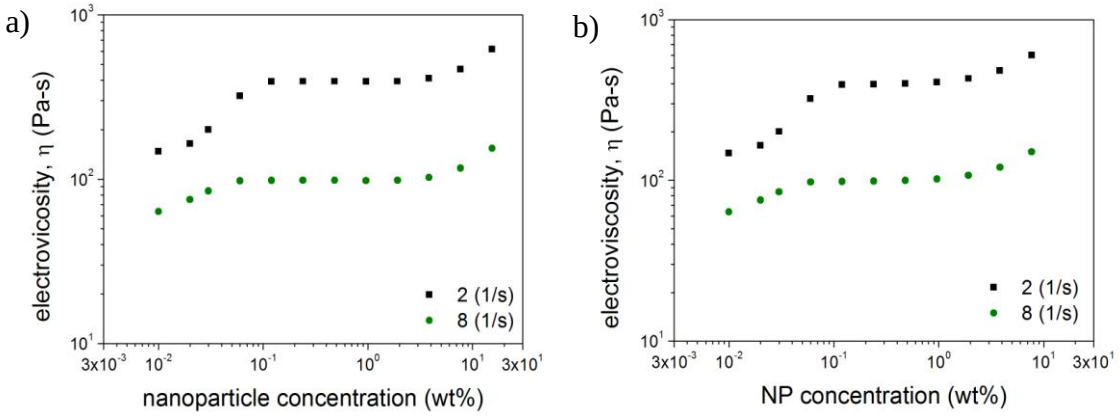

Figure 6.10: Nanoparticle concentration effect on the steady-state electroviscosity of 34 wt% PHIC/*p*-xylene solutions at different shear rates (2 (1/s) – black squares and 8 (1/s) green circles) and 25°C at zero electric field for single-nanotubes (d=8m) (a) and bundles (d=48nm) (b)

The loading effect on the electrorheological behavior of 34wt% PHIC/*p*-xylene solutions was experimentally determined and theoretically predicted at 25°C and 1(1/s). As Figure 6.11 shows, a qualitative agreement between the experimental and the predicted data was obtained. The electroviscosity of the neat matrix was not significantly affected with the inclusion of a small nanoparticle concentration.

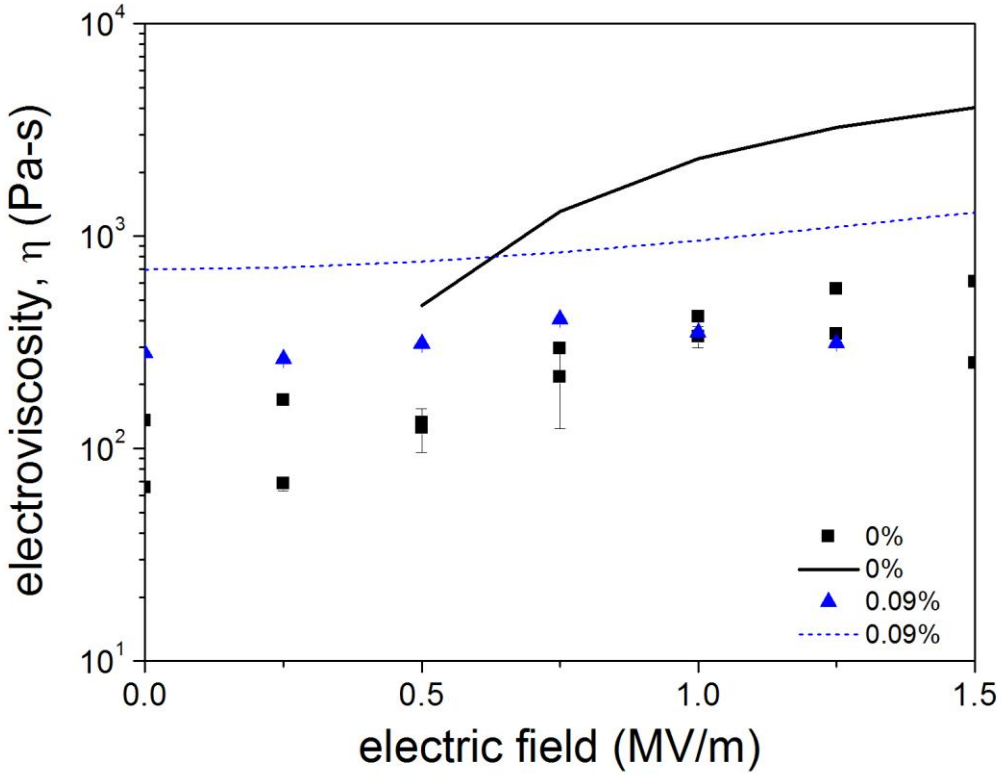

Figure 6.11 Electrorheological behavior of neat and 0.09wt% i-MWCNTs PHIC/*p*-xylene solutions at 25°C and 1(1/s); lines and symbols represent the predicted and experimental values, respectively.

6.4 Conclusions

The electrorheological properties of PHIC do not change significantly with particle loading in the experimental window. A negative ER effect (viscosity decrease) was obtained with particle inclusion up to 2 wt% when a non-responsive matrix was used. The results suggest an aggregation of the carbon nanotubes due to the application of an external DC electric field. Consequently, the addition of carbon nanotubes do not seems to have a positive impact on electrorheological applications under the experimental window.

CONCLUSIONS

A well-dispersed solution and attractive interactions between the polymer molecules and the nanoparticles are important parameters that should be considered when working with composite material. The incorporation of a high concentration of well-disperse anisotropic rod-like nanoparticles promote the formation of a liquid crystalline phase around the surface of the nanoparticles (a liquid crystal phase is obtained using a smaller polymer concentration). A composite material containing well-dispersed rod-like nanoparticles up to 0.45wt% may be developed without affecting the characteristic structure of the liquid crystalline phase. Well-disperse nanoparticles may be incorporated and oriented along the nematic director without affect the microstructural rearrangements of liquid crystalline polymer molecules. Molecular theories such as Doi-Edwards molecular theory may be used to predict the rheological properties of liquid crystalline polymers loaded with rod-like nanoparticles since the polymer dynamics is governed by the polymer molecules using effective average properties.

Core-shell structures may be obtained with the incorporation of well-dispersed nanoparticles that have attractive interactions with the polymer molecules. Consequently, an isotropic solution with low particle concentrations may be processed using a smaller stress.

The application of an electric field is not a feasible method to control the orientation of a non- electrorheological liquid crystalline polymer solution containing carbon nanotubes since it promotes the agglomeration of the nanoparticles. The electrorheological properties of an electrorheological liquid crystalline polymer

solution loaded a small concentration of rod-like nanoparticle (less than 1 wt%) may improve when electric fields with strength higher than 10MV/m is applied.

Future experiments involving the processing and characterization of the composite materials may be useful to complement this research work. Based on the experimental results, an electro-spinning process may be a useful way to develop aligned and reinforced materials working with an isotropic polymer solution loaded with a low nanoparticle concentration.

REFERENCES

1. Biercuk, M.J., et al., *Carbon nanotube composites for thermal management.* Applied Physics Letters, 2002. **80**(15): p. 2767.
2. Kim, H.-S., et al., *Thermal Properties of Poly(ε-Caprolactone)/Multiwalled Carbon Nanotubes Composites.* Advanced Composite Materials, 2008. **17**(2): p. 157-166.
3. Bonnet, P., et al., *Thermal properties and percolation in carbon nanotube-polymer composites.* Applied Physics Letters, 2007. **91**(20): p. 201910.
4. Wen, Z., et al., *Thermal, electrical, and mechanical properties of composite polymer electrolytes based on cross-linked poly(ethylene oxide-co-propylene oxide) and ceramic filler.* Solid State Ionics, 2003. **160**(1-2): p. 141-148.
5. Cadek, M., et al., *Mechanical and Thermal Properties of CNT and CNF Reinforced Polymer Composites.* AIP Conference Proceedings, 2002. **633**(1): p. 562.
6. Wenqing, J., et al., *Carbon Nanotubes Incorporated within Lyotropic Hexagonal Liquid Crystal Formed in Room-Temperature Ionic Liquids.* Langmuir, 2007. **23**(16): p. 8549-8553.
7. Allaoui, A., et al., *Mechanical and electrical properties of a MWNT/epoxy composite.* Composites Science and Technology, 2002. **62**(15): p. 1993-1998.
8. Kumar, H. and Siddaramaiah, *Study of Chemical and Tensile Properties of PU and PU/PS Coated Bamboo Fibers.* Polymer-Plastics Technology & Engineering, 2005. **44**(7): p. 1369-1377.
9. Ounaies, Z., et al., *Electrical properties of single wall carbon nanotube reinforced polyimide composites.* Composites Science and Technology Modeling and Characterization of Nanostructured Materials, 2003. **63**(11): p. 1637-1646.
10. Du, F., et al., *Nanotube Networks in Polymer Nanocomposites: Rheology and Electrical Conductivity.* Macromolecules, 2004. **37**(24): p. 9048-9055.
11. Pötschke, P., T.D. Fornes, and D.R. Paul, *Rheological behavior of multiwalled carbon nanotube/polycarbonate composites.* Polymer, 2002. **43**(11): p. 3247-3255.
12. Fan, Z.H. and S.G. Advani, *Rheology of multiwall carbon nanotube suspensions.* Journal of Rheology, 2007. **51**(4): p. 585-604.
13. Busick, D.N., R.J. Spontak, and C.M. Balik, *Effects of graphite content on the morphology and barrier properties of poly(vinylidene fluoride) composites.* Polymer, 1999. **40**(22): p. 6023-6029.

14. Bharadwaj, R.K., et al., *Structure-property relationships in cross-linked polyester-clay nanocomposites.* Polymer, 2002. **43**(13): p. 3699-3705.
15. Manias, E., et al., *Intercalation kinetics of long polymers in 2 nm confinements.* Macromolecules, 2000. **33**(21): p. 7955-7966.
16. Krishnamoorti, R., R.A. Vaia, and E.P. Giannelis, *Structure and Dynamics of Polymer-Layered Silicate Nanocomposites.* Chemistry of Materials, 1996. **8**(8): p. 1728-1734.
17. DuPont. *Aircraft/Aerospace*. 2010 [cited 2010 March 29, 2010]; Available from: http://www2.dupont.com/Aircraft_Aerospace/en_US/.
18. Hartmann, V., et al., *Effects of particles on the steady state and transient rheology of lyotropic hydroxypropylcellulose solutions.* Journal of Rheology, 2000. **44**(6): p. 1417-1432.
19. Moldenaers, P., et al., *Effect of fillers on the steady state rheological behaviour of liquid crystalline polymers.* Rheologica Acta, 1998. **37**(5): p. 463-469.
20. Hoekstra, H., et al., *Rheology and Structure of Suspensions in Liquid Crystalline Hydroxypropylcellulose Solutions.* Langmuir, 2002. **18**(15): p. 5695-5703.
21. Evmenenko, G., et al., *Structural reorganization in films of cellulose derivatives in the presence of colloidal particles.* Polymer, 2004. **45**(18): p. 6269-6273.
22. Duran, H., et al., *Effect of carbon nanotubes on phase transitions of nematic liquid crystals.* Liquid Crystals, 2005. **32**(7): p. 815-821.
23. Santiago-Quinones, D.I., A. Acevedo, and C. Rinaldi, *Magnetic and magnetorheological characterization of a polymer liquid crystal ferronematic.* Journal of Applied Physics, 2009. **105**(7).
24. Baik, I.S., et al., *Electrical-field effect on carbon nanotubes in a twisted nematic liquid crystal cell.* Applied Physics Letters, 2005. **87**(26).
25. Goncharuk, A.I., et al., *Aggregation, percolation and phase transitions in nematic liquid crystal EBBA doped with carbon nanotubes.* Journal of Physics D-Applied Physics, 2009. **42**(16).
26. Lisetski, L.N., et al., *Dispersions of multiwalled carbon nanotubes in different nematic mesogens: The study of optical transmittance and electrical conductivity.* Physica E-Low-Dimensional Systems & Nanostructures, 2009. **41**(3): p. 431-435.
27. Jiang, W., et al., *Carbon Nanotubes Incorporated within Lyotropic Hexagonal Liquid Crystal Formed in Room-Temperature Ionic Liquids.* Langmuir, 2007. **23**(16): p. 8549-8553.
28. Weiss, V., R. Thiruvengadathan, and O. Regev, *Preparation and Characterization of a Carbon Nanotube-Lyotropic Liquid Crystal Composite.* Langmuir, 2006. **22**(3): p. 854-856.
29. Dierking, I., *Textures of Liquid Crystals* First ed. 2003: Wiley-VCH Verlag GmbH and Company. 218.

30. Singh, S., *Liquid Crystals: Fundamentals (Foreword by Davis A. Dunmur)*. First ed. 2002: World Scientific Publishing Company. 531.
31. Chung, T.-S., ed. *Thermotropic Liquid Crystal Polymers: Thin-film Polymerization, Characterization, Blends, and Applications* First ed. 2001, Technomic Publishing Company, Inc. 364.
32. Larson, R.G., *The structure and Rheology of Complex Fluids*. 1999, New York: Oxford University Press Inc.
33. Huang, C.M., J.J. Magda, and R.G. Larson, *The effect of temperature and concentration on N-1 and tumbling in a liquid crystal polymer.* Journal of Rheology, 1999. **43**(1): p. 31-50.
34. Gabor, K. and S.P. Roger, *Rheology of concentrated solutions of poly(gamma-benzyl-glutamate).* Journal of Polymer Science: Polymer Symposia, 1978. **65**(1): p. 193-211.
35. Moldenaers, P. and J. Mewis, *Transient Behavior of Liquid Crystalline Solutions of Poly(benzylglutamate).* Journal of Rheology, 1986. **30**(3): p. 567-584.
36. Grizzuti, N., S. Cavella, and P. Cicarelli, *Transient and steady-state rheology of a liquid crystalline hydroxypropylcellulose solution.* Journal of Rheology, 1990. **34**(8): p. 1293-1310.
37. Moldenaers, P. and J. Mewis, *Relaxational phenomena and anisotrophy in lyotropic polymeric liquid crystals.* Journal of Non-Newtonian Fluid Mechanics, 1990. **34**(3): p. 359-374.
38. Picken, S.J., et al., *Structure and rheology of aramid solutions: transient rheological and rheooptical measurements.* Macromolecules, 1991. **24**(6): p. 1366-1375.
39. Walker, L.M., et al., *The rheology of highly concentrated PBLG solutions.* Journal of Rheology, 1995. **39**(5): p. 925-952.
40. Larson, R.G. and D.W. Mead, *The Ericksen number and Deborah number cascades in sheared polymeric nematics.* Liquid Crystals, 1993. **15**(2): p. 151-169.
41. Navard, P. and J.M. Haudin, *Rheology of Hydroxypropylcellulose Solutions.* Journal of Polymer Science Part B-Polymer Physics, 1986. **24**(1): p. 189-201.
42. Walker, L. and N. Wagner, *Rheology of region I flow in a lyotropic liquid-crystal polymer: The effects of defect texture.* Journal of Rheology, 1994. **38**(5): p. 1525-1547.
43. Viale, S., E. Mendes, and S. Picken, *A Direct Observation by XRD of Reorientation in a Supramolecular Liquid Crystal Polymer Induced by Magnetic Field.* Molecular Crystals & Liquid Crystals, 2005. **437**(1): p. 43-52.
44. T. J. Menna, F.E.F., *Effect of high electric fields on the isotropic phase of a lyotropic liquid-crystalline system.* Journal of Polymer Science Part B: Polymer Physics, 2004. **42**(22): p. 4116-4125.

45. Halamus, T., P. Wojciechowski, and I. Bobowska, *Synthesis and characterization of (hydroxypropyl)cellulose/TiO2 nanocomposite films.* Polymers for Advanced Technologies, 2008. **19**(7): p. 807-811.
46. Wojciechowski, P.H., T. ; Pietsch, U., *Mesomorphic organisation of (2-hydroxypropyl)cellulose under the influence of silica networks.* Materials Science-Poland, 2006. **24**(2/2): p. 507-516.
47. Antypov, D. and D.J. Cleaver, *Orientational and phase-coexistence behaviour of hard rod-sphere mixtures.* Chemical Physics Letters, 2003. **377**(3-4): p. 311-316.
48. Tian, P. and G.D. Smith, *Molecular dynamics simulations of nanoparticles in dense isotropic nematogens: The role of matrix-induced long-range repulsive interactions.* Journal of Chemical Physics, 2006. **124**(18).
49. Koda, T., M. Numajiri, and S. Ikeda, *Smectic-A phase of a bidisperse system of parallel hard rods and hard spheres.* Journal of the Physical Society of Japan, 1996. **65**(11): p. 3551-3556.
50. Lee, K.J., et al., *The influence of carbon fiber orientation on the mechanical and tribological behavior of carbon fiber/LCP composites.* Materials Chemistry and Physics, 2007. **102**(2-3): p. 187-194.
51. Wang, X., et al., *Synthesis and characterization of thermotropic liquid crystalline polyester/multi-walled carbon nanotube nanocomposites.* Applied Surface Science, 2010. **256**(6): p. 1739-1743.
52. Hu, W.-Q., et al., *Synthesis and characterization of rodlike liquid crystalline polyester/multi-walled carbon nanotubes and study of their thermal stability.* Applied Surface Science, 2011. **258**(1): p. 507-512.
53. Kim, J.Y., D.K. Kim, and S.H. Kim, *Effect of modified carbon nanotube on physical properties of thermotropic liquid crystal polyester nanocomposites.* European Polymer Journal, 2009. **45**(2): p. 316-324.
54. Scalia, G., et al., *Effect of phenyl rings in liquid crystal molecules on SWCNTs studied by Raman spectroscopy.* physica status solidi (b), 2006. **243**(13): p. 3238-3241.
55. Lebovka, N., et al., *Phase transitions, intermolecular interactions and electrical conductivity behavior in carbon multiwalled nanotubes/nematic liquid crystal composites.* Journal of Molecular Structure, 2008. **887**(1-3): p. 135-143.
56. Ji, Y., Y.Y. Huang, and E.M. Terentjev, *Dissolving and Aligning Carbon Nanotubes in Thermotropic Liquid Crystals.* Langmuir, 2011. **27**(21): p. 13254-13260.
57. Basu, R. and G.S. Iannacchione, *Orientational coupling enhancement in a carbon nanotube dispersed liquid crystal.* Physical Review E, 2010. **81**(5).
58. Sigdel, K.P. and G.S. Iannacchione, *Effect of carbon nanotubes on the isotropic to nematic and the nematic to smectic- A phase transitions in liquid crystal and carbon nanotubes composites.* The European Physical Journal E C7 - 34, 2011. **34**(4): p. 1-9.

59. Zadoina, L., et al., *Liquid crystalline magnetic materials.* Journal of Materials Chemistry, 2009. **19**(43): p. 8075-8078.
60. Kumar, S. and H.K. Bisoyi, *Aligned Carbon Nanotubes in the Supramolecular Order of Discotic Liquid Crystals.* Angewandte Chemie International Edition, 2007. **46**(9): p. 1501-1503.
61. Kuhnast, M., C. Tschierske, and J. Lagerwall, *Tailor-designed polyphilic promotors for stabilizing dispersions of carbon nanotubes in liquid crystals.* Chemical Communications, 2010. **46**(37): p. 6989-6991.
62. Schymura, S., et al., *Towards Efficient Dispersion of Carbon Nanotubes in Thermotropic Liquid Crystals.* Advanced Functional Materials, 2010. **20**(19): p. 3350-3357.
63. Liu, Q., et al., *Self-Alignment of Plasmonic Gold Nanorods in Reconfigurable Anisotropic Fluids for Tunable Bulk Metamaterial Applications.* Nano Letters, 2010. **10**(4): p. 1347-1353.
64. Lagerwall, J., et al., *Nanotube Alignment Using Lyotropic Liquid Crystals.* Advanced Materials, 2007. **19**(3): p. 359-364.
65. Zhao, M., Y. Gao, and L. Zheng, *Lyotropic liquid crystalline phases formed in binary mixture of 1-tetradecyl-3-methylimidazolium chloride/ethylammonium nitrate and its application in the dispersion of multi-walled carbon nanotubes.* Colloids Surf A Physicochem Eng Asp, 2010. **369**(1-3): p. 95-100.
66. Xin, X., et al., *Single-Walled Carbon Nanotube/Lyotropic Liquid Crystal Hybrid Materials Fabricated by a Phase Separation Method in the Presence of Polyelectrolyte.* Langmuir, 2010. **26**(11): p. 8821-8828.
67. Xin, X., et al., *Incorporation of Carbon Nanotubes into a Lyotropic Liquid Crystal by Phase Separation in the Presence of a Hydrophilic Polymer.* Langmuir, 2010. **26**(5): p. 3562-3568.
68. Okano, K., I. Noguchi, and T. Yamashita, *Anisotropic Carbon Nanotube Films Fabricated from a Lyotropic Liquid-Crystalline Polymer.* Macromolecules, 2010. **43**(13): p. 5496-5499.
69. Tardani, F. and C. La Mesa, *Elasticity of Dispersions Based on Carbon Nanotubes Dissolved in a Lyotropic Nematic Solvent.* The Journal of Physical Chemistry C, 2011. **115**(19): p. 9424-9431.
70. Abe, A. and P.J. Flory, *Statistical Thermodynamics of Mixtures of Rodlike Particles .2. Ternary-Systems* Macromolecules, 1978. **11**(6): p. 1122-1126.
71. Speranza, A. and P. Sollich, *Simplified Onsager theory for isotropic-nematic phase equilibria of length polydisperse hard rods.* Journal of Chemical Physics, 2002. **117**(11): p. 5421-5436.
72. Speranza, A. and P. Sollich, *Isotropic-nematic phase equilibria in the Onsager theory of hard rods with length polydispersity.* Physical Review E, 2003. **67**(6).
73. Speranza, A. and P. Sollich, *Isotropic-nematic phase equilibria of polydisperse hard rods: The effect of fat tails in the length distribution.* The Journal of Chemical Physics, 2003. **118**(11): p. 5213-5223.

74. Varga, S., et al., *Nematic-nematic phase separation in binary mixtures of thick and thin hard rods: Results from Onsager-like theories.* Physical Review E, 2005. **72**(5): p. 051704.
75. Purdy, K.R., et al., *Nematic Phase Transitions in Mixtures of Thin and Thick Colloidal Rods.* Physical Review Letters, 2005. **94**(5): p. 057801.
76. Chen, Z.Y., *Effect of polydispersity on the isotropic-nematic phase transition of rigid rods* Physical Review E, 1994. **50**(4): p. 2849-2855.
77. Wensink, H.H. and G.J. Vroege, *Isotropic-nematic phase behavior of length-polydisperse hard rods.* Journal of Chemical Physics, 2003. **119**(13): p. 6868-6882.
78. Lekkerkerker, H.N.W., et al., *On the isotropic-liquid crystal phase separation in a solution of rodlike particles of different lengths.* The Journal of Chemical Physics, 1984. **80**(7): p. 3427-3433.
79. Itou, T. and A. Teramoto, *Multi-phase equilibrium in aqueous-solutions of the triple-helical polysaccharide, schizophyllan.* Polymer Journal, 1984. **16**(10): p. 779-790.
80. Itou, T. and A. Teramoto, *Triphase equilibrium in aqueous solutions of the rodlike polysaccharide schizophyllan.* Macromolecules, 1984. **17**(7): p. 1419-1420.
81. Sato, T., et al., *Phase equilibrium in ternary solutions containing two semiflexible polymers with different lengths.* Polymer, 1989. **30**(2): p. 311-316.
82. Acevedo, A., *Electrorheology of concentrated nematic solutions of rodlike polymers: Molecular weight and polydispersity dependence*, in *Department of Chemical Engineering*. 2006, University of Delaware: Newark, DE. p. 630.
83. Hine, P., et al., *Fibre orientation: measurement, modelling and knowledge based design.* Plastics, Rubber & Composites, 2005. **34**(9): p. 417-424.
84. Russell, J.M., et al., *Alignment of nematic liquid crystals using carbon nanotube films.* Thin Solid Films, 2006. **509**(1/2): p. 53-57.
85. Vigolo, B., et al., *Macroscopic Fibers and Ribbons of Oriented Carbon Nanotubes.* Science, 2000. **290**(5495): p. 1331-1334.
86. Zamora-Ledezma, C., et al., *Anisotropic Thin Films of Single-Wall Carbon Nanotubes from Aligned Lyotropic Nematic Suspensions.* Nano Letters, 2008. **8**(12): p. 4103-4107.
87. Lee, H.W., et al., *Lyotropic Liquid-Crystalline Solutions of High-Concentration Dispersions of Single-Walled Carbon Nanotubes with Conjugated Polymers.* Small, 2009. **5**(9): p. 1019-1024.
88. Lu, L. and W. Chen, *Large-Scale Aligned Carbon Nanotubes from Their Purified, Highly Concentrated Suspension.* Acs Nano, 2010. **4**(2): p. 1042-1048.
89. Becraft, M.L. and A.B. Metzner, *The rheology, fiber orientation, and processing behavior of fiber-filled fluids.* Journal of Rheology, 1992. **36**(1): p. 143-174.

90. Kumar, S., et al., *Synthesis, Structure, and Properties of PBO/SWNT Composites.* Macromolecules, 2002. **35**(24): p. 9039-9043.
91. Dierking, I. and S.E. San, *Magnetically steered liquid crystal-nanotube switch.* Applied Physics Letters, 2005. **87**(23).
92. Mauter, M.S., M. Elimelech, and C.O. Osuji, *Nanocomposites of Vertically Aligned Single-Walled Carbon Nanotubes by Magnetic Alignment and Polymerization of a Lyotropic Precursor.* Acs Nano, 2010. **4**(11): p. 6651-6658.
93. Shi, D.L., et al., *Magnetic alignment of carbon nanofibers in polymer composites and anisotropy of mechanical properties.* Journal of Applied Physics, 2005. **97**(6).
94. Choi, E.S., et al., *Enhancement of thermal and electrical properties of carbon nanotube polymer composites by magnetic field processing.* Journal of Applied Physics, 2003. **94**(9): p. 6034.
95. Gupta, S., et al., *"Self-Corralling" Nanorods under an Applied Electric Field.* Nano Lett., 2006. **6**(9): p. 2066-2069.
96. Dierking, I., K. Casson, and R. Hampson, *Reorientation Dynamics of Liquid Crystal-Nanotube Dispersions.* Japanese Journal of Applied Physics, 2008. **47**(8): p. 6390-6393.
97. Scalia, G., et al., *Carbon nanotubes in liquid crystals as versatile functional materials.* physica status solidi (b), 2007. **244**(11): p. 4212-4217.
98. Martin, D.C., *Controlled local organization of lyotropic liquid crystalline polymer thin films with electric fields.* Polymer, 2002. **43**(16): p. 4421-4436.
99. Senthil Kumar, M., et al., *Influence of electric field type on the assembly of single walled carbon nanotubes.* Chemical Physics Letters, 2004. **383**(3-4): p. 235-239.
100. Chen, X.Q., et al., *Aligning single-wall carbon nanotubes with an alternating-current electric field.* Applied Physics Letters, 2001. **78**(23): p. 3714.
101. Baik, I.S., et al., *Local deformation of liquid crystal director induced by translational motion of carbon nanotubes under in-plane field.* Journal of Applied Physics, 2006. **100**(7).
102. Park, C., et al., *Aligned single-wall carbon nanotube polymer composites using an electric field.* Journal of Polymer Science Part B-Polymer Physics, 2006. **44**(12): p. 1751-1762.
103. Ma, C., et al., *Alignment and dispersion of functionalized carbon nanotubes in polymer composites induced by an electric field.* Carbon, 2008. **46**(4): p. 706-710.
104. Zhu, Y.-F., et al., *Preparation and properties of alumina composites modified by electric field-induced alignment of carbon nanotubes.* Applied Physics A, 2007. **89**(3): p. 761-767.
105. Wongsuwarn, S., et al., *Fast and reversible microscale formation of columns in carbon nanotube suspensions.* Soft Matter, 2013. **9**(1): p. 235-240.

106. Bhattacharyya, S.S., et al., *Electric-field induced elastic stretching of multiwalled carbon nanotube clusters: a realistic model.* Physical Chemistry Chemical Physics, 2011. **13**(45): p. 20435-20440.
107. Jeong, S.J., et al., *Electroactive Superelongation of Carbon Nanotube Aggregates in Liquid Crystal Medium.* Nano Letters, 2007. **7**(8): p. 2178-2182.
108. Wakaya, F., T. Nagai, and K. Gamo, *Position control of carbon nanotube using patterned electrode and electric field.* Microelectronic Engineering, 2002. **63**(1-3): p. 27-31.
109. Senthil Kumar, M., et al., *DC electric field assisted alignment of carbon nanotubes on metal electrodes.* Solid-State Electronics, 2003. **47**(11): p. 2075-2080.
110. Bubke, K., et al., *Optical anisotropy of dispersed carbon nanotubes induced by an electric field.* Applied Physics Letters, 1997. **71**(14): p. 1906-1908.
111. Shah, H.J., et al., *Field controlled nematic-to-isotropic phase transition in liquid crystal-carbon nanotube composites.* Journal of Applied Physics, 2008. **103**(6): p. 064314.
112. Martin, C.A., et al., *Electric field-induced aligned multi-wall carbon nanotube networks in epoxy composites.* Polymer, 2005. **46**(3): p. 877-886.
113. Tse, K.L. and A.D. Shine, *Steady-State Electrorheology of Nematic Poly(n-hexyl isocyanate) Solutions.* Macromolecules, 2000. **33**(8): p. 3134-3141.
114. Lozano, K., et al., *Electrorheological analysis of nano laden suspensions.* Journal of Colloid and Interface Science, 2006. **297**(2): p. 618-624.
115. Lynch, M.D. and D.L. Patrick, *Organizing Carbon Nanotubes with Liquid Crystals.* Nano Letters, 2002. **2**(11): p. 1197-1201.
116. Lagerwall, J.P.F., et al., *Simultaneous alignment and dispersion of carbon nanotubes with lyotropic liquid crystals.* Physica Status Solidi B-Basic Solid State Physics, 2006. **243**(13): p. 3046-3049.
117. Schymura, S., et al., *Macroscopic-scale carbon nanotube alignment via self-assembly in lyotropic liquid crystals.* Synthetic Metals, 2009. **159**(21-22): p. 2177-2179.
118. Thomas, M.R., et al., *Nematic director-induced switching of assemblies of hexagonally packed gold nanorods.* Adv Mater, 2012. **24**(32): p. 4424-4429.
119. Dierking, I., et al., *Aligning and Reorienting Carbon Nanotubes with Nematic Liquid Crystals.* Advanced Materials, 2004. **16**(11): p. 865-869.
120. Scalia, G., et al., *Spontaneous macroscopic carbon nanotube alignment via colloidal suspension in hexagonal columnar lyotropic liquid crystals.* Soft Matter, 2008. **4**(3): p. 570-576.
121. Zhao, Y., et al., *Alignment of Single-Walled Carbon Nanotubes with Ferroelectric Liquid Crystal.* The Journal of Physical Chemistry C, 2012. **116**(31): p. 16694-16699.
122. Davis, V.A., et al., *Phase Behavior and Rheology of SWNTs in Superacids.* Macromolecules, 2004. **37**(1): p. 154-160.

123. Song, W., I.A. Kinloch, and A.H. Windle, *Nematic Liquid Crystallinity of Multiwall Carbon Nanotubes.* Science, 2003. **302**(5649): p. 1363-1363.
124. Song, W.H. and A.H. Windle, *Isotropic-nematic phase transition of dispersions of multiwall carbon nanotubes.* Macromolecules, 2005. **38**(14): p. 6181-6188.
125. Rai, P.K., et al., *Isotropic-Nematic Phase Transition of Single-Walled Carbon Nanotubes in Strong Acids.* Journal of the American Chemical Society, 2006. **128**(2): p. 591-595.
126. Song, W. and A.H. Windle, *Size-Dependence and Elasticity of Liquid-Crystalline Multiwalled Carbon Nanotubes.* Advanced Materials, 2008. **20**(16): p. 3149-3154.
127. Dierking, I., G. Scalia, and P. Morales, *Liquid crystal--carbon nanotube dispersions.* Journal of Applied Physics, 2005. **97**(4): p. 044309-5.
128. Doi, M., and Edwards S. F, *The Theory of Polymer Dynamics*. reprinted ed. The International Series of Monographs on Physics, ed. S.F.E. J. Birman, C. H. Llewellyn Smith, and M. Rees. 1986, New York: Oxford University Press. 391.
129. Burgers, J.M., *On the Motion of Small Particles of Elongated Form Suspended in a Viscous Liquid*, in *Second Report on Viscosity and Plasticity*. 1938, North-Holland: Amsterdam. p. 113.
130. Doi, M., *Rotational relaxation time of rigid rod-like macromolecule in concentrated solution.* J. Phys. France, 1975. **36**(7-8): p. 607-611.
131. Doi, M. and S.F. Edwards, *Dynamics of rod-like macromolecules in concentrated solution. Part 1.* Journal of the Chemical Society, Faraday Transactions 2: Molecular and Chemical Physics, 1978. **74**(0): p. 560-570.
132. Teraoka, I. and R. Hayakawa, *Anisotropic rotational diffusion of entangled rodlike polymers under elongational flow.* The Journal of Chemical Physics, 1989. **91**(12): p. 7951-7956.
133. Teraoka, I., N. Ookubo, and R. Hayakawa, *Molecular Theory on the Entanglement Effect of Rodlike Polymers.* Physical Review Letters, 1985. **55**(24): p. 2712-2715.
134. Acevedo, A., P.M. Cotts, and A.D. Shine, *Molecular Weight Dependence of the Rotational Diffusivity of Rodlike Polymers in Concentrated Nematic Solutions.* Macromolecules, 2005. **38**(15): p. 6648-6655.
135. Doi, M., *Rheological properties of rodlike polymers in isotropic and liquid crystalline phases.* Ferroelectrics, 1980. **30**(1): p. 247-254.
136. Doi, M., *Molecular dynamics and rheological properties of concentrated solutions of rodlike polymers in isotropic and liquid crystalline phases.* Journal of Polymer Science: Polymer Physics Edition, 1981. **19**(2): p. 229-243.
137. Marrucci, G. and P.L. Maffettone, *A description of the liquid-crystalline phase of rodlike polymers at high shear rates.* Macromolecules, 1989. **22**(10): p. 4076-4082.

138. Tse, K.-L. and A.D. Shine, *Two-dimensional modeling of the electrorheological behavior of liquid crystalline polymer solutions.* Journal of Rheology, 1995. **39**(5): p. 1021-1040.
139. Yang, I.K. and A.D. Shine, *Transient shear flow of a unidomain liquid-crystalline polymer.* Macromolecules, 1993. **26**(7): p. 1529-1536.
140. Bur, A.J. and L.J. Fetters, *The chain structure, polymerization, and conformation of polyisocyanates.* Chemical Reviews, 1976. **76**(6): p. 727-746.
141. Tse, K.L., *Electrorheology of Liquid Crystalline Polymer Solutions*, in *Chemical Engineering*. 1996, University of Delaware: Delaware. p. 448.
142. Baughman, R.H., A.A. Zakhidov, and W.A. de Heer, *Carbon nanotubes - the route toward applications.* Science, 2002. **297**(5582): p. 787-792.
143. Zhao, C., et al., *Functionalized carbon nanotubes containing isocyanate groups.* Journal of Solid State Chemistry, 2004. **177**(12): p. 4394-4398.
144. Levis, S.R. and P.B. Deasy, *Characterisation of halloysite for use as a microtubular drug delivery system.* International Journal of Pharmaceutics, 2002. **243**(1-2): p. 125-134.
145. Vergaro, V., et al., *Cytocompatibility and Uptake of Halloysite Clay Nanotubes.* Biomacromolecules, 2010. **11**(3): p. 820-826.
146. Liu, M., et al., *Chitosan/halloysite nanotubes bionanocomposites: Structure, mechanical properties and biocompatibility.* International Journal of Biological Macromolecules, 2012. **51**(4): p. 566-575.
147. Wilson, I.R., *Kaolin and halloysite deposits of China.* Clay Minerals, 2004. **39**(1): p. 1-15.
148. Ye, Y.P., et al., *High impact strength epoxy nanocomposites with natural nanotubes.* Polymer, 2007. **48**(21): p. 6426-6433.
149. Veerabadran, N.G., et al., *Organized Shells on Clay Nanotubes for Controlled Release of Macromolecules.* Macromolecular Rapid Communications, 2009. **30**(2): p. 99-103.
150. Shchukin, D.G., et al., *Halloysite nanotubes as biomimetic nanoreactors.* Small, 2005. **1**(5): p. 510-513.
151. Fried, F. and P. Sixou, *Lyotropic Mesophases of Hydroxypropylcellulose in Pure Acetic Acid, in Water, and in Mixed Solvents* Journal of Polymer Science Part a-Polymer Chemistry, 1984. **22**(1): p. 239-247.
152. Suto, S., et al., *Rheology of liquid crystalline solutions of hydroxypropyl cellulose in m-cresol.* Journal of Applied Polymer Science, 1989. **37**(4): p. 1147-1151.
153. Itou, T. and A. Teramoto, *Isotropic-liquid crystal phase equilibrium in solutions of semiflexible polymers: poly(hexyl isocyanate).* Macromolecules, 1988. **21**(7): p. 2225-2230.
154. Conio, G., et al., *Mesophase formation by semirigid polymers: poly(n-hexyl isocyanate) in dichloromethane and toluene.* Macromolecules, 1984. **17**(4): p. 856-861.

155. Fleurot, O. and D.D. Edie, *Steady and transient rheological behavior of mesophase pitches.* Journal of Rheology, 1998. **42**(4): p. 781-793.
156. Kundu, S. and A.A. Ogale, *Rheostructural studies on a synthetic mesophase pitch during transient shear flow.* Carbon, 2006. **44**(11): p. 2224-2235.
157. Khokhlov, A.R. and A.N. Semenov, *Liquid-crystalline ordering in the solution of long persistent chains.* Physica A: Statistical Mechanics and its Applications, 1981. **108**(2â€“3): p. 546-556.
158. Purdy, K.R. and S. Fraden, *Isotropic-cholesteric phase transition of filamentous virus suspensions as a function of rod length and charge.* Physical Review E, 2004. **70**(6): p. 061703.
159. Gorkunov, M.V. and M.A. Osipov, *Mean-field theory of a nematic liquid crystal doped with anisotropic nanoparticles.* Soft Matter, 2011. **7**(9): p. 4348-4356.
160. Shundyak, K., R. van Roij, and P. van der Schoot, *Theory of the isotropic-nematic transition in dispersions of compressible rods.* Physical Review E, 2006. **74**(2): p. 021710.
161. Matsuyama, A., *Theory of binary mixtures of a rodlike polymer and a liquid crystal.* The Journal of Chemical Physics, 2010. **132**(21): p. 214902.
162. Zhang, Q., D.R. Lippits, and S. Rastogi, *Dispersion and Rheological Aspects of SWNTs in Ultrahigh Molecular Weight Polyethylene.* Macromolecules, 2006. **39**(2): p. 658-666.
163. Ohl, N. and W. Gleissle, *The characterization of the steady-state shear and normal stress functions of highly concentrated suspensions formulated with viscoelastic liquids.* Journal of Rheology (1978-present), 1993. **37**(2): p. 381-406.
164. Vega, J.F., et al., *Rheology, Processing, Tensile Properties, and Crystallization of Polyethylene/Carbon Nanotube Nanocomposites.* Macromolecules, 2009. **42**(13): p. 4719-4727.
165. Nuel, L. and M.M. Denn, *Effect of processing and particulate fillers on the rheology of a nematic polymer melt.* Rheologica Acta, 1991. **30**(1): p. 65-70.
166. Mackay, M.E., et al., *Nanoscale effects leading to non-Einstein-like decrease in viscosity.* Nature Materials, 2003. **2**(11): p. 762-766.
167. Tuteja, A., et al., *Effect of Ideal, Organic Nanoparticles on the Flow Properties of Linear Polymers: Non-Einstein-like Behavior.* Macromolecules, 2005. **38**(19): p. 8000-8011.
168. Gao, Y., Y. Song, and Q. Zheng, *Miniemulsion polymerized titania/polystyrene core-shell nanocomposite particles based on nanotitania powder: Morphology, composition and suspension rheology.* Colloids and Surfaces A: Physicochemical and Engineering Aspects, 2012. **411**(0): p. 40-49.
169. Jain, S., et al., *Strong decrease in viscosity of nanoparticle-filled polymer melts through selective adsorption.* Soft Matter, 2008. **4**(9): p. 1848-1854.
170. Nusser, K., et al., *Viscosity Decrease and Reinforcement in Polymer-Silsesquioxane Composites.* Macromolecules, 2011. **44**(19): p. 7820-7830.

171. Schmidt, R.G., et al., *A Critical Size Ratio for Viscosity Reduction in Poly(dimethylsiloxane)-Polysilicate Nanocomposites.* Macromolecules, 2010. **43**(23): p. 10143-10151.
172. Pan, N., *Theoretical determination of the optimal fiber volume fraction and fiber-matrix property compatibility of short fiber composites.* Polymer Composites, 1993. **14**(2): p. 85-93.
173. Brenner, H., *Rheology of a dilute suspension of axisymmetric Brownian particles.* International Journal of Multiphase Flow, 1974. **1**(2): p. 195-341.
174. Kuhn, W. and H. Kuhn, *Die Abhängigkeit der Viskosität vom Strömungsgefälle bei hochverdünnten Suspensionen und Lösungen.* Helvetica Chimica Acta, 1945. **28**(1): p. 97-127.
175. Nemilentsau, A.M., et al., *Scattering of the near field of an electric dipole by a single-wall carbon nanotube.* Journal of Nanophotonics, 2010. **4**(1): p. 041685-041685.
176. Viswanath, D.S. and G. Natarajan, *Data book on the viscosity of liquids*. 1989, New York: Hemisphere Pub. Corp.
177. Folgar, F. and C.L. Tucker, *Orientation Behavior of Fibers in Concentrated Suspensions.* Journal of Reinforced Plastics and Composites, 1984. **3**(2): p. 98-119.
178. Koch, D.L., *A model for orientational diffusion in fiber suspensions.* Physics of Fluids, 1995. **7**(8): p. 2086-2088.